Institut für Theoretische Physik

Fakultät Mathematik und Naturwissenschaften

TU Dresden

Effect of Distributed Delays in Systems of Coupled Phase Oscillators

DISSERTATION

zur Erlangung des akademischen Grades

Doctor rerum naturalium

(Dr. rer. nat.)

vorgelegt von

Lucas Wetzel

MAX-PLANCK-INSTITUT FÜR

PHYSIK KOMPLEXER SYSTEME

Dresden, 2012

Verfasser: Lucas Wetzel, geboren am 22/07/1981

Abstract

Communication delays are common in many complex systems. It has been shown that these delays cannot be neglected when they are long enough compared to other timescales in the system. In systems of coupled phase oscillators discrete delays in the coupling give rise to effects such as multistability of steady states. However, variability in the communication times inherent to many processes suggests that the description with discrete delays maybe insufficient to capture all effects of delays.

An interesting example of the effects of communication delays is found during embryonic development of vertebrates. A clock based on biochemical reactions inside cells provides the periodicity for the successive and robust formation of somites, the embryonic precursors of vertebrae, ribs and some skeletal muscle. Experiments show that these cellular clocks communicate in order to synchronize their behavior. However, in cellular systems, fluctuations and stochastic processes introduce a variability in the communication times. Here we account for such variability by considering the effects of distributed delays. Our approach takes into account entire intervals of past states, and weights them according to a delay distribution.

We find that the stability of the fully synchronized steady state with zero phase lag does not depend on the shape of the delay distribution, but the dynamics when responding to small perturbations about this steady state do. Depending on the mean of the delay distribution, a change in its shape can enhance or reduce the ability of these systems to respond to small perturbations about the phase-locked steady state, as compared to a discrete delay with a value equal to this mean. For synchronized steady states with non-zero phase lag we find that the stability of the steady state can be altered by changing the shape of the delay distribution.

We conclude that the response to a perturbation in systems of phase oscillators coupled with discrete delays has a sharper functional dependence on the

mean delay than in systems with distributed delays in the coupling. The strong dependence of the coupling on the mean delay time is partially averaged out by distributed delays that take into account intervals of the past.

Acknowledgement

First of all, I would like to thank Prof. Jülicher for giving me the opportunity to work in his group and for the many helpful suggestions as well as the guidance during the last years. I would like to express my gratitude to Dr. Saúl Ares and Dr. Luis G. Morelli for their criticism, patience and great effort in guiding me through my projects.

The collaboration with the Oates Lab at MPI-CBG was very instructive and a great pleasure; many good memories are related to Dr. Andrew Oates and all the members of the lab.

Furthermore, I owe sincere and earnest thankfulness to my friend Dr. Douglas Staple for proofreading the thesis, and for the many fruitful discussions and helpful ideas he shared. I am also obliged to my colleagues Dr. Koichiro Uriu and David Jörg for the many discussions and comments.

Last but not least, I wish to thank my whole family for supporting me, especially my loved girlfriend Deborah Schmidt for her great support and keen mind.

Contents

III. APPENDICES 117

A. 119

B. Simulation methods 129

Notation of variables

- θ_k – phase of oscillator k

- ω – intrinsic frequency

- Ω – global frequency

- $k, l \in \mathbb{N}$ – indices of oscillators in the system

- $r(t)$ – synchronization order parameter

- β – phase frustration parameter

- N – total number of oscillators in the system

- n_k – number of coupling partners of oscillator k

- K – coupling strength

- h – 2π-periodic coupling function

- $g(s)$ – probability density of delay times

- $\hat{g}(\lambda)$ – Laplace transform of the delay distribution $g(s)$

- $\mathbb{D}$ – connectivity matrix

- d_{kl} – components of the connectivity matrix $\mathbb{D}$

- τ – mean of the delay distribution $g(s)$

- σ^2 – variance of the delay distribution $g(s)$

- γ – skewness of the delay distribution $g(s)$

- $q_k(t)$ – perturbation on oscillator k

- ζ – eigenvalues of the matrix $\mathbb{D}$

- λ – solutions of the characteristic equation

- x – real part of λ

- y – imaginary part of λ

- ψ, ξ and Ξ – phases of complex variables

- m – integer number of phase twists on a ring

- a, b – shape and scale parameter of the gamma distribution

- $\bar{m}, b, c$ – median and widths of the two step delay distribution

Abbreviations

- PSM – pre-somitic mesoderm

- AP axis – anterior posterior axis

- DCT – Delayed Coupling Theory (of vertebrate segmentation)

- FGF – Fibroblast growth factor

Part I.

INTRODUCTION

This part introduces the concepts needed throughout this work.

In Chapter 1 and 2 we give a short introduction to systems of coupled phase oscillators. Such systems are comprised of many autonomously oscillating parts that interact and can yield organized collective behaviour, e.g. synchronization. They play a major role in the work presented in this thesis. We take a look at some of the earliest work on synchronization phenomena in systems of coupled oscillators, for example by Christiaan Huygens and outline the contributions to the field by Winfree, Kuramoto and others. We define phase oscillators and discuss synchronization phenomena. The Kuramoto order parameter as a measure of coherence is introduced, and the effects of delayed coupling are discussed. We also give a short overview on how these oscillators are connected; this is described by the coupling topology. At the end we discuss the solutions to systems of coupled phase oscillators that are investigated in this work.

Chapter 3 puts these concepts into a biological context, the vertebrate segmentation clock. It is thought to act as a pacemaker during the developmental process of vertebrate segmentation. We present the concept of the clock and wavefront mechanism, present biological processes that have been suggested to be involved in vertebrate segmentation, and introduce the Delayed Coupling Theory of vertebrate segmentation, a model based on the clock and wavefront mechanism. The Delayed Coupling Theory is the starting point for the work in this thesis. We discuss the effects of replacing the dependence of the current state on solely one past time, by a dependence on intervals of past times.

Finally, Chapter 4 provides an outline of how the results part of the thesis is organized.

1. Coupled Phase Oscillators Enter the Stage

In this chapter we introduce the concept of synchronization in systems of coupled phase oscillators. This organized collective behaviour, which results from the interactions of many autonomously oscillating parts, can be quantified with the Kuramoto order parameter [1]. We give historical examples on synchronization phenomena, and introduce phase oscillator models. Two different ways of how the oscillators are arranged with respect to each other in the system are discussed, and the effects of communication delays are addressed.

1.1. Adjusting rhythms – synchronization

Synchronization is the coordination of rhythms of many individually oscillating parts that interact in order to show coherent behaviour on the population level.

Figure 1.1.: Synchronization of applause. (Dresden Monarchs)

For example, a cheering audience as shown in Fig. 1.1, usually starts clapping in a disordered fashion, but eventually synchronizes to a common rhythm shared

by all members [2]. Each member of the group receives audio-visual input from the others, upon which the own behaviour can be adjusted to that of the group. A detailed and rigorous introduction to synchronization phenomena is given in [3].

In this work we consider different types of synchronized states. When each member of an applauding crowd claps their hands with the same repetition speed, or frequency, and starts each clap at the exact same time as the other group members, we denote that as phase-locked synchronization with no phase lags.

The case that all members clap again with the same frequency but do not start each clap at the exact same time as their neighbours, we call splay state or m-twist synchronization. Here the integer number m is related to the difference of the fixed time-points at which neighbours start their individual claps. These solutions are introduced in more detail in Chapter 2.

The Kuramoto order parameter [1] is a measure of synchrony in systems of interacting oscillators, which we introduce later in this chapter, see Section 1.4.

1.2. Historical remarks

Christiaan Huygens, the Dutch astronomer, physicist and mathematician was one of the first scientists to observe and write about synchronization, and to give a detailed description back in the seventeenth century. He invented and worked with pendulum clocks, kept advancing them and made efforts to make them reliable even for travelling on ships on the open sea [3]. When he hung two pendulum clocks on a common support, a wooden beam (see Fig. 1.2), he discovered that they align (synchronize) the motion of their pendulum, despite the small inevitable differences in their intrinsic frequencies. In his memoirs he described his observation of a pair of such clocks [4, 5]:

"...It was quite worth noting that when we suspended two clocks so constructed from two hooks imbedded in the same wooden beam, the motions of each pendulum in opposite swings were so much in agreement that they never receded the least bit from each other and the sound of each was always heard simultaneously. Further, if this agreement was disturbed by some interference, it re-established itself in a short time. For a long time I was amazed at this unexpected result, but after a careful examination finally found that the cause of this is due to the

6
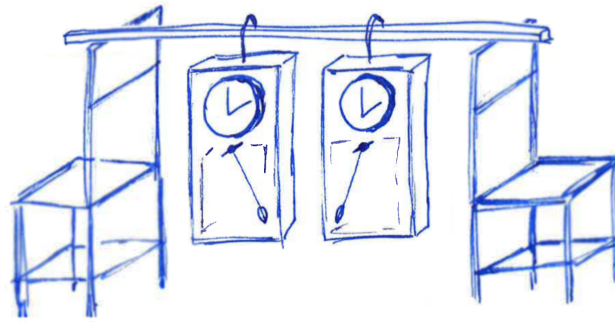
Figure 1.2.: Suspended pendulum clocks as used in a sketch by Christiaan Huygens and described in *Horologium Oscillatorium* (1673) [4].

motion of the beam, even though this is hardly perceptible. The cause is that the oscillations of the pendulum, in proportion to their weight, communicate some motion to the clocks. This motion, impressed onto the beam, necessarily has the effect of making the pendulum come to a state of exactly contrary swings if it happened that they moved otherwise first, and from this finally the motion of the beam completely ceases. But this cause is not sufficiently powerful unless the opposite motions of the clocks are exactly equal and uniform."

Huygens had given one of the first qualitative descriptions of the concept of mutual synchronization. By mentioning that *"the pendulum come to a state of exactly contrary swings"*, Huygens describes a phase-locked state of the system [6].

Another historic example, where the observation of synchronization phenomena is described, goes back to a travel diary of the Dutch physician Engelbert Kämpfer [3, 7]. In his notes from a travel to Siam in 1680 he wrote [8]:

"The glowworms [...] represent another shew, which settle on some Trees, like a fiery could, with this surprising circumstance, that a whole swarm of these insects, having taken possession of one Tree, and spread themselves over its branches, sometimes hide their Light all at once, and a moment after make it appear again with their utmost regularity and exactness ... ."

Here Kämpfer describes the observation of a phase-locked state in a large population of glowworms [7].

Synchronization phenomena of large interacting populations are abundant in many physical [9, 10], chemical [11, 12], engineering [13], and biological systems [14, 15]. In 1976 Winfree formulated the idea that many rhythmic processes in biology can be modelled by large systems of interacting oscillators [16]. Win-

7

free realized that organized collective behaviour and formation of patterns are possible, despite the differences between oscillators, for example due to genetic variability, noisy environments and other factors inherent to biological systems [16]. However the mathematical treatment of large systems of interacting oscillators is not simple, and the formulation used by Winfree in his first attempts was intractable. Despite the difficulties, he recognized that the description would simplify for weak interactions and nearly identical oscillators. In this limit a separation of timescales occurs. On the short timescale the oscillators relax to their limit cycles and can be described by their phases only, while on the long timescale the phases are influenced by their weak interaction and the differences in their intrinsic frequencies [17]. Another simplification Winfree proposed for his model was to take a mean-field like approach, where each oscillator interacts with the collective rhythm of all oscillators in the system:

$$\dot{\theta}_k = \omega_k + \left(\sum_{l=1}^{N} X(\theta_l) \right) Z(\theta_k). \tag{1.1}$$

In this formulation, θ_k is the phase of the oscillators $k = 1, 2, \ldots, N$, ω_k is the associated intrinsic frequency, $X(\theta_l)$ is the phase dependent influence of oscillator l, and $Z(\theta_k)$ is a sensitivity function, which governs the response to the interaction dependent on the phase θ_k. Winfree then used analytical approximations and numerical simulations to analyze his model [17]. He found a phase transition from asynchronous to synchronous behaviour, as he decreased the spread in the intrinsic frequencies of the individual oscillators below a certain threshold.

Another important contribution following Winfree's work was made by Kuramoto in 1975 [1]. Kuramoto employed perturbation methods and averaging to derive generally valid phase equations for systems of many weakly interacting autonomous oscillators that are almost identical. For the tractable case of "all to all" interaction, Kuramoto derived a set of coupled differential equations that are known as the Kuramoto model. In the following years Kuramoto kept developing his model and clarifying the presentation. A broad overview on Kuramoto's work can be found in his book [11]. Since then, many important contributions and advances have been made [18–26], reviewed in [2, 3, 15, 17, 27–30]. In the next section we introduce phase models in more detail.

1.3. Reducing variables – phase models

In terms of dynamical systems, a self-sustained oscillatory process is described by a limit cycle, which is a closed trajectory in phase space [19]. Here phase space denotes the space spanned by the variables of the oscillatory process. In steady state, the time evolution of these variables takes place on the limit cycle which is an attractor of nearby trajectories [3]. During one period of oscillation, the system variables traverse the limit cycle in phase space once. For quasilinear oscillators with a nearly circular limit cycle, the amplitude and phase correspond to the polar coordinates of this point [3].

The amplitude is the intensity of the oscillation, and by definition, the phase grows linearly in time and describes the fraction of one period of oscillation T
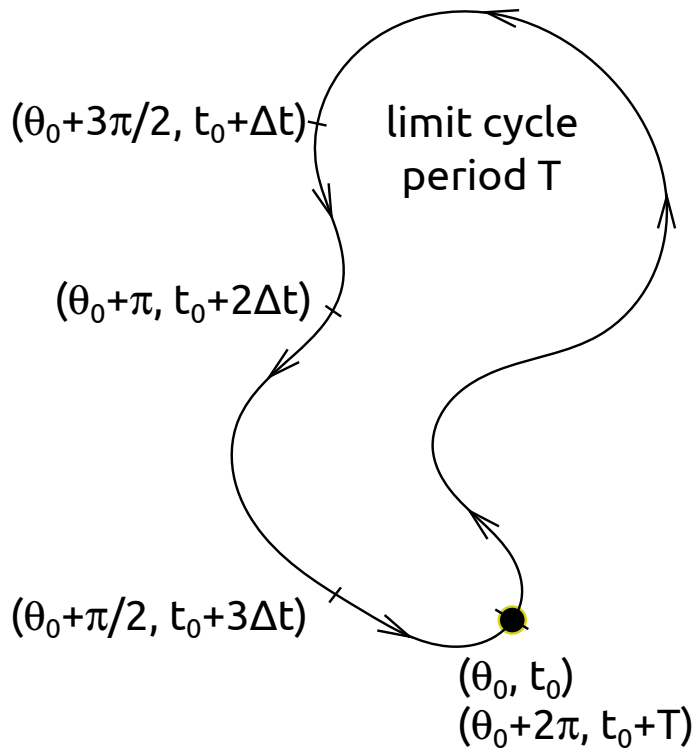

Figure 1.3.: Sketch of a limit cycle [3] with period T. The marks on the limit cycle depict four equidistant times. As the point moves once around the limit cycle during one period of oscillation, it advances with different speeds. Despite that, by definition, the phase grows linearly with time.

that has been completed [3], see Fig. 1.3:

$$\theta(t) = \theta_0 + \frac{2\pi}{T}(t - t_0). \tag{1.2}$$

Here θ_0 is the initial phase. Since every point on the limit cycle is equivalent, the phase is neutrally stable with regard to shifts (along the cycle), while the amplitude is stable, and perturbations imposed to it decay [3]. Even if the point has gone through different parts of the cycle with non-uniformly growing angle, as sketched in Fig. 1.3, a linearly growing phase can be defined by an appropriate transformation. Hence the phase always grows linearly in time.

When we talk of phase models of coupled oscillators we mean systems with reduced dynamics on a sub-manifold of the original system. Neglecting the amplitude, and the interactions of amplitude and phase and vice versa, is valid in the limit of weakly coupled oscillators [11, 31]. In such systems with weak mutual interactions, the neutrally stable phase can be freely shifted by perturbations, while the limit cycle is stable and will relax back to its original value. Averaging and perturbation techniques can be used to derive a phase dynamics approximation in these cases [32, 33]. The description of the oscillator is reduced to its phase.

Note that such reduced descriptions of systems of coupled oscillators do not provide a complete picture of the original system. For example amplitude death [34–36] cannot be identified in a phase model, since the amplitude is not defined. The process of synchronization however, where a population of oscillators orchestrates its dynamics to exhibit a periodic and coherent outcome, can be studied in systems of coupled phase oscillators.

1.4. The Kuramoto order parameter

We introduce a measure of coherence in a system of coupled phase oscillators, the so-called Kuramoto order parameter [1]:

$$r(t)e^{i\Xi(t)} \equiv \frac{1}{N} \sum_{k=1}^{N} e^{i\theta_k(t)}. \tag{1.3}$$

Here $\theta_k(t)$, with $k = 1, 2, \ldots, N$, corresponds to the phases of the individual oscillators at time t, and N denotes the number of oscillators in the system. The order parameter is a complex number and defined as the normalized sum over the real
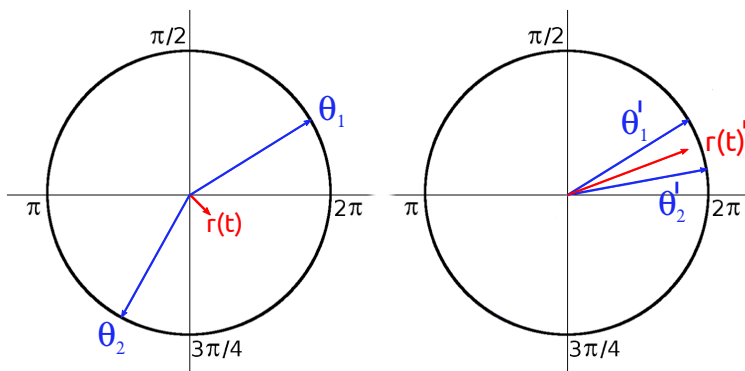
Figure 1.4.: Sketch of $r(t)$ for a system of two oscillators. On the left the oscillators with phase θ_1 and θ_2 are almost in anti-phase, resulting in a small order parameter $r(t)$. On the right the phases θ_1' and θ_2' are similar, which leads to a large order parameter $r(t)'$.

and imaginary parts of all phases in the complex plane. In Eq. (1.3) $r(t) \in \mathbb{R}$ is a measure of phase coherence in the system of phase oscillators, and $\Xi(t)$ denotes the average phase [17]. $\Xi(t)$ and $r(t)$ characterize the so-called mean-field in systems where all members are connected to each other, which will be explained in Section 1.5.

For phase-locked solutions, where all oscillators share the same frequency and start each cycle of the oscillations at the same time, the oscillators are completely synchronized and $r(t) = 1$. Examples for this state are the synchronized flashing of glowworms [7], or applause where the entire audience starts each individual clap at the same time. Note however, that other synchronized states can exist that have $r(t) = 0$ following the definition in Eq. (1.3). For example, this can occur if all oscillators share a common frequency, but do not start each cycle of the oscillations at the same time, but rather in a defined relation that is constant in time, due to their common frequency. That applies for solutions where the phases are equally distributed in $[0, 2\pi)$, e.g. splay states or so-called m-twist solutions [37, 38]. In systems where the number of oscillators becomes large, the incoherent state approaches $r(t) = 0$ [18]. Hence, in such systems the Kuramoto order parameter has to be modified such that these different states can be distinguished.

A generalized order parameter that becomes $r(t) = 1$ for m-twist steady states

can be defined in terms of the number of clusters $C \in \mathbb{N}$ [39]:

$$r(t)e^{i\Xi(t)} \equiv \frac{1}{N} \sum_{k=1}^{N} e^{iC\theta_k(t)}. \tag{1.4}$$

The cluster number denotes how many groups of oscillators with the same phase form in steady state. This can also be formulated in terms of the m-twist and number N of oscillators in the system, calculating $\theta_k(t)$ modulo the constant phase difference between adjacent clusters $\Delta \equiv 2\pi\, m/N$ in the system, and rescaling by $2\pi/\Delta$:

$$r(t)e^{i\Xi(t)} \equiv \frac{1}{N} \sum_{k=1}^{N} e^{i\frac{2\pi}{\Delta}\mathrm{mod}[\theta_k(t),\,\Delta]}. \tag{1.5}$$

1.5. Who talks to whom – coupling topologies

An important characterization of systems of coupled oscillators is the coupling topology. It contains the information about the connections between different members in the system. In a previous section we had already heard about "all to all" mean-field coupling [18, 40, 41], where all oscillators couple to every other oscillator in the system.

There are many other types of coupling topologies, such as randomly connected networks [13, 42–44], networks with mobile oscillators where the topology constantly changes [13, 38, 45], and nearest neighbour interactions on different lattices implying different numbers of neighbours [46–48]. A few examples are shown in Fig. 1.5. These coupling topologies can be distinguished further, e.g.
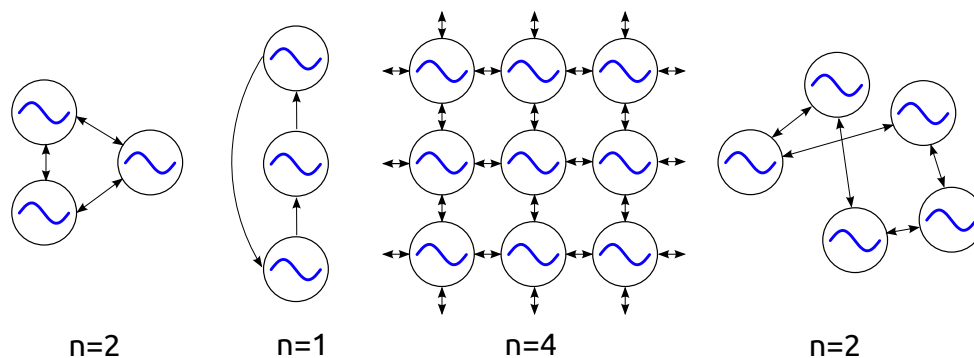
Figure 1.5.: Left to right: all-to-all connected system, ring topology with unidirectional connections, square lattice, and randomly connected system.

into unidirectional, bidirectional and mixed connections within the system [49–53], and into systems with different boundary conditions, such as reflecting, periodic or closed boundaries. In addition to the mutual arrangement of the oscillators, the boundary conditions and the directionality of the connection, the character of the coupling function plays an important role in the coupling. For example both attractive [1] and repulsive [54] coupling functions are possible.

Mean field coupling – "all to all"

The mean field coupling topology describes an "all to all" coupling within the system, such as in the Kuramoto model [1]:

$$\dot{\theta}_k(t) = \omega_k + \frac{K}{N} \sum_{l=1}^{N} \sin\left(\theta_l(t) - \theta_k(t)\right). \tag{1.6}$$

Here $\theta_k(t)$ denotes the phase of the oscillators for $k = 1, 2, \ldots, N$, ω_k the intrinsic frequencies, and K the coupling strength. The frequencies ω_k are drawn from a unimodal and symmetric distribution. In such models the individual coupling interactions can be replaced by an effective coupling to the mean-field:

$$\dot{\theta}_k(t) = \omega_k + K\,r(t)\sin(\Xi(t) - \theta_k(t)), \tag{1.7}$$

using the Kuramoto order parameter Eq. (1.3), which characterizes the mean-field [1]. It is an average or effective description of the entire system of oscillators [16, 55]. This can simplify analytic and numerical treatment drastically, especially when dealing with large systems of oscillators.

Nearest neighbour coupling

We refer to nearest neighbour coupling when looking at coupled oscillators arranged on a lattice, if each oscillator couples only to its nearest neighbours, see Fig. 1.5 B. For square lattices this implies the number of neighbours for each oscillator is $2D$, where D denotes the dimension [48, 56].

2. Coupled Phase Oscillators with Delay in the Coupling

2.1. Communication needs time – coupling delays

When information is processed and exchanged between different elements in a system, finite signal propagation speed leads to communication delay. In many cases such delay is not negligible. It can introduce qualitatively new effects that are not present in the description without delay.

Delays in signal transduction are inherent to many complex processes; for example due to molecular transport processes, or in general finite propagation times [57–62]. Also intermediate steps or states of the process [63], such as transcription and translation times in protein synthesis [64, 65] introduce delays.

In systems of coupled oscillators delays in the coupling lead to new phenomena, not present in systems without delay [66, 67]. This can be seen from a
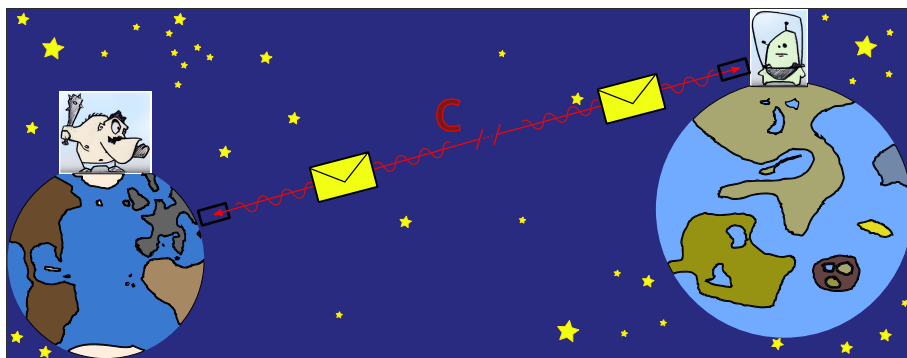

Figure 2.1.: Sketch of interaction with finite signal transmission speed c. Such finite transmission speed leads to delayed communication. (Earthling and alien images courtesy of Steffen Kleine.)

simple example: two persons who would attempt to synchronize their 24 hour wrist watches by sending letters to each other, easily succeed if the letters take exactly 24 hours. In contrast, letters that take 12 hours would correspond to a repulsive interaction, and result in watches that run in anti-phase unless the people know the transit time. Hence, replacing an instantaneous by a delayed action in a model can lead to qualitatively different outcomes [68].

Two coupled limit cycle oscillators can synchronize to a common frequency and phase despite the presence of a time delay, as shown by Schuster and Wagner for systems of coupled phase oscillators [68]. In [69], Yeung and Strogatz derive exact formulas for the stability of the coherent and incoherent states as a function of the delay in a mean-field coupled system. Dependent on the mean value of the delay, the global frequency in the synchronized state is different compared to the frequencies of the individual oscillators. It is not given by the mean of the intrinsic frequencies [68]. For values of the delay that exceed a critical value there are multiple stable and unstable steady states [68, 70–72]. Hence, above the critical delay multistability of steady states can be found.

In systems of coupled oscillators that also contain the amplitude of oscillation [73], for example in coupled Stuart-Landau oscillators, amplitude death [34–36, 74, 75] can occur. Amplitude death denotes the coupling-induced state of zero amplitude [76], which requires sufficiently strong coupling, and a sufficiently wide-spread distribution of intrinsic frequencies [77]. With delay in the coupling amplitude death is also possible if the individual frequencies of the oscillators are identical [78]. If the intrinsic frequencies of the oscillators are not identical, an increasing delay value leads to an increase in the size of amplitude death regions [30], compared to systems without delay. Another reported phenomenon introduced by delay, in this specific case by distance dependent delays, is the formation of various patterns such as spirals, targets and travelling rolls [79].

In the next two subsections we introduce distributed and discrete delays and discuss previous results.

2.1.1. Discrete delays consider one past time

There are many types of delay [80]. One major classification of delay systems is into systems with discrete or with distributed delays [67]. However, there is some ambiguity in the literature as to what is meant by these two terms.

In discrete delay formulations, only the state at one past time is taken into

account for the present time evolution. However, if a discrete delay is randomly drawn of a distribution at each time-step [81], this is often termed as distributed delays. In that case we face a temporal distribution of delay times. There is also the case of discrete delays drawn randomly from a distribution for different connections in the system, e.g. [82, 83]. Then the time delays throughout the system are heterogeneous, and despite their individual discrete character, they are called distributed delays. Due to the difficulties to unambiguously distinguish the different delay models in the literature by just the two major classifications, we define discrete delays for this thesis as follows. Systems of coupled phase oscillators that take into account one past time that is homogeneous throughout all connections and constant in time, are called discrete delays. Note that discrete delays are a simplified description; real time delays are usually not constant in time, nor homogeneous throughout a system.

2.1.2. Distributed delays consider multiple past times

Delay models that fall under the category of distributed delays are manifold. They all share the property that not only one discrete past time, but rather different past times or entire intervals of the past [67], are considered.

The number of different formulations of distributed delays is large; it reaches from delay times τ_{kl} that are drawn from a distribution for each of the connections in a system individually [23, 26, 82], to formulations where an effective information of the past $\bar{x}$ is computed by a normalized integral [34, 36, 84–86] over intervals of past states. The first formulation mentioned, describes heterogeneous interaction delays throughout the system, whereas the latter is mostly used homogeneously throughout the system:

$$\bar{x}(t) = \int_a^b ds \, g(s) x(t-s). \tag{2.1}$$

Here $g(s)$ is a so-called delay kernel, which weights the different past times, and $x(t-s)$ provides the history of the variable.

The references mentioned so far study systems with distributed delays, which are abundant in many fields of engineering and natural sciences; e.g. in dynamical systems [65, 84, 86], or in chemical reactions of coupled reaction-diffusion systems [85]. Also the field of neuronal networks has made many contributions [82, 83, 87–91] to systems coupled with distributed delays.

Effects introduced by distributed delays are often compared to the case of a discrete delay, with a value equal to the mean of the delay distribution, see e.g. [92]. In systems of delay coupled Stuart-Landau oscillators it has been shown [34] that amplitude death regions are increased in parameter space, if one uses distributed delays in the coupling instead of discrete delays. As a threshold value of the variance of the delay distribution is crossed, the amplitude death region becomes unbounded and any mean value of the delay can lead to amplitude death [34].

2.2. Coupled phase oscillators with discrete delay

In this section we introduce systems of coupled phase oscillators with a discrete delay τ in the coupling function [68]:

$$\dot{\theta}_k(t) = \omega + \frac{K}{n_k} \sum_{l=1}^{N} d_{kl} \, h \left(\theta_l(t-\tau) - \theta_k(t) \right), \qquad (2.2)$$

where $\theta_k(t)$, with $k = 1, 2, \ldots, N$, corresponds to the phases of the individual oscillators at time t, N is the number of oscillators in the system, n_k is the number of connections that oscillator k has to other oscillators in the system, K is the coupling strength that couples an oscillator to its neighbours, h is a 2π-periodic coupling function, and ω is the intrinsic frequency of the identical oscillators. The d_{kl} are either one, if oscillator k is connected to oscillator l, or zero, if not. These are the components of the connectivity matrix $\mathbb{D}$, which contains the information about all connections between the oscillators in the system. The next two sections introduce phase-locked solutions in such systems of coupled phase oscillators with delay.

2.2.1. Phase locked steady states with no phase lags

One type of phase-locked solution to Eqs. (2.2) is the phase-locked steady state with no phase lags, $\theta_k(t) = \Omega t$, characterized by a common phase and global frequency Ω shared by all oscillators in the system. Steady states describe the long term behavior of the system, when transient dynamics have died away [19]. The ansatz made for this phase-locked solution:

$$\theta_k(t) = \Omega t, \qquad (2.3)$$

considers linear growth of all phases with the global frequency Ω [68]. Ansatz (2.3) is substituted into Eq. (2.2) in order to obtain the solution for Ω via a self-consistent approach:

$$\Omega = \omega + K h(-\Omega\tau) \frac{1}{n_k} \sum_{l=1}^{N} d_{kl}. \tag{2.4}$$

The sum of entries l in the kth row of the connectivity matrix is given by $n_k \ \forall \ k$:

$$\frac{1}{n_k} \sum_{l=1}^{N} d_{kl} = 1 \quad \forall \ k. \tag{2.5}$$

This leads to an implicit expression for Ω in the case of discrete delays:

$$\Omega = \omega + Kh(-\Omega\tau). \tag{2.6}$$

This relation can be plotted parametrically in the $\Omega - \tau$ plane by substituting $\Omega\tau \equiv f$ [56]:

$$\Omega = \omega + Kh(-f),$$
$$\tau = \frac{f}{\omega + Kh(-f)}. \tag{2.7}$$
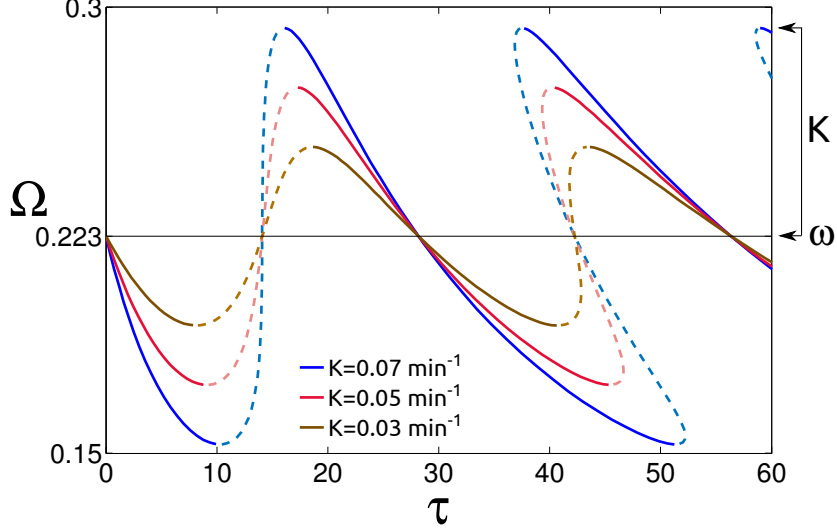
Figure 2.2.: Global frequency Ω plotted versus the mean of delay τ for a sinusoidal coupling function h. The plot shows three curves for different coupling strengths K, intrinsic frequency $\omega = 0.223\text{min}^{-1}$, arbitrary number of oscillators N and connections n_k. Dashed lines denote unstable solutions and solid lines denote stable solutions as determined in Section 6.2.
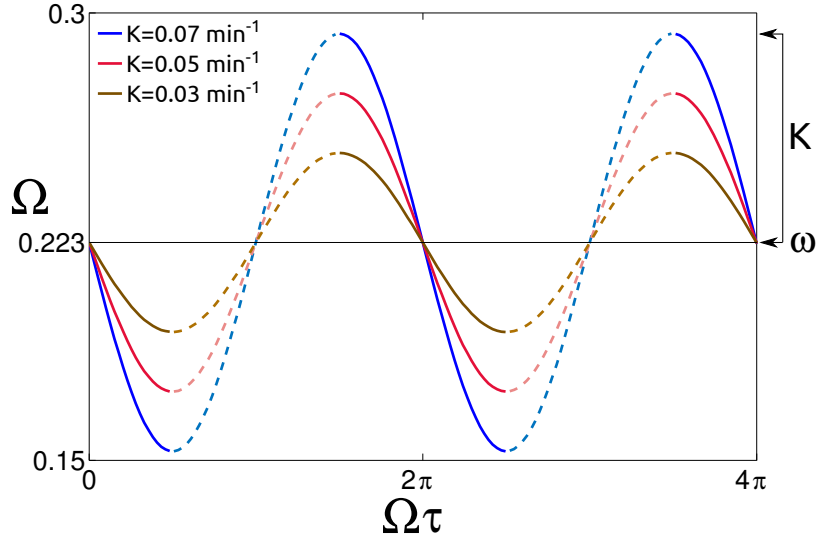
Figure 2.3.: Global frequency Ω plotted versus $\Omega\tau$ for a sinusoidal coupling function h. The plot shows three curves for different coupling strengths K, intrinsic frequency $\omega = 0.223\,\mathrm{min}^{-1}$, arbitrary number of oscillators N and connections n_k. Dashed lines denote unstable solutions and solid lines denote stable solutions as determined in Section 6.2.

It is plotted for different coupling strengths K in Fig. 2.2. An effect introduced by the delay is the multistability of steady states: there are multiple solutions for the global frequency Ω for one value of the mean delay τ [68]. This can be seen in Fig. 2.2 for sufficiently large τ.

With increasing coupling strength K, the deviation of the global frequency Ω from the intrinsic frequency ω grows for all $\Omega\tau \neq j\pi \ \forall \ j \in \mathbb{N}_0$. The τ-intervals with multiple solutions also grow as K increases, see Fig. 2.2. The relation between Ω and the product of Ω times the mean τ is plotted in Fig. 2.3. This unfolds the curve and we will later use this representation for other plots. We will see that this is convenient since many expressions that are evaluated often depend on $\Omega\tau$. In the remainder of this thesis we set $K = 0.07\,\mathrm{min}^{-1}$ and $\omega = 0.223\,\mathrm{min}^{-1}$.

20
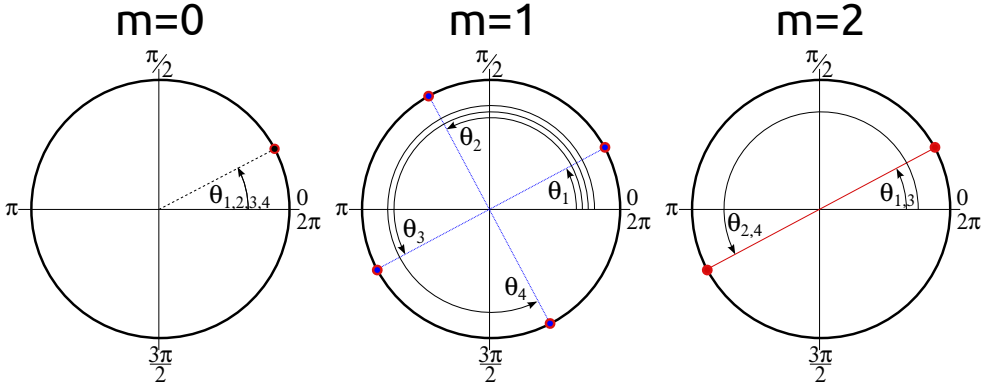
Figure 2.4.: Snapshots of the phases in different m-twist steady state configurations for $N = 4$ oscillators. The coloured circles mark the phases.

2.2.2. m-twist solutions: phase-locked steady states with phase lags

Phase locked solutions with non-zero phase lags are introduced in this section [35, 37, 38]. We consider these solutions only in $1D$ systems with periodic boundary conditions and nearest neighbour interactions. The accordingly modified Eqs. (2.2) then read:

$$\dot{\theta}_k(t) = \omega + \frac{K}{2} \sum_{l=k\pm1} h\left(\theta_l(t-\tau) - \theta_k(t)\right). \tag{2.8}$$
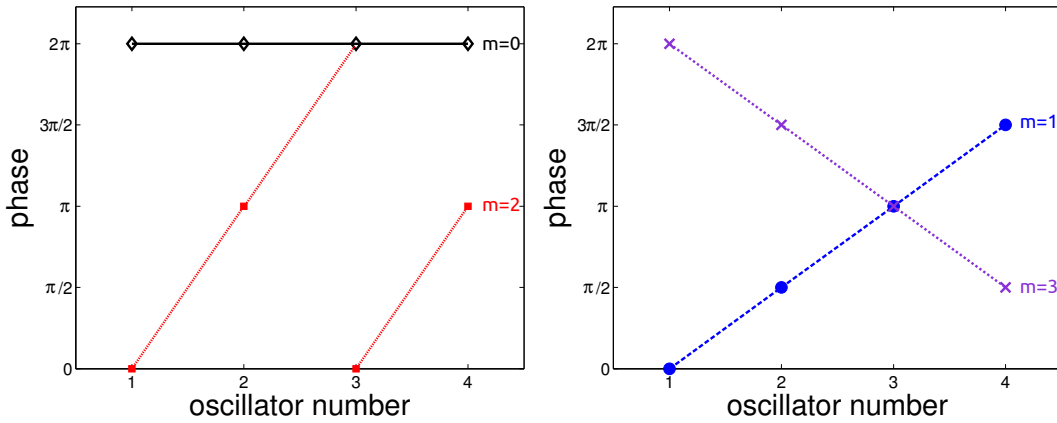
Figure 2.5.: Sketch of steady state phases for a system of $N = 4$ oscillators for $m = \{0, 2\}$ twist state with $\Delta = \{0, \pi\}$ respectively in the left plot and $m = \{1, 3\}$ twist state with $\Delta = \left\{\frac{\pi}{2}, \frac{3\pi}{2}\right\}$ respectively in the right plot.
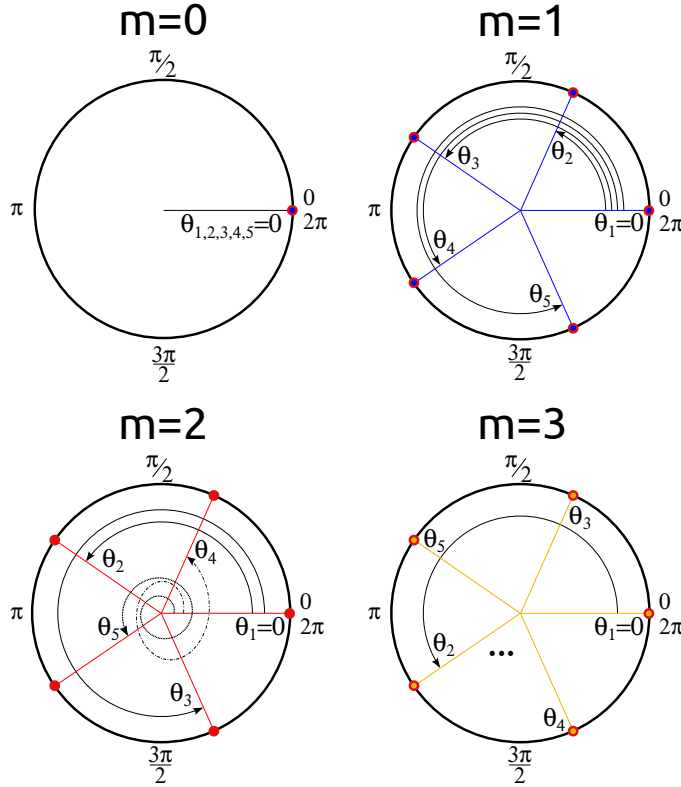
Figure 2.6.: Snapshots of the phases in different m-twist steady state configurations for $N = 5$ oscillators. Note: $m = 4$ corresponds to $m = -1$.

In this system the steady state solutions are characterized by a global frequency Ω shared by all oscillators in the system, and phase differences $\pm\Delta$ between adjacent neighbours. The phase difference Δ is identical between all adjacent pairs of oscillators. Hence the phases of the oscillators are evenly arranged in $[0, 2\pi)$, see Fig. 2.4 for a chain of $N = 4$, and Fig. 2.6 for a chain of $N = 5$ oscillators. These solutions are also called m-twist or splay states [37, 93], related to the multiples m of 2π accumulated when summing all phase differences Δ between the oscillators on the ring. The case $m = 0$ recovers the phase-locked solution with zero phase lags. Hence, all oscillators share the same phase in steady state and the phase differences are zero. For $m = 1$ the sum over the phase differences yields 2π. Since these phase differences are identical for all adjacent pairs by definition, the oscillators arrange evenly spaced in the interval $[0, 2\pi)$ – e.g. a snapshot yields $\{\theta_1 = 2\pi, \theta_2 = \frac{\pi}{2}, \theta_3 = \pi, \theta_4 = \frac{3\pi}{2}\}$. In this configuration they evolve with a common global frequency Ω in time, maintaining their mutual phase differences.
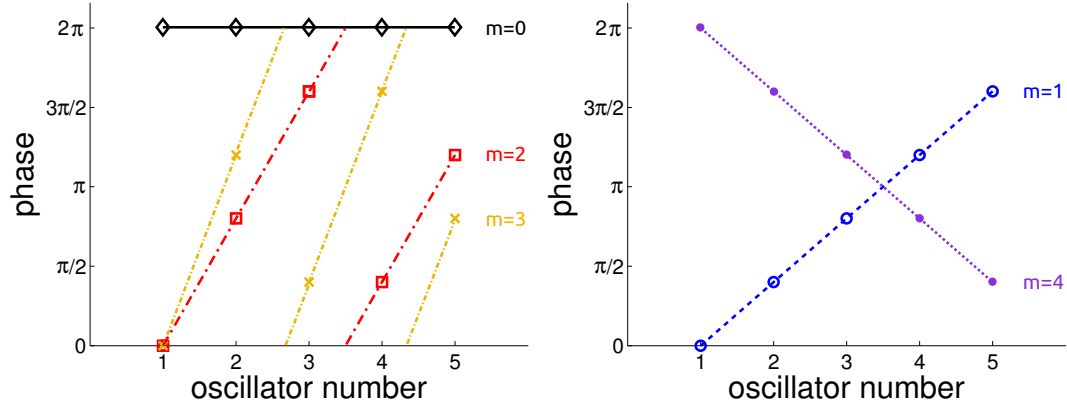
Figure 2.7.: Sketch of steady state phases for a system of $N = 5$ oscillators for $m = \{0, 2, 3\}$ twist state with the associated $\Delta = \left\{0, \frac{4\pi}{5}, \frac{6\pi}{5}\right\}$ in the left plot and in the right plot $m = \{1, 4\}$ twist state with $\Delta = \left\{\frac{2\pi}{5}, \frac{8\pi}{5}\right\}$, respectively.

Following Wiley et al. [37], and Peruani et al. [38], these m-twist or splay state solutions with $m \in \mathbb{N}_0$ are defined by:

$$\theta_k(t) = \Omega t + \frac{2\pi m}{N} k. \tag{2.9}$$

The phase lag between neighbouring oscillators is given by:

$$\Delta \equiv \frac{2\pi m}{N}, \tag{2.10}$$

according to the associated m-twist number. This integer $m \in \{0, 1, \dots, N-1\}$ denotes the winding number that determines how many multiples of 2π accumulate, as one goes once trough the chain of oscillators, and sums up their phase lags with respect to the next oscillator, see Figs. 2.7 and 2.5.

Summary

In this chapter we introduced the concept of synchronization in systems of coupled phase oscillators, presented the coupling topologies that are considered in this work, and gave an introduction to known effects of discrete and distributed delays in such systems. Furthermore we introduced phase-locked solutions with zero and non-zero phase lags in systems of coupled phase oscillators with delay in the coupling function.

The next chapter introduces the vertebrate segmentation clock that plays an important role in the developmental process of vertebrate segmentation. This

process has been successfully treated with a phase oscillator model with discrete delays, the Delayed Coupling Theory of vertebrate segmentation [56].

3. The Vertebrate Segmentation Clock – What Provides the Rhythm?

The aim of this chapter is to introduce an essential mechanism that we believe is a core component to vertebrate segmentation, the vertebrate segmentation clock. It is thought to provide the rhythm for the developmental process of vertebrate segmentation. During this developmental process, vertebrates sequentially form pairs of structures aligned on both sides of the elongating head to tail body axis

Figure 3.1.: The vertebrate body axis is segmented. (A-B) Lateral view of a zebrafish embryo at two different stages of development. Time relative to bud stage at about 10 hours past fertilization [94] (image courtesy of Christian Schröter). (C) Segmented body axis of wild-type adult zebrafish. Adult zebrafish body length varies from $2.5 - 4$ cm [95] (image courtesy of A. Oates).
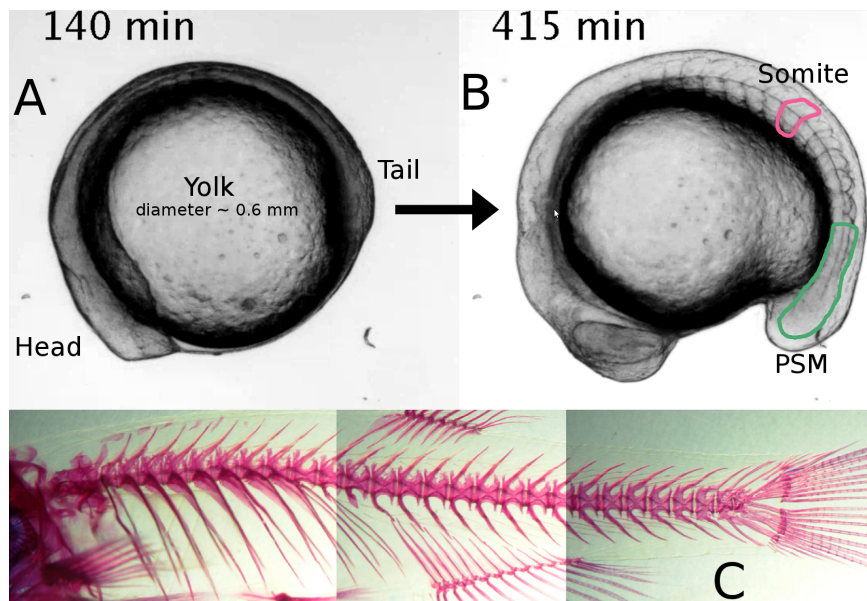
[96], see Fig. 3.1. These structures, called somites, are blocks of mesodermal cells [97, 98] and are the precursors of vertebrae, ribs and skeletal muscle. How these periodic structures are formed reliably in a noisy environment is the subject of intense research [32, 99–101]. For more detailed descriptions on the process of vertebrate segmentation we refer the reader to the literature [56, 98, 102–105].

3.1. The clock and wavefront mechanism

There are different theoretical models and concepts [106] that aim to describe how biological systems measure distances, achieve diversity from an undifferentiated state, or self organize. Such models and concepts are for example morphogen gradients [107, 108], reaction-diffusion systems [109, 110] and the clock and wavefront mechanism [96, 102]. The clock and wavefront mechanism is currently favoured as the basis for theoretical description of somitogenesis [98, 111] and well supported by experiments [112, 113].

In 1976 Cooke and Zeeman [96] proposed the clock and wavefront mechanism, a general scheme that aims to describe how structure formation in developing organisms can be achieved, without specifying the underlying biological and biochemical details. They propose a clock, composed of unspecified cellular oscillators that show synchronized oscillations, and provide the timing for the regular and periodic formation of each somite. Superimposed to these coherent oscillations, a wavefront sweeps through the tissue and arrests the oscillations in their current state, leaving behind a frozen image of the state of oscillation at the time of arrest. Assuming the wavefront moves through the tissue at constant speed and direction, implies a well defined length l of the structures that are left behind. It is given by the product of the period of oscillation T and the wavefront speed v, i.e. $l = vT$.

Based on the concept of the clock and wavefront mechanism, various modelling approaches on vertebrate segmentation [56, 114, 115] have been made. In the next two sections we give a closer description on what we believe is the unspecified cellular oscillator proposed by the clock and wavefront mechanism, and how these oscillators communicate their states to organize the tissue level coherent oscillations, that provide the period of the segmentation clock [98].

3.2. Cyclic gene expression on the cellular and the tissue level

In recent years experiments in chick [116, 117], zebrafish [118] and other organisms [119] have been carried out, identifying travelling waves of cyclic gene expression on the tissue level, see Fig. 3.2. This is observed in the pre-somitic mesoderm (PSM) of vertebrates, Figs. 3.1 and 3.3, a tissue located in the tail region of the growing embryo. With each newly formed somite the pattern of gene expression repeats, i.e. the rhythm of cyclic gene expression on the tissue level matches the rate of somite formation [98].

Cyclic gene expression has been observed by mRNA *in situ* hybridization [118, 120–122] and also *in vivo*, using yellow fluorescent protein (YFP)-based, real-time fluorescence imaging systems [123–125]. The observed waves of cyclic gene expression are independent from material transport. This is evident in dissection experiments [116, 123], where surgically removed pieces of the PSM continue to show cyclic gene expression patterns. However, the question is raised whether cyclic gene expression exists autonomously also at the cellular level.

There is evidence that supports cyclic gene expression at the single cell level [123, 126]. Time series of endogenous gene expression from *in situ* hybridization experiments, in which single cells were dissociated from PSM tissue and fixed, show variable gene expression levels [117]. Time-lapse images of cells that are marked by a luciferase reporter that is under control of the Hes1 cyclic gene promoter yield additional indications for sustained oscillations at single cell level [123]. Period measurements in these and other experiments suggest that the noise level in the individual oscillating cell is higher than at the tissue level [32, 127].
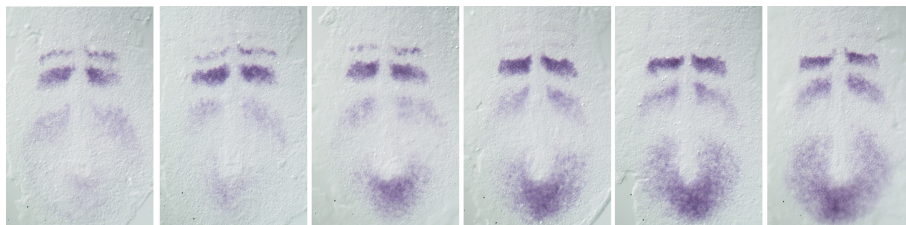
Figure 3.2.: Dorsal view of the PSM of fixed embryos at similar stages of development. mRNA expression levels made visible by *in situ* hybridization technique. (Image courtesy of Andrew Oates.)
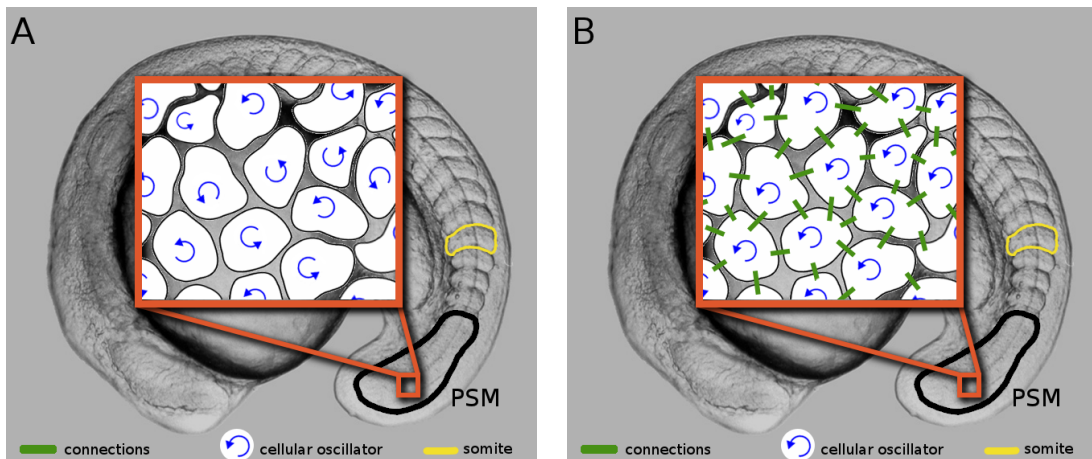
Figure 3.3.: Lateral view of a zebrafish embryo. Insets: uncoupled incoherent (A) and coupled coherent (B) cellular oscillators in the PSM. (Image courtesy of Christian Schröter.)

Different theoretical models that have been proposed to describe single cell genetic oscillators suggest an auto-inhibitory feedback loop with a transcriptional time delay [63, 64, 128, 129]. The idea is that protein products can bind to the promoters of their own genes and inhibit further gene expression, and hence the formation of new mRNA, see Fig. 3.4. The number of mRNA molecules of this gene decreases due to degradation according to their half-lives. Consequently the the number of gene products in the cell will drop, until it cannot continue to suppress its own gene expression. Then the cycle starts over. The time delays associated to transcription, translation and molecule trafficking, as new mRNA copies are made and processed in the cell, play an important role for the period [64] of this proposed biochemical oscillation in the cell.
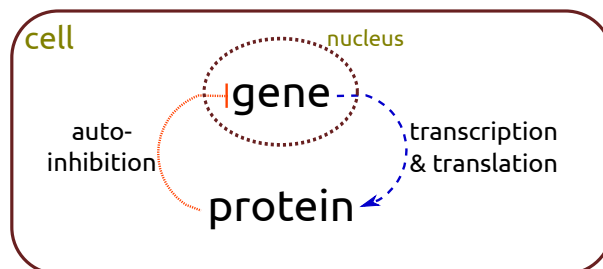
Figure 3.4.: Sketch of a negative feedback loop in gene expression. Protein products inhibit the transcription of their own gene.

Oscillations on the tissue level have the same period as the successive formation of the somites. This suggests that the period of oscillation at the tissue level constitutes the clock period in vertebrate segmentation. These coherent tissue level oscillations may be the result of synchronized periodic gene expression in the cells of the PSM. If so, there must to be some kind of signalling pathway that allows many individual oscillators to coordinate their expression levels. It has been suggested that cells in the PSM of zebrafish embryos communicate their states using the Delta-Notch signalling pathway [32, 99, 100], which requires cell-cell contact to function [130, 131].

3.3. Coupling by Delta-Notch signalling

The intercellular Delta-Notch signalling pathway is highly conserved and present in most multicellular organisms [130]. It allows cells to process external signals and communicate cell state information to the cell membrane [131]. Contact areas of adjacent cells allow for transactivation and cis-inhibition of Delta and Notch proteins [132, 133]. Here transactivation denotes the interaction of Delta and Notch proteins on the cell membrane of adjacent cells, that leads to the cleavage of the Notch intracellular domain, see Fig. 3.5. The interaction of Delta
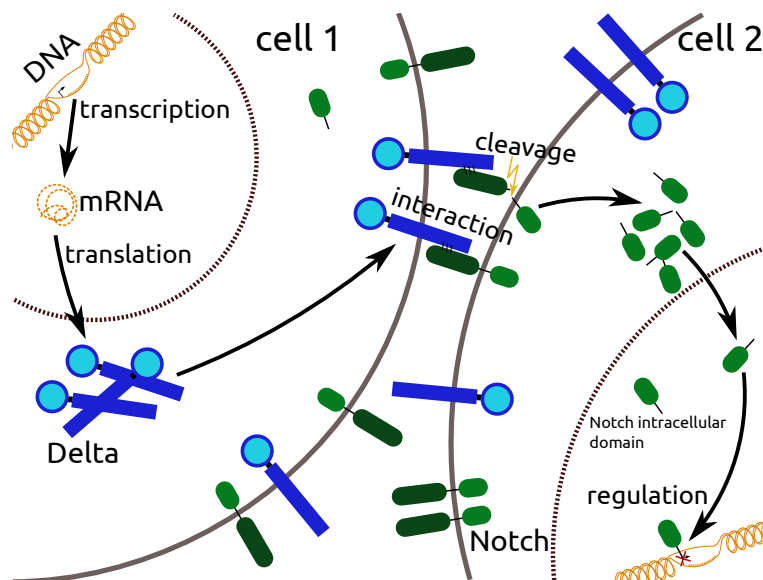
Figure 3.5.: Delta-Notch intercellular signalling pathway. Delta protein shown in blue and Notch protein in green.

and Notch proteins located at the same cell membrane leads to the inhibition of Notch and is called cis-inhibition. The interaction of Delta and Notch proteins at the cell contact area of two cells leads to the cleavage of the Notch extracellular domain and releases the intracellular domain to the signal receiving cell. This domain can in turn fulfil regulatory tasks in the cell, see Fig. 3.5.

The coherent levels of gene expression observed on the tissue level in travelling waves of gene expression suggest that there must be a mechanism that coordinates the behaviour of individual cellular oscillators in vertebrate segmentation. The Delta-Notch signalling pathway has been shown to be involved in the local synchronization of oscillators across the PSM [113]. As Delta-Notch coupling is lost, the patterns of travelling waves of gene expression show 'salt and pepper' like expression patterns [32], indicating that synchrony between cellular oscillators is lost [99, 118]. Mutations that lead to loss of function of the Delta-Notch signalling pathway cause defective somite boundaries and the disruption of somitogenesis [134–136]. Inhibition of the Delta-Notch pathway leads to gradual disruption of somite formation, and eventually leading to defective somite boundaries. This can be reversed when Delta-Notch signalling is re-established, and recovers the formation of somites after a transient time [32].

3.4. The Delayed Coupling Theory

Different modelling approaches to vertebrate segmentation conducted in recent years rely on the clock and wavefront mechanism [56, 96, 137, 138]. For example, the Delayed Coupling Theory (DCT) of vertebrate segmentation [56], is based on this mechanism, which considers the vertebrate segmentation clock to provide the rhythm for the segmentation process [56]. In terms of the clock and wavefront mechanism the wavefront is given by a globally acting frequency profile that gradually slows down the oscillations until they arrest [56].

In Oates et. al. [98], the vertebrate segmentation clock is defined as a multiscale rhythmic pattern generator that yields the gene expression patterns at the tissue level. The underlying processes are organized in a three tier model.

The first tier describes single cell genetic oscillations. It is based on the assumption that the individual cells in the PSM contain autonomous genetic oscillators [117, 123], which are capable of sustaining their oscillations even if separated from the tissue [116]. The DCT models the patterns of cyclic gene expres-

sion on the tissue level by a system of phase oscillators. The second tier describes the local synchronization of single cell genetic oscillators. Experimental data suggests that Delta-Notch signalling allows for locally synchronized patterns on population level [99, 117], despite the dynamical noise acting upon the system [56]. This intercellular communication is non-instantaneous, due to finite signal transmission time in complex biochemical signalling pathways [32, 99–101]. In the DCT discrete delays account for these communication delays in the coupling function [56]. The third tier describes the arrest of the oscillations, when the phase of the oscillators is converted into a stable spatial pattern. Experiments have been conducted that suggest that the slowdown and arrest of the oscillations, and the gene expression patterns on the tissue level are under the control of morphogen gradients [116, 119, 139], such as Fibroblast growth factors (FGF) [140, 141] or Wnt signalling protein (Wnt) gradients [124, 142]. These build from sources at the posterior end of the PSM [140, 142]. In the DCT this is accounted for by a superimposed frequency profile, which slows down the intrinsic frequencies as the oscillators move from the posterior to the anterior end of the PSM. We omit this frequency profile in our description, and focus on the effects of distributed delays in systems of coupled phase oscillators.

Experimental evidence [32] suggests that the coupling strength is weak compared to other timescales present in the system [56]. Hence, the cyclic gene expression patterns [118] on the tissue level can be represented by a system of coupled phase oscillators, that takes into account the three tiers:

$$\dot{\theta}_k(t) = \omega_k(t) + \frac{\epsilon_k(t)}{na^2} \sum_l \sin\left[\theta_l(t - \tau_l(t)) - \theta_k(t)\right] + \zeta_k(t). \qquad (3.1)$$

This set of k equations, with $k = 1, 2, \ldots, N$, describes the time evolution of the phases $\theta_k(t)$, given by their intrinsic frequencies $\omega_k(t)$, and the coupling terms over all neighbours l; these terms evaluate the phase differences for the different connections. The phase information of oscillator l is delayed by a discrete time $\tau_l(t)$, and dynamic noise $\zeta_k(t)$ is added to the equations. The prefactor contains more system parameters, the lattice constant a, the number of neighbours n of each oscillator, and the coupling strength $\epsilon_k(t)$. This model of coupled phase oscillators with discrete delays in the coupling successfully predicts the dependence of the length of the self-organized structures (somites) on the time delays of intercellular communication. This was experimentally confirmed in [113].

3.5. Discrete delay is an approximation − is it sufficient?

Intercellular communication mediated by biochemical signalling pathways is not instantaneous [67]. Cellular processes, such as transcription, translation and molecule processing introduce time delays in this communication [56, 64]. Delays can introduce qualitatively new behaviour in systems of coupled phase oscillators [68] and cannot be neglected if they are long enough compared to other timescales of the system [31]. However, fluctuations in processes like gene expression and the transport of macromolecules introduce a variability to such delay times [67]. Discrete delays are an approximation, and a more realistic model of the delay would use distributed delays [67], to account for the variability in biochemical signalling pathways. Distributed delays consider different past times, weighted according to a delay time distribution. The delay statistics could in principle be obtained from the analysis of a stochastic model of the microscopic dynamics involved in such biochemical signalling pathways [143], or measured experimentally.

In the framework of the Delayed Coupling Theory of vertebrate segmentation [56] we ask how the approximation with discrete time delays involved in intercellular coupling compares to models with distributed delays in the coupling. There is no experimental data available that can be used to tackle this question. Hence, this work aims to conceptually understand the differences that distributed delays in the coupling introduce. We use tools from dynamical systems theory to analyze the stability of steady state solutions. Furthermore, we investigate the linearized dynamics close to the steady state for discrete and distributed delays in the coupling. For different values of the mean, the variance, and the skewness of the delay time distribution, we determine how the system reacts to small perturbations about its steady state.

4. Outline of the Thesis

In the previous chapter we briefly introduced a model based on a system of coupled phase oscillators with a discrete delay in the coupling, the Delayed Coupling Theory of vertebrate segmentation [56]. We raised the question, whether the formulation with discrete delays in the coupling of the oscillators is sufficient to capture all effects introduced by delayed communication in noisy systems.

In order to answer this question, we introduce a model of phase oscillators with distributed delays in the coupling, using the Delayed Coupling Theory of vertebrate segmentation as a basis. We give a detailed explanation of the delay formulation, and discuss different types of distributed delays.

From the viewpoint of dynamical systems, we ask how stability and linearized dynamics close to the steady states of different phase-locked solutions are affected by distributed delays in contrast to discrete delays.

In Part II of this thesis we present our results. Using the new formulation of the system of delay coupled phase oscillators with distributed delays, which we introduce and discuss in Chapter 5, we investigate phase-locked solutions in such systems. In Chapter 6 we discuss the dependence of global frequency on the mean delay, and present the results on the steady state stability of phase-locked solutions with zero phase lags. We discuss the characteristic equation and present a general result on the stability of the steady state of these solutions. Chapter 7 presents the results on the transient dynamics of the model equations in Chapter 5, as the system settles into steady state or reacts to small perturbations about its steady state. In Chapter 8 we present the results on the steady state stability of m-twist solutions in a system with distributed delays, and the relation between the mean delay and the global frequency in steady state. Chapter 9 contains first results on the transient dynamics of the model equations in Chapter 5 with distributed delays, as the system settles into m-twist steady state or reacts to small perturbations about this steady state. In Chapter 10 we present the conclusions of this work and discuss open questions.

Part II.

DISTRIBUTED DELAYS

5. Setting the Stage for Distributed Delays

5.1. Model equations with distributed delays

In this section we introduce a general model of phase oscillators that are coupled with a delay, which accounts for the entire past of the neighbour:

$$\dot{\theta}_k(t) = \omega_k + \frac{K}{n_k} \sum_{l=1}^{N} d_{kl}\, h\left(-\theta_k(t) - \beta + \int_0^\infty ds\, g(s)\theta_l(t-s)\right), \qquad (5.1)$$

where $\theta_k(t)$, with $k = 1,2,\ldots,N$, corresponds to the phases of the individual oscillators at time t, N denotes the number of oscillators in the system, n_k is the number of connections that oscillator k has to other oscillators in the system, K is the coupling strength that couples an oscillator to its neighbours, h is a 2π-periodic coupling function, β is a phase frustration parameter, $g(s)$ denotes the delay distribution and ω_k the intrinsic frequency of oscillator k. The d_{kl} are either one, if oscillator k is connected to oscillator l, or zero, if not. This is how the connection topology of the system is formulated and we define the connectivity matrix $\mathbb{D}$, whose components are the coefficients d_{kl}, and which contains the information about all connections between the oscillators in the system. The phase frustration parameter β introduces a constant phase shift in the evaluation of the phase differences in the coupling function h. This can lead to repulsive coupling, e.g., for $\beta = \pi$ with a sinusoidal coupling function. The effects of phase frustration are being investigated in a separate work. Here, we focus on the effects of distributed delays in the coupling, setting $\beta = 0$ for the remainder of the thesis.

This formulation of Eqs. (5.1) encompasses a large class of systems. One example is the original Kuramoto model [1], which is recovered for a sinusoidal coupling function $h(\theta) = \sin(\theta)$, with zero delay $g(s) = \delta(0)$, $\beta = 0$, mean field coupling $d_{kl} = 1 \; \forall \, k,l$ and $n_k = N \; \forall \, k$. Another example is the Delayed Coupling

Theory of vertebrate segmentation [56]. It is recovered for a Dirac delta delay distribution $g(s) = \delta(s - \tau)$, sinusoidal coupling function, zero phase frustration parameter $\beta = 0$, time dependent intrinsic frequencies $\omega_k(t)$, and nearest neighbour coupling topology, see Eqs. (3.1).

The delay distribution $g(s)$ can be any probability density function defined for non-negative delay times. It can be characterized by the mean delay τ, defined as:

$$\tau = \int_0^\infty ds\, g(s)s, \tag{5.2}$$

and higher central moments [144], for example the variance σ^2 and skewness γ:

$$\sigma^2 = \int_0^\infty ds\, g(s)(s - \tau)^2, \tag{5.3}$$

$$\gamma = \frac{1}{\sigma^3} \int_0^\infty ds\, g(s)(s - \tau)^3. \tag{5.4}$$

To characterize the effects of distributed delays we compare to the case of discrete delays in the coupling. Discrete delays can be recovered by a shifted Dirac delta delay distribution $g(s) = \delta(s - \tau)$, where τ is the value of the discrete delays.

5.2. How we include distributed delays

In this study the distributed delays are given by an integral over all past times [67] of the phase history of the oscillator l:

$$\tilde{\theta}_l(t) \equiv \int_0^\infty ds\, g(s)\theta_l(t - s), \tag{5.5}$$

where the different past times are weighted by a probability density $g(s)$. The value of the delayed phase $\tilde{\theta}_l(t)$ represents a condensed information about the past phases of oscillator l. The delay integral appears inside the coupling function h in the phase evolution Eqs. (5.1).

In intercellular communication processes, biochemical signalling pathways play an important role [130]. They consist of many molecular processes such as transcription, translation and molecule trafficking [145]. Completion times of these processes are stochastic [146]. The resulting fluctuations can be described by delay distributions $g(s)$ that govern the statistics [147] of the underlying stochastic process.

In general, the formulation of distributed delays, as shown in Eq. (5.5) and throughout this study, describes systems in which the phase information that is
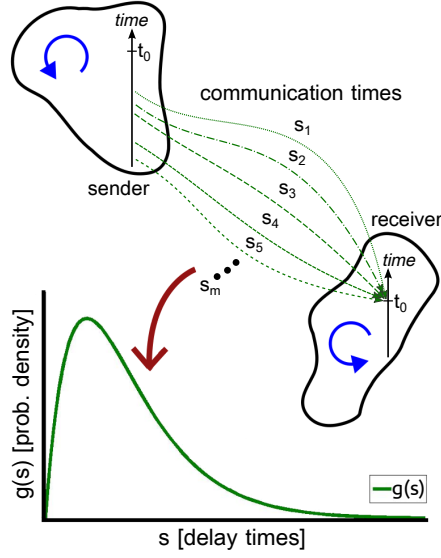
Figure 5.1.: When many individual coupling processes with delay times s_m occur in parallel, the overall communication process can be described using the probability distribution of the delay times.

evaluated by the coupling function consists of many individual signalling events in parallel. We consider signals, originated at different past times, that reach the receiver in an infinitesimal time window, see Fig. 5.1. Together these signalling events yield the delayed phase information of the sender. Statistics on the waiting times for completing an individual signalling event are encoded by the delay distribution. It provides the information of how likely it is to receive a signalling event of a specific past time. We assume the delay is homogeneous throughout the system of oscillators, i.e., the delay time statistics encoded by $g(s)$ are identical for each connection. Coupled systems that communicate their states in this way can be described by the formulation of distributed delays with the integral inside the coupling function. This formulation of distributed delays is also used in neural networks, e.g. [88, 148, 149], where neurons have a multitude of parallel connections [87] that introduce a distribution of propagation delays for incoming signals.

Alternative representations of distributed delays could have the integral outside the coupling function h:

$$\dot{\theta}_k(t) = \omega_k + \frac{K}{n_k} \sum_{l=1}^{N} d_{kl} \int_0^\infty ds\, g(s)\, h\left(\theta_l(t-s) - \theta_k(t)\right). \qquad (5.6)$$

This corresponds to individually evaluated signalling events. These individual events are summed and weighted after the evaluation of the event by the coupling function. We do not employ this model of distributed delays here, because we do not consider individually evaluated signalling events.

Systems that use heterogeneous interaction delays [82, 83] take into account link-dependent interaction time delays [23, 26]:

$$\dot{\theta}_k(t) = \omega_k + \frac{K}{N} \sum_{l=1}^{N} h\left(\theta_l(t - \tau_{kl}) - \theta_k(t)\right), \tag{5.7}$$

where discrete, time-independent delays τ_{kl} inherent to the connections between the oscillators, are drawn of a distribution for each connection individually. Such a description is different than the one considered in this work [compare Eqs. (5.1)], because the distribution governing the different connection delays τ_{kl}, accounts for the variability in delay times between different connections kl, rather than the variable delay times possible within a connection.

5.3. Summary

In this chapter we introduced the model Eqs. (5.1) for a system of identical phase oscillators that are coupled according to one, so far, unspecified coupling topology. The coupling function includes a delay term, see Eq. (5.5), accounting for non-instantaneous signal transduction and considering past states of the coupling partner. This delay term returns an effective phase information of the phase history of the coupling partner, consisting of weighted influences from different past times. The weight with which these delay times enter the effective phase information is given by a distribution which encodes the probability of their occurrence. Therefore we call this term distributed delays. Note however, that Eqs. (5.1) are entirely deterministic.

This formulation of distributed delays is motivated by situations where many individual signalling events reach the receiver in an infinitesimal time window, each of them having originated at some delayed time in the past with a probability given by the delay distribution, see Fig. 5.1.

6. The Phase-Locked Steady State Solution

We introduced the phase-locked solution with no phase lags in Subsection 2.2.1. In steady state it is characterized by a global frequency Ω, with which all oscillators evolve in time, and a common phase shared by all oscillators in the system. This solution is a special case of the phase-locked solution with phase lags, denoted by m-twist or splay state solution, with phase lags equal to zero ($m = 0$) between all oscillators.

6.1. Global frequency of phase-locked steady states

Here we make an analogy to the phase-locked steady state in a system with discrete delay in the coupling was introduced in Subsection 2.2.1, in order to obtain a similar relation for the case of distributed delays in the coupling in Eqs. (5.1). The ansatz for the phase-locked solution is:

$$\theta_k(t) = \Omega t. \tag{6.1}$$

This denotes linear growth of the phases with the global frequency Ω. We substitute this ansatz into Eqs. (5.1) with $\omega_k = \omega \ \forall \ k$, implying identical oscillators, in order to obtain the solution for Ω by a self-consistent approach [68, 69]:

$$\Omega = \omega + \frac{K}{n_k} \sum_{l=1}^{N} d_{kl}\, h\left(-\Omega t + \Omega t \int_0^\infty ds\, g(s) - \Omega \int_0^\infty ds\, g(s)s\right). \tag{6.2}$$

Since the delay distribution $g(s)$ is normalized, the left integral in the coupling function yields 1. The right integral denotes the first moment of $g(s)$ which we defined in Eq. (5.2) and which yields after substituting:

$$\Omega = \omega + K\, h(-\Omega\tau)\, \frac{1}{n_k} \sum_{l=1}^{N} d_{kl}. \tag{6.3}$$

41

The sum of entries l in the kth row of the connectivity matrix is given by n_k $\forall\, k$:

$$\frac{1}{n_k} \sum_{l=1}^{N} d_{kl} = 1 \quad \forall\, k. \tag{6.4}$$

This leads to an implicit expression for Ω in the case of distributed delays:

$$\Omega = \omega + K h(-\Omega \tau). \tag{6.5}$$

Note that Eq. (6.5) only depends on the mean delay, and not on the particular shape of the delay distribution $g(s)$. It is also independent from the number of oscillators in the system or the number of neighbours of each of them.

The global frequency Ω in the phase-locked steady state, where all oscillators have synchronized to a common phase and global frequency, only depends on the mean of the delay distribution. No higher moments, that characterize the shape or symmetry of the distribution, are involved. Hence, the functional dependence of the global frequency in steady state is identical for distributed and discrete delays, if their mean value is chosen to be the same. The according plots to Eq. (6.5) are given in Subsection 2.2.1 in Figs. 2.2 and 2.3.

6.2. Linear stability of the steady state

In general the linear stability of a solution to a dynamical system, e.g. Eqs. (5.1), can be determined by linear stability analysis [19]. We ask how the synchronized system in steady state responds to small perturbations. This is studied for linearized dynamics and only valid close to the steady state. For unstable steady states, the perturbation will grow because the system is not attracted back to the steady state, whereas the perturbation will converge to zero eventually when the steady state is stable. In cases where linear stability analysis is not sufficient to decide whether a steady state is stable or not, higher order terms have to be taken into account [19]. Following this idea and assuming identical oscillators, $\omega_k = \omega$ $\forall\, k$ for the remainder of the thesis, we add a perturbation $q_k(t)$ to the phase-locked solution:

$$\theta_k(t) = \Omega t + \epsilon q_k(t), \tag{6.6}$$

with $\epsilon \ll 1$ and substitute this into Eqs. (5.1), which yields:

$$\Omega + \epsilon \dot{q}_k(t) = \omega + \frac{K}{n_k} \sum_{l=1}^{N} d_{kl} h\left(-\Omega \tau + \epsilon\left[-q_k(t) + \int_0^\infty ds\, g(s) q_l(t-s)\right]\right), \tag{6.7}$$

where τ is the mean of the delay distribution as defined in Eq. (5.2). Taylor expansion for $\epsilon \ll 1$ leads to:

$$\Omega + \epsilon \dot{q}_k(t) = \omega$$
$$+ \frac{K}{n_k} \sum_{l=1}^{N} d_{kl} \left(h(-\Omega\tau) + \epsilon h'(-\Omega\tau) \left[-q_k(t) + \int_0^\infty ds\, g(s) q_l(t-s) \right] \right) + O(\epsilon^2), \quad (6.8)$$

with h' being the first derivative of h with respect to its argument. Eq. (6.8) can be separated in powers of ϵ to yield the equation for the global frequency in zeroth order:

$$\Omega = \omega + K h(-\Omega\tau), \qquad (6.9)$$

and the linear dynamic equations for the evolution of the perturbation in first order:

$$\dot{q}_k(t) = \frac{\alpha}{n_k} \sum_{l=1}^{N} d_{kl} \left[-q_k(t) + \int_0^\infty ds\, g(s) q_l(t-s) \right], \qquad (6.10)$$

where:

$$\alpha \equiv K h'(-\Omega\tau). \qquad (6.11)$$

We are interested in whether the perturbation grows or decays as the system evolves. For general linear dynamical systems the solutions are linear combinations of exponentials [150, 151]. Hence, for the functional form of the perturbation we introduce the ansatz:

$$q_k(t) = c_k e^{\lambda t}. \qquad (6.12)$$

The terms c_k are the components of the perturbation mode associated to the solutions $\lambda \in \mathbb{C}$. These λ are obtained by substituting Eq. (6.12) into (6.10), for which the result is shown in the next section.

6.3. Linear dynamics of the perturbation − the characteristic equation

The characteristic equation describes the linear dynamics of the perturbation. It can be derived from Eqs. (6.10) and (6.12). Substituting the description of the perturbation into the dynamic equations yields:

$$c_k \lambda e^{\lambda t} = \frac{\alpha}{n_k} \sum_{l=1}^{N} d_{kl} e^{\lambda t} \left[-c_k + c_l \int_0^\infty ds\, g(s) e^{-\lambda s} \right]. \qquad (6.13)$$

The integral in Eq. (6.13) represents the Laplace transform $\hat{g}(\lambda)$ of the delay distribution [152, 153]:

$$\hat{g}(\lambda) = \int_0^\infty ds\, g(s) e^{-\lambda s}. \tag{6.14}$$

Simplified, this set of equations reads:

$$c_k \lambda = \frac{\alpha}{n_k} \sum_{l=1}^N d_{kl} [c_l \hat{g}(\lambda) - c_k]. \tag{6.15}$$

In order to find an expression for the λ for arbitrary delay distributions that fulfil the normalization condition:

$$\int_0^\infty ds\, g(s) = 1, \tag{6.16}$$

Eq. (6.15) is rearranged in order to obtain:

$$(\lambda + \alpha)c_k = \frac{\alpha \hat{g}(\lambda)}{n_k} \sum_{l=1}^N d_{kl}\, c_l, \tag{6.17}$$

which under the condition

$$\alpha \neq 0 \tag{6.18}$$

can be further rearranged to yield:

$$\frac{n_k}{\hat{g}(\lambda)} \left(\frac{\lambda}{\alpha} + 1 \right) c_k = \sum_{l=1}^N d_{kl}\, c_l. \tag{6.19}$$

Additionally only values of λ that ensure $\hat{g}(\lambda) \neq 0$ are allowed, otherwise physically not meaningful singularities can arise. If not stated otherwise, the number of connections of each oscillator is set to $n_k = n \; \forall \, k$ for the remainder of this work, meaning that each oscillator in the system has the same number of connections n:

$$\frac{n}{\hat{g}(\lambda)} \left(\frac{\lambda}{\alpha} + 1 \right) c_k = \sum_{l=1}^N d_{kl}\, c_l. \tag{6.20}$$

We use the last two Eqs. (6.20) and (6.18) to determine the λ. The sign of the real part of λ determines the stability of the corresponding solution. In case of a negative real part, $\text{Re}(\lambda) < 0$, the perturbation decays exponentially and the solution is called stable, whereas for positive real part, $\text{Re}(\lambda) > 0$, the perturbation grows exponentially and is therefore called unstable [154]. A real part of λ equal to zero corresponds to neutral stability and linearized dynamics are not sufficient

to determine stability [19]. The value of the real part of λ contains the information on how fast the associated perturbation modes decay or grow, depending on the sign. Because λ can be a complex number the growth or decay of the perturbation can be oscillatory. The imaginary part of λ denotes the frequency of oscillation of the perturbation growth or decay dynamics.

Stability of phase-locked solutions

We look at Eq. (6.20) which can be rewritten in matrix notation:

$$\frac{n}{\hat{g}(\lambda)}\left(\frac{\lambda}{\alpha}+1\right)\vec{c} = \mathbb{D}\vec{c}, \tag{6.21}$$

with $\vec{c}$ being the vectors defined by the components of the perturbation c_k. We define:

$$\zeta \equiv \frac{n}{\hat{g}(\lambda)}\left(\frac{\lambda}{\alpha}+1\right), \tag{6.22}$$

and substitute into Eq. (6.21):

$$\zeta\vec{c} = \mathbb{D}\vec{c}. \tag{6.23}$$

This eigenvalue problem is solved for the matrix $\mathbb{D}$ that contains the connection topology of the system of coupled phase oscillators given by Eqs. (5.1).

Earl and Strogatz [155] outline how to proceed to find a stability condition for a class of connection topologies that will be defined below. The result holds for phase-locked solutions in a system of phase oscillators coupled with discrete delays. This corresponds to $g(s) = \delta(s-\tau)$ in the notation of Eqs. (5.1). We extend this result for arbitrary delay distributions $g(s)$. In order to prove the stability condition for such cases, we need a few prerequisites that will be given in the following paragraphs.

Gerschgorin's circle theorem [156–158], also see Appendix A.4, is used to find an upper bound on the modulus of the eigenvalues of a square matrix. The matrix elements can be complex. So called Gerschgorin disks are defined by their center and radius in the complex plane. The center of each of the N Gerschgorin disks associated to a $N \times N$ matrix, is given by the lth diagonal entry for $l = 1, 2, \ldots, N$. The radius of the Gerschgorin disks is calculated as the sum over the absolute value of each element of the lth row, with the diagonal entry excluded [156]. Gerschgorin's circle theorem states that the eigenvalues of such matrices all lie within the Gerschgorin disks. This means that if the diagonal
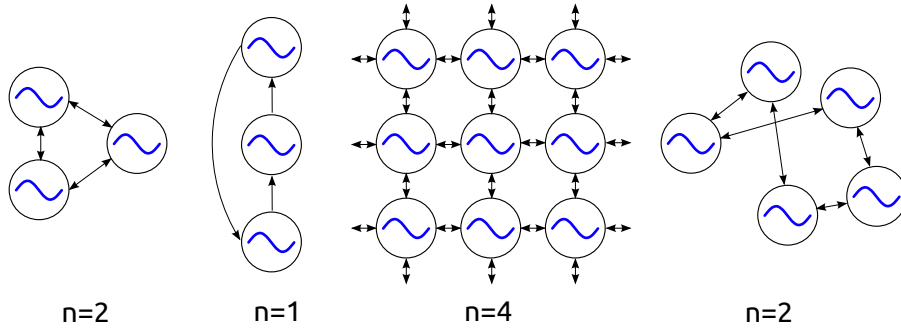
Figure 6.1.: These are examples of the class of connection topologies for which the following result 6.3 on steady state stability holds. Left to right: all-to-all connected system, ring topology with unidirectional connections, square lattice, and randomly connected system. All these systems have in common, that each oscillator has the same number of connections to other oscillators.

entries of the matrix are all zero, all Gerschgorin disks are centered at the origin, and the one that has the largest radius provides an upper bound on the magnitudes of the eigenvalues.

We derive the stability condition for a class of coupling topologies characterized by the properties that each oscillator has the same number of connections n to other oscillators, but is not coupled to itself. Hence, all Gerschgorin disks are centered at the origin. Some examples of coupling topologies are shown in Fig. 6.1. We exclude self coupling of the oscillators in this section to make use of Gerschgorin's circle theorem to find an upper bound on the modulus of the eigenvalues. For the connectivity matrix $\mathbb{D}$ in Eq. (6.23), this implies that all Gerschgorin disks are centered at the origin, since all diagonal entries are zero. All radii are of equal length, since each oscillator couples to the same number of oscillators in the system. Note that in Section 7.3 of this thesis, cases with self coupling will be investigated without using Gerschgorin's theorem.

Using Gerschgorin's theorem, an upper bound on the modulus of the eigenvalues ζ is given by the number n of connections each oscillator has:

$$|\zeta| \leq \sum_{l \neq k} |d_{kl}| = n, \tag{6.24}$$

and we conclude:

$$\frac{|\zeta|}{n} \leq 1. \tag{6.25}$$

This upper bound on the eigenvalues ζ of the connectivity matrix will be used when we analyze Eq. (6.22).

The absolute value of the Laplace transform $|\hat{g}(\lambda)|$ is also bounded. With $\lambda = x + iy$, where $x > 0$ and for normalized delay distributions $g(s)$ one finds:

$$|\hat{g}(\lambda)| = \left| \int_0^\infty ds\, g(s)\, e^{-(x+iy)s} \right| \leq \int_0^\infty ds\, g(s)\, \left| e^{-(x+iy)s} \right|, \qquad (6.26)$$

where we made use of the triangle inequality, and $|g(s)| = g(s)$ since $g(s) \geq 0 \ \forall \ s$. Taking into account that for the phase related term $\left| e^{iys} \right| = 1$ holds and:

$$\left| e^{-xs} \right| \in [0, 1] \ \ \forall \ x \geq 0,$$

we obtain:

$$
\begin{aligned}
|\hat{g}(\lambda)| &= \left| \int_0^\infty ds\, g(s)\, e^{-(x+iy)s} \right| \leq \int_0^\infty ds\, g(s)\, \left| e^{-(x+iy)s} \right| \\
&= \int_0^\infty ds\, g(s)\, \underbrace{\left| e^{-xs} \right|}_{\forall\, x \geq 0 \in [0,1]}\, \underbrace{\left| e^{iys} \right|}_{1} \leq 1.
\end{aligned}
\qquad (6.27)
$$

Whereas $\hat{g}(\lambda)$, ζ and λ can be complex, we define:

$$\hat{g}(\lambda) \equiv |\hat{g}(\lambda)|\, e^{i\psi}, \qquad (6.28)$$

$$\zeta \equiv |\zeta|\, e^{i\xi}, \qquad (6.29)$$

where ψ and ξ are angular coordinates in the complex plane. Rewriting Eq. (6.22) using this notation, we obtain:

$$\alpha\, |\hat{g}(\lambda)|\, e^{i\psi}\, \frac{|\zeta|}{n}\, e^{i\xi} = (x + iy + \alpha), \qquad (6.30)$$

which can be divided into real and imaginary parts:

$$\alpha\, |\hat{g}(\lambda)|\, \frac{|\zeta|}{n}\, \cos(\psi + \xi) = x + \alpha, \qquad (6.31)$$

$$\alpha\, |\hat{g}(\lambda)|\, \frac{|\zeta|}{n}\, \sin(\psi + \xi) = y. \qquad (6.32)$$

Squaring both equations and adding them yields:

$$\alpha^2\, |\hat{g}(\lambda)|^2 \left(\frac{|\zeta|}{n} \right)^2 = (x + \alpha)^2 + y^2. \qquad (6.33)$$

Theorem on linear stability of phase-locked solutions

These are the equations and bounds we need to prove the result on steady state stability for the phase-locked solutions of coupled phase oscillators, given that there is no self coupling and each oscillator has the same number of connections, as defined in the previous paragraph. We state the theorem on linear stability:

Proposition: For all λ that satisfy Eq. (6.22), $x = \mathrm{Re}(\lambda) < 0$ holds if and only if
$$\alpha \equiv K h'(-\Omega\tau) > 0.$$

Proof: ($\Leftarrow$) *by contradiction*: Suppose there exists an $\alpha > 0$ such that
$$x = \mathrm{Re}(\lambda) \geq 0$$

The contradiction can be seen by looking at Eq. (6.33) after division of both sides of the equation by α^2, which implies:

$$|\hat{g}(\lambda)|^2 \left(\frac{|\zeta|}{n}\right)^2 = 1 + \frac{(x^2 + y^2 + 2|\alpha||x|)}{\alpha^2}. \tag{6.34}$$

Since $(|\zeta|/n)^2 \leq 1$ as shown in Eq. (6.25) and $|\hat{g}(\lambda)| \leq 1 \ \forall \ x \geq 0$ as shown in Eq. (6.27), the product on the left hand side of the above equation is smaller or equal than 1. The case of equality to 1 implies $x = y = 0$, i.e. $\lambda = x + iy = 0$. This corresponds to the eigenvector $(1, 1, \ldots, 1)^T$, which reflects the rotational symmetry of the system. The system is neutrally stable under such a perturbation. For all $\lambda \neq 0$, the right hand side of the equation will always be greater than 1. This poses a contradiction and it follows that for $\alpha > 0$ there are no solutions with $\mathrm{Re}(\lambda) > 0$. This means from $\alpha > 0$ linear stability can always be deduced.

($\Rightarrow$) *contrapositive*: if $\alpha < 0$, suppose there exists at least one $x = \mathrm{Re}(\lambda) \geq 0$

Here Eq. (6.31), with $\alpha = -|\alpha| < 0$, is analyzed and yields:

$$-|\alpha||\hat{g}(\lambda)|\frac{|\zeta|}{n} cos(\psi + \xi) = x - |\alpha|. \tag{6.35}$$

A case differentiation for the cosine term is necessary to cover all possible signs of the left hand side. For the case of $\cos(\psi + \xi) \leq 0$ we have $\cos(\psi + \xi) = -\big|\cos(\psi + \xi)\big|$. Rearranging the equation to find x yields:

$$x = |\alpha|\left(1 + |\hat{g}(\lambda)|\frac{|\zeta|}{n}\big|\cos(\psi + \xi)\big|\right), \tag{6.36}$$

and we see that $x = \text{Re}(\lambda) > 0$. The other case with $\cos(\psi + \xi) > 0$:

$$x - |\alpha| = -|\alpha||\hat{g}(\lambda)|\frac{|\zeta|}{n}\left|\cos(\psi + \xi)\right|, \tag{6.37}$$

can be understood by plotting both sides of Eq. (6.35), as demonstrated in Fig. 6.2, where the left hand side is plotted in red, and the right hand side in blue. In the limit of x approaching infinity we have: $x \to +\infty \Rightarrow |\hat{g}(\lambda)| \to 0$, whereas for the case of x approaching minus infinity: $x \to -\infty \Rightarrow |\hat{g}(\lambda)| \to \infty$ holds, see Eq. (6.27). For $x = 0$ we find for 1-normalized delay distributions:

$$|\hat{g}(\lambda)| = \left|\int_0^\infty ds\, g(s) e^{-iys}\right| \leq \int_0^\infty ds\, g(s) \underbrace{\left|e^{-iys}\right|}_{=1} = 1, \tag{6.38}$$

and the right hand side of Eq. (6.37) can not be smaller than $-|\alpha|$. Hence it can be seen that for $\alpha < 0$ there always exists a solution $x \geq 0$, and hence the system is linearly unstable.

This result shows, that the linear stability of the phase-locked steady state for systems of coupled phase oscillators with identical intrinsic frequencies and with distributed delays in the coupling, only depends on the mean τ of the delay dis-
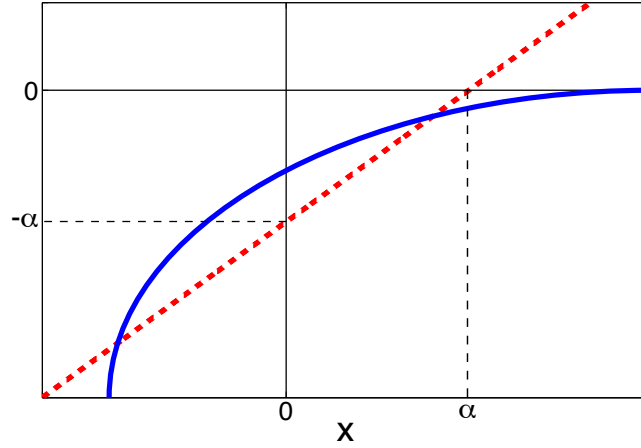
Figure 6.2.: The left and right hand side of Eq. (6.37) plotted as a function of x in red (dashed) and blue (solid), respectively. The red dashed curve always crosses the the y-axis at $y = -|\alpha|$ and the blues solid curve always crosses in the interval $[-|\alpha|, 0)$. Since the blue curve approaches zero for $x \to \infty$, but crosses the y-axis at values $\geq -|\alpha|$, there must always be an intersection of the two curves for $x \geq 0$, and hence a solution to Eq. (6.37).

tribution:

$$Kh'(-\Omega\tau) > 0 \quad \Leftrightarrow \quad \mathrm{Re}(\lambda) < 0. \tag{6.39}$$

Higher moments, such as the variance or the skewness do not affect linear stability.

6.4. Summary and application to the Delayed Coupling Theory

We have shown that the linear stability and the global frequency of the phase-locked steady state with no phase lags is not altered by introducing delay distributions, with variance greater than zero and a mean equal to the discrete delay. In other words, the shape of the delay distribution does not affect the phase-locked steady state with no phase lags which only depends on the mean delay. Hence, we have extended the steady state stability condition for phase-locked solutions with no phase lags in systems of coupled phase oscillators with discrete delays obtained by Earl and Strogatz [155].

We conclude that in systems of coupled phase oscillators that obey the assumptions we made on the coupling topology, the utilisation of discrete delays are a valid approximation to describe the steady state, if the discrete delay equals the mean of the delay distribution. An example is the Delayed Coupling Theory of vertebrate segmentation [56], introduced in Section 3.4. In this model discrete delays are used to account for finite communication in the coupling of phase oscillators, and the dependence of the length of somites on the value of the time delay is predicted.

However, transient dynamics close to steady state might depend on the delay distribution. The nonlinear equation that relates the eigenvalues ζ of the connectivity matrix with the dependence on the Laplace transform of the delay distribution:

$$\zeta_j \equiv \frac{n}{\hat{g}(\lambda_j)} \left(\frac{\lambda_j}{\alpha} + 1 \right) \quad \text{with } j = 1, 2, \ldots, N, \tag{6.40}$$

suggests that for different $\hat{g}(\lambda)$ the real and imaginary parts of λ change, while the sign of the real part is independent of $\hat{g}(\lambda)$. We therefore hypothesize, that perturbation modes can decay or grow with different rates for delay distributions with different variance and skewness. However, for any given set of solutions λ, we know that the first λ whose real part becomes greater than zero always

crosses the imaginary axis for the same mean delay τ, independent of the delay formulation.

For example the gamma distribution, see Appendix A.2:

$$g_\Gamma(s; a, b) = s^{a-1} \frac{e^{-\frac{s}{b}}}{b^a \Gamma(a)}, \qquad (6.41)$$

with shape parameter a and scale parameter b, has a mean given by $\tau = a\,b$. The Laplace transform reads:

$$\hat{g}_\Gamma(\lambda) = (1 + b\lambda)^{-a}. \qquad (6.42)$$

Substituted into Eq. (6.40) this yields:

$$\frac{\zeta_j}{n} \equiv \left(1 + b\lambda_j\right)^a \left(\frac{\lambda_j}{\alpha} + 1\right). \qquad (6.43)$$

The shape parameter a of the delay distribution determines the order of the polynomial that has to be solved, and therefore the number of solutions λ. The linear dynamics close to the steady state will be discussed in detail in the next chapter. Later we will propose how this transient dynamics could be observed experimentally in zebrafish embryonic cells.

7. Dynamics Close to the Phase-Locked Steady State

In the last chapter we have shown that the stability of the phase-locked steady states, in systems with equal connectivity degree for each oscillator, only depends on the first moment of the delay distribution, but not on its shape.

We now address the question of whether linearized dynamics close to the steady state of the system are also independent of the shape of the delay distribution. To analyze the dynamics, a small perturbation is added to the steady state solution. This pushes the system slightly off the steady state; linearized dynamic equations can be used to analyze the response to such a perturbation. The synchronization order parameter $r(t)$, as defined in Eq. (1.3), is used to quantify the perturbation to the steady state and the perturbation decay rate when relaxing back to steady state.

7.1. The response to small perturbations

The response of a dynamical system subjected to a small perturbation about its steady state can be investigated by looking at the linearized dynamics [19, 154], given here by Eq. (6.10). The steady state stability of the phase-locked solution in the previous chapter was determined by the sign of $\text{Re}(\lambda)$ of the perturbation Eq. (6.12). Similarly we determine how the perturbation modes in the system decay or grow. This is given by the real and imaginary parts of λ.

The inverse of the real part of λ is the characteristic timescale of the decay or growth of the associated perturbation mode [19]. This means for stable solutions, that the largest $\text{Re}(\lambda) < 0$ describes the decay rate of the slowest relaxation mode in the system, before the steady state is reached. Sufficiently close to the steady state this perturbation mode is the only one that can be observed, because all others will have already decayed. In the case that $\text{Im}(\lambda) \neq 0$ the decay of the

associated perturbation mode takes place in an oscillatory manner [19], with the frequency given by the imaginary part $y = \text{Im}(\lambda)$.

In order to determine the resynchronization properties and decay rates, the characteristic Eq. (6.21) has to be solved for the connectivity topology of the given system. In the present chapter the mean field and the nearest neighbour coupling topologies are treated. Those were introduced in Section 1.5.

7.2. Relation between order parameter and perturbation modes

Since the measure of the system's synchrony is given by the order parameter $r(t)$, introduced in Section 1.4, but the perturbation decays with rates given by $x = \text{Re}(\lambda)$, and frequency $y = \text{Im}(\lambda)$, a relation between the two measures has to be derived. This will be used to compare analytic solutions obtained for λ to time series of the order parameter measured in simulation. We use Eq. (6.6):

$$\theta_k(t) = \Omega t + \epsilon q_k(t),$$

for the perturbed phase-locked solution with no phase lags. It describes the time evolution of the phases of the oscillators, when subject to a small perturbation $\epsilon q_k(t)$. Substituting this into Eq. (1.3):

$$r(t)e^{i\Xi(t)} \equiv \frac{1}{N} \sum_{k=1}^{N} e^{i\theta_k(t)},$$

for the synchronization order parameter $r(t)$ yields:

$$r(t)e^{i\Xi(t)} = \frac{1}{N} \sum_{k=1}^{N} e^{i(\Omega t + \epsilon q_k(t))}, \tag{7.1}$$

that means:

$$r(t)e^{i(\Xi(t)-\Omega t)} = \frac{1}{N} \sum_{k=1}^{N} e^{i\epsilon q_k(t)}. \tag{7.2}$$

We seek the modulus of the order parameter, $r(t)$. Squaring both sides eliminates the phases:

$$r(t)^2 = \frac{1}{N^2} \left\{ \left(\sum_{k=1}^{N} \cos(\epsilon q_k(t)) \right)^2 + \left(\sum_{k=1}^{N} \sin(\epsilon q_k(t)) \right)^2 \right\}, \tag{7.3}$$

and since $\epsilon \ll 1$, we can expand the sine and cosine terms to first order in ϵ. Then we evaluate the squares:

$$r(t)^2 = \frac{1}{N^2}\left\{N^2 - N\epsilon^2\sum_{k=1}^{N}q_k^2(t) + \frac{\epsilon^4}{4}\left(\sum_{k=1}^{N}q_k^2(t)\right)^2 + \epsilon^2\left(\sum_{k=1}^{N}q_k(t)\right)^2\right\}. \qquad (7.4)$$

Dropping all orders of ϵ greater than 2 yields:

$$r(t)^2 = 1 - \frac{\epsilon^2}{N}\sum_{k=1}^{N}q_k^2(t) + \frac{\epsilon^2}{N^2}\left(\sum_{k=1}^{N}q_k(t)\right)^2 + O(\epsilon^3). \qquad (7.5)$$

The functional form of the perturbation is given by:

$$\epsilon q_k(t) = \frac{1}{2}\left(c_k e^{\lambda t} + c.c.\right) = e^{xt}\left(c_k^{Re}\cos(yt) - c_k^{Im}\sin(yt)\right), \qquad (7.6)$$

where $c.c.$ denotes the complex conjugate, $\lambda = x + iy$ and $c_k = c_k^{Re} + i\,c_k^{Im}$. The c_k are the components of the eigenvector of the characteristic equation.

In this chapter we assume the components of the eigenvectors to be purely real and set $c_k^{Im} = 0$:

$$\epsilon q_k(t) = e^{xt}c_k\cos(yt), \qquad (7.7)$$

which is true for the mean field coupling case, and as well for nearest neighbour interaction in a system of $N = 2$ oscillators; both cases will be treated in the next sections. However, note that in nearest neighbour coupled systems with $N \geq 3$, this relation has to be derived accounting for complex eigenvector components. This will be explained in more detail in Section 7.4.

The functional form of the perturbation as given in Eq. (7.7) is substituted into Eq. (7.5):

$$r(t)^2 = 1 - \cos^2(yt)e^{2xt}\underbrace{\left(\frac{1}{N}\sum_{k=1}^{N}c_k^2 + \frac{1}{N^2}\left\{\sum_{k=1}^{N}c_k\right\}^2\right)}_{\equiv \overline{w}}. \qquad (7.8)$$

The last term in Eq. (7.8), defined as $\overline{w}$, contains sums over the components of the eigenvectors associated to the perturbation modes. These amplitudes of perturbation are all small by definition:

$$r(t) = \left[1 - \cos^2(yt)e^{2xt}\overline{w}\right]^{\frac{1}{2}} \approx 1 - \frac{1}{2}\cos^2(yt)e^{2xt}\overline{w}. \qquad (7.9)$$

With this expression we have derived the desired relation between order parameter $r(t)$ and the solutions λ. Whereas we use plots where $\log[1 - r(t)]$ is plotted versus t, e.g. in Fig. 7.5, the expression is rearranged to yield:

$$\log[1 - r(t)] = 2xt + \log\left[\cos^2(yt)\right] + \log\left[\frac{1}{2}\overline{w}\right], \qquad (7.10)$$

with the $\overline{w}$-term depending on the initial setup of the perturbation.

7.3. Perturbation dynamics in mean-field coupled systems

In this section we investigate the resynchronization dynamics of a system of coupled phase oscillators with delays for the case of "all to all" coupling. In this case, we will show that dynamics close to the steady state are equivalent in systems with discrete and distributed delays. The latter delay type is realized with a gamma distribution delay kernel.

The resynchronization properties, given by the real and imaginary part of λ, can be obtained by solving Eq. (6.21). We do this in two steps; first calculating the eigenvalues ζ of the connectivity matrix $\mathbb{D}$:

$$\zeta \vec{c} = \mathbb{D}\vec{c}, \tag{7.11}$$

and in the second step we determine the solutions λ of the characteristic equation for the Laplace transform $\hat{g}(\lambda)$ of the given delay distribution:

$$\zeta = \frac{n}{\hat{g}(\lambda)}\left(\frac{\lambda}{\alpha} + 1\right). \tag{7.12}$$

With this procedure one first takes into account the connectivity in the system, and then considers the influence of the delay distribution. At the end it has to be checked whether the solutions λ fulfil the conditions:

$$\begin{aligned}
\hat{g}(\lambda) &\neq 0 \quad \forall\ \lambda, \\
\alpha &\neq\quad 0,
\end{aligned} \tag{7.13}$$

obtained during the derivation of the characteristic equation, see Eqs. (6.17-6.18). Hence, only values of λ that ensure $\hat{g}(\lambda) \neq 0$ are allowed, otherwise physically not meaningful singularities can arise.

The $N \times N$ connectivity matrix in the case of mean field coupling is given by:

$$\mathbb{D}_{MF} = \begin{pmatrix} 1 & 1 & \dots & 1 \\ 1 & 1 & \dots & 1 \\ \vdots & \vdots & \ddots & \vdots \\ 1 & 1 & \dots & 1 \end{pmatrix}, \tag{7.14}$$

for which the corresponding eigenvalues ζ are given by:

$$\zeta_1 \;=\; 0 \;\; \text{with multiplicity } N-1 \tag{7.15}$$

$$\zeta_2 \;=\; N \;\; \text{with multiplicity } 1. \tag{7.16}$$

Note that the constraint of no self-coupling was only considered for the results in the last chapter, but does not apply for the calculation carried out here. The eigenvalues ζ_j, $j = 1,2$ of $\mathbb{D}$ are substituted into Eq. (7.11):

$$\zeta_j c_k = \sum_{l=1}^{N} c_l, \tag{7.17}$$

in order to obtain conditions for the corresponding eigenvectors:

$$\zeta_1 : \qquad 0 \;=\; \sum_{l=1}^{N} c_l, \tag{7.18}$$

$$\zeta_2 : \qquad N c_k \;=\; \sum_{l=1}^{N} c_l. \tag{7.19}$$

Eq. (7.18) states that the sum over the components c_l, of the $N-1$ eigenvectors corresponding to the eigenvalue $\zeta_1 = 0$, with multiplicity $N-1$, must add up to zero. The other Eq. (7.19) holds for the single eigenvector, related to $\zeta_2 = N$ with multiplicity 1, and is solved for $c_l = 1 \;\; \forall \;\; l$. Since there is only one eigenvector associated to $\zeta_2 = N$, and we found a valid solution to Eq. (7.19), this must be the eigenvector. The perturbation associated with this eigenvector shifts the phases of all oscillators in the system by the same value. This means that the phase differences, which drive the synchronization dynamics, do not change. The system is invariant under such a uniform phase shift of all oscillators, see [69] and [3].

Now that we know the eigenvalues ζ and the associated eigenvectors $\vec{c}$ we return to Eq. (6.15). For mean field coupling we have $n = N$ and $d_{kl} = 1 \;\; \forall \;\; k, l$, which leads to the characteristic equation:

$$\lambda c_k = -\alpha c_k + \frac{\alpha \hat{g}(\lambda)}{N} \sum_{l=1}^{N} c_l. \tag{7.20}$$

This implies that for the eigenvector $\vec{c}_1$ related to ζ_1 as given in Eq. (7.18):

$$\lambda_1 c_k = -\alpha c_k, \tag{7.21}$$

holds and

$$\lambda_1 = -\alpha, \tag{7.22}$$

is the only solution regardless of the delay distribution. This solution $\lambda_1 = -\alpha$ must be present for any choice of distribution. It is independent of the Laplace transform of the delay distribution, see Eqs. (7.18) and (7.20).

For the eigenvector $\vec{c}_2$ related to ζ_2 in Eq. (7.19) one finds:

$$\lambda_2 = \alpha\,(\hat{g}(\lambda_2) - 1), \tag{7.23}$$

which depends on the Laplace transform of the delay distribution. However the solutions given by Eq. (7.23) are associated to the eigenvector $\vec{c}_2$, which changes each oscillator's phase equally. Furthermore we want to understand how these results are obtained for different delay distributions from the characteristic equation.

Dirac delta and gamma distribution delay kernel

We now obtain results for explicit choices of distributed delays. This is achieved by formulating a discrete delay in terms of distributed delays [67], described by a shifted Dirac delta delay kernel:

$$g_\delta(s) = \delta(s - \tau), \tag{7.24}$$

with the corresponding Laplace transform:

$$\hat{g}_\delta(\lambda) = \int_0^\infty ds\, g_\delta(s) e^{-\lambda s} = e^{-\lambda \tau}. \tag{7.25}$$

In this section, the case of distributed delays is realized with the gamma distribution, introduced in Eq. (A.27) with parameters a and b:

$$g_\Gamma(s; a, b) = s^{a-1} \frac{e^{-\frac{s}{b}}}{b^a \Gamma(a)}. \tag{7.26}$$

Its Laplace transform, compare to subsection A.2, reads:

$$\hat{g}_\Gamma(\lambda) = \int_0^\infty ds\, g_\Gamma(s) e^{-\lambda s} = (1 + b\lambda)^{-a}, \tag{7.27}$$

which depends on both parameters a and b. This leads to two distinct characteristic equations for the case of discrete delays and the case of distributed delays:

$$\text{discrete:} \qquad N e^{\lambda_j \tau} \left(\frac{\lambda_j}{\alpha} + 1 \right) = \zeta_j, \tag{7.28}$$

$$\text{gamma:} \quad N \left(1 + \lambda_{ji} b\right)^a \left(\frac{\lambda_{ji}}{\alpha} + 1 \right) = \zeta_j, \tag{7.29}$$

where $j = 1, 2, \ldots, N$ and $i = 1, 2, \ldots, a$. Note that with the ζ_j from mean-field coupling, the number of oscillators N does not play a role in Eq. (7.29). The λ are solely determined by $\alpha = K h'(-\Omega \tau)$ and the shape and scale parameters a, b of the delay distribution. We start by solving Eq. (7.28) for the case of discrete delays. This can be done using the Lambert W-function denoted by W, with $W e^W = x$, see [159–162] and Appendix A.5:

$$\lambda_j = -\alpha + \frac{1}{\tau} W \left(\frac{\zeta_j \alpha \tau}{N} e^{\alpha \tau} \right), \tag{7.30}$$

yielding two real valued solutions λ_j for $j = 1, 2$:

$$\lambda_1 = 0, \tag{7.31}$$

$$\lambda_2 = -\alpha. \tag{7.32}$$

Here we made use of the properties $W(0) = 0$ and $W(\alpha \tau e^{\alpha \tau}) = \alpha \tau$, see [153]. These solutions are plotted in dependence of the mean delay in Fig. 7.1. The solution $\lambda_1 = 0$ corresponds to neutral stability of the phase variable and is associated to the eigenvector that shifts the phases of all oscillators by the same value. The other solution $\lambda_2 = -\alpha$ describes the linear dynamics of the perturbation mode with the eigenvector whose components sum up to zero.

For the case of the gamma distribution described by Eq. (7.29), expressions that can be solved analytically are obtained for exponents $a = 1, 2$ of the gamma distribution. This leads to polynomials in λ of order two or three, respectively. We consider the case $a = 1$, which corresponds to an exponential distribution. This choice of the parameter a of the gamma distribution represents the case for which the width and asymmetry of the distribution are most distinct from a discrete delay. The variance of the gamma distribution is given by $\sigma_\Gamma^2 = ab^2$ and the skewness by $\gamma_\Gamma = \frac{2}{\sqrt{a}}$. Hence for $a = 1$ (which implies $b = \tau$ since the first moment of the gamma distribution is $\tau \equiv \mu_\Gamma = ab$) we find:

$$N \left(1 + \lambda_{ji} \tau \right) \left(\frac{\lambda_{ji}}{\alpha} + 1 \right) = \zeta_j. \tag{7.33}$$

This implies four different solutions λ_{ji} because we have a quadratic equation and two values of ζ:

$$\lambda_{11} = -\alpha,$$
$$\lambda_{12} = -\frac{1}{\tau},$$
$$\lambda_{21} = 0,$$
$$\lambda_{22} = -\left(\frac{1}{\tau} + \alpha \right).$$

Because Eq. (7.12) is only valid if the conditions given in Eq. (7.13) are fulfilled, each of the above λ has to satisfy these conditions. The λ_{ji} are substituted into Eq. (7.13):

$$
\begin{aligned}
\hat{g}(\lambda_{11}) &= (1 - \tau\alpha)^{-1}, \\
\hat{g}(\lambda_{12}) &= \text{not defined}, \\
\hat{g}(\lambda_{21}) &= 1, \\
\hat{g}(\lambda_{22}) &= (-\tau\alpha)^{-1},
\end{aligned}
$$

and we find that λ_{12} is not a valid solution with $\hat{g}(\lambda_{12})$ undefined and only:

$$
\lambda_{11} = -\alpha, \tag{7.34}
$$

$$
\lambda_{21} = 0, \tag{7.35}
$$

$$
\lambda_{22} = -\left(\frac{1}{\tau} + \alpha\right), \tag{7.36}
$$

are solutions of the characteristic equation. Because $\tau \geq 0$, λ_{11} is larger than λ_{22} for all τ, λ_{11} governs the dynamics close to steady state. The eigenvector associated to λ_{22} rotates all phases in the system the same phase value and does not affect the dynamics.

Discussion

Comparing the values of λ for discrete and distributed delays, reveals that there are no differences in how the system approaches the phase-locked steady state with no phase lags, see Fig. 7.1. The largest non-zero real part of the solutions is given by $\mathrm{Re}(\lambda) = -\alpha$, and the imaginary parts are zero in both cases. With this in mind, Fig. 7.1 holds for both discrete and distributed delays. It shows the rate at which the last perturbation mode present in the system decays for stable solutions with $\mathrm{Re}(\lambda) < 0$, or how fast the system in the unstable case escapes the phase-locked solution with $\mathrm{Re}(\lambda) > 0$. We simulated 50 realizations of Eqs. (5.1) with $N = 20$ mean-field coupled phase oscillators, coupling strength $K = 0.07\,\mathrm{min}^{-1}$, identical intrinsic frequencies $\omega = 0.223\,\mathrm{min}^{-1}$, at different values of discrete τ, and with sinusoidal coupling. These values of K, ω are representative and were used for the DCT in [56]. The oscillators were set to identical initial phases, which we randomly perturbed, such that a random initial order parameter in an interval of $r(t) \in [0.99, 0.999]$ was realized. The initial phase
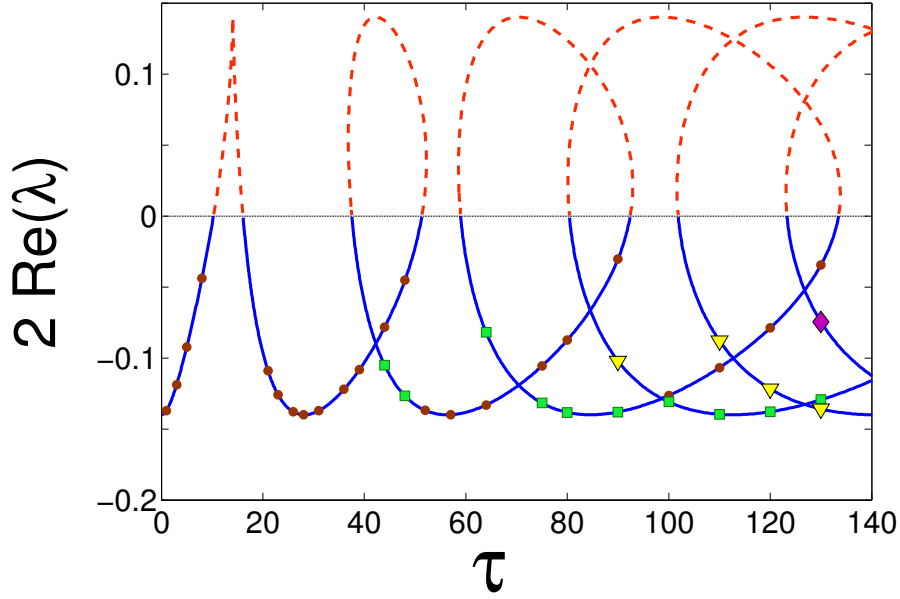
Figure 7.1.: $2\,\mathrm{Re}(\lambda)$ plotted versus τ for discrete and distributed delays, as obtained by solving Eqs. (7.28-7.29). The solid blue line corresponds to the perturbation decay of stable solutions, whereas the dashed red line above zero denotes the perturbation growth of unstable solutions. This is plotted for $N = 20$ mean-field coupled phase oscillators with coupling strength $K = 0.07\,\mathrm{min}^{-1}$, identical intrinsic frequencies $\omega = 0.223\,\mathrm{min}^{-1}$ and sinusoidal coupling function. The markers represent the average of 50 resynchronization rates obtained by simulations with random initial conditions. The brown dots, green squares, yellow triangles and magenta diamond markers denote the different states in the multistable regime for the given values of τ.

history, necessary for delay systems, was given by evolving the uncoupled oscillators with an intrinsic frequency equal to the global frequency of the closest phase-locked steady state. Then the relation between the order parameter and the λ, given in Eq. (7.10), is used to compare the slope of $\log[1 - r(t)]$ versus t with the analytically obtained results. We then placed markers for the mean slope over these realizations in Fig. 7.1. The associated error bars are so small that they cannot be seen in the plot and are therefore omitted.

We conclude, that for mean field coupling the phase-locked steady state and the resynchronization dynamics close to steady state are independent of moments higher than the first moment of the delay distribution. In other words,

the shape of the delay distribution has no effects on linear stability, nor on resynchronization dynamics in systems of mean field coupled phase oscillators.

7.4. Nearest neighbour coupling with periodic boundary conditions
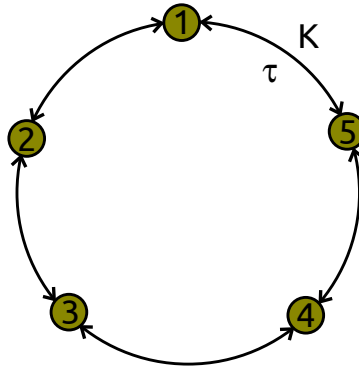

Figure 7.2.: Schematic of $N = 5$ oscillators coupled bidirectionally via nearest neighbour interaction in $1D$ with periodic boundary conditions and time delays.

In the last section for mean-field coupling, no differences in resynchronization dynamics were found, comparing discrete and distributed delays. In this section, nearest neighbour coupling on a $1D$ ring (periodic boundary conditions) will be investigated. For such a connection topology, the $N \times N$ matrix $\mathbb{D}$ reads:

$$\mathbb{D} = \begin{pmatrix} 0 & 1 & 0 & \dots & \dots & \dots & 0 & 1 \\ 1 & 0 & 1 & 0 & \dots & \dots & 0 & 0 \\ 0 & 1 & 0 & 1 & 0 & \dots & 0 & 0 \\ \vdots & & \ddots & \ddots & \ddots & & & \vdots \\ \vdots & & & \ddots & \ddots & \ddots & & \vdots \\ 0 & 0 & 0 & \dots & 1 & 0 & 1 & 0 \\ 0 & 0 & 0 & \dots & \dots & 1 & 0 & 1 \\ 1 & 0 & 0 & \dots & \dots & \dots & 1 & 0 \end{pmatrix}, \tag{7.37}$$

with zeros in the main diagonal, since there is no self coupling, and two entries with 1 indicating the connection to the two nearest neighbours in each row. The

eigenvalues of such a matrix can be found using the solutions to the N-th cyclotomic polynomial, namely the roots of unity, see Appendix A.6 and [163, 164], as given by:

$$w_j^k = \exp\left(i\frac{2\pi jk}{N}\right) \quad \text{where} \quad j = 1, 2, \ldots, N, \tag{7.38}$$

which we use to construct the eigenvectors $\vec{c}$ as a basis:

$$\vec{c}_j = (w_j^1, w_j^2, \ldots, w_j^N)^T. \tag{7.39}$$

Note that these components are complex variables, and that eigenvectors associated to systems with $N \geq 3$ can have complex components. The eigenvectors are only purely real if $2k/N \in \mathbb{N} \, \forall \, k = 1, 2, \ldots, N$. This implies real eigenvectors in a system of $N = 2$ oscillators. Since $w^N = w^0 = 1$ and $w^{-1} = w^{N-1}$, we find from the evaluation of:

$$\mathbb{D}\vec{c} = \begin{pmatrix} w^N + w^2 \\ w + w^3 \\ \vdots \\ w^{N-1} + w \end{pmatrix} = \underbrace{\left(w + w^{N-1}\right)}_{=\zeta_j} \begin{pmatrix} w^1 \\ w^2 \\ \vdots \\ w^N \end{pmatrix}, \tag{7.40}$$

that a term $\left(w + w^{N-1}\right)$ can be separated, which must be the eigenvalues ζ_j of the matrix $\mathbb{D}$ for N oscillators on a ring. Eq. (7.38) and $w^N = w^0 = 1$ implies:

$$\zeta_j = 2\cos\left(\frac{2\pi j}{N}\right), \quad j = 1, 2 \ldots, N. \tag{7.41}$$

Note that one eigenvalue $\zeta_1 = 2$ exists independently of N. This always relates to the solution $\lambda = 0$ of the characteristic Eq. (6.22), and corresponds to the perturbation mode that shifts all oscillators by the same phase. The system is neutrally stable to this mode.

As in the previous case of mean-field coupling we compare discrete delays described by the delay distribution $g_\delta(s)$ in Eq. (7.24) to distributed delays, described by the gamma distribution $g_\Gamma(s)$ in Eq. (7.26). The corresponding Laplace transforms are given by Eq. (7.25) for the discrete case, and by Eq. (7.27) for the gamma distribution. We use these expressions to write down the characteristic equations for the two delay cases:

$$\text{discrete:} \qquad 2e^{\lambda_j \tau}\left(\frac{\lambda_j}{\alpha} + 1\right) = \zeta_j, \tag{7.42}$$

$$\text{gamma:} \qquad 2\left(1 + \lambda_{ji}b\right)^a \left(\frac{\lambda_{ji}}{\alpha} + 1\right) = \zeta_j, \tag{7.43}$$

where $j = 1, 2, \ldots, N$ and $i = 1, 2, \ldots, a$. Differences in the characteristic equations presented here for the case of nearest neighbour coupling are two-fold as compared to the mean field coupling case. Firstly, $n = 2$ instead of $n = N$, because each oscillator couples only to the two nearest neighbours. Furthermore, the eigenvalues ζ_j are different. In the case of an arbitrary number N of oscillators in the system, Eq. (7.41) is used to determine the eigenvalues ζ_j. The characteristic equations for λ_j are then given by Eq. (7.42) and Eq. (7.43). Note that Eqs. (7.42-7.43) hold for arbitrary 2π-periodic coupling functions h. The derivative h' of the coupling function h appears in the parameter $\alpha = K h'(-\Omega\tau)$, defined in Eq. (6.11).

A system of two oscillators

We discuss the simple case of $N = 2$ coupled oscillators with the associated connectivity matrix:

$$\mathbb{D}_{N=2} = \begin{pmatrix} 0 & 1 \\ 1 & 0 \end{pmatrix}, \tag{7.44}$$

where the eigenvalues ζ_j given by Eq. (7.41) for $j = 1, 2$ are:

$$\zeta_1 = -2, \tag{7.45}$$

$$\zeta_2 = 2. \tag{7.46}$$

Note that the eigenvectors corresponding to these eigenvalues have real components, $\vec{c}_1 = (-1, 1)^T$ and $\vec{c}_2 = (1, 1)^T$, see Eq. (7.38). The eigenvalues are substituted into Eq. (7.42) for discrete delay, that written in terms of the Lambert W-function W reads:

$$\lambda_j = -\alpha + \frac{1}{\tau} W \left(\frac{\zeta_j \alpha\tau}{2} e^{\alpha\tau} \right). \tag{7.47}$$

For $\zeta_2 = 2$ we use the property of the Lambert W-function that $W(\alpha\tau e^{\alpha\tau}) = \alpha\tau$ [159], which provides one solution for Eq. (7.47):

$$\lambda_1 = 0. \tag{7.48}$$

With the other eigenvalue, $\zeta_1 = -2$, substituted into the argument of the Lambert W-function, the solution is given by:

$$\lambda_2 = -\alpha + \frac{1}{\tau} W \left(-\alpha\tau e^{\alpha\tau} \right). \tag{7.49}$$

These solutions for discrete delay are plotted in Fig. 7.3 with dashed lines.

The solutions λ_{ji} to the characteristic Eq. (7.43) for distributed delays described by a gamma distribution, with shape parameter $a = 1$ and scale parameter $b = \tau$ in a system of $N = 2$ oscillators, are given by:

$$\lambda_{ji} = -\frac{1}{2}\left(\frac{1}{\tau} + \alpha\right) \pm \sqrt{\frac{1}{4}\left(\frac{1}{\tau} + \alpha\right)^2 - \frac{\alpha}{\tau}\left(1 - \frac{\zeta_j}{2}\right)}, \tag{7.50}$$

where $j, i \in [1, 2]$. Substituting in the eigenvalue ζ_2 gives:

$$\lambda_{21} = -\left(\frac{1}{\tau} + \alpha\right), \tag{7.51}$$

$$\lambda_{22} = 0. \tag{7.52}$$

Similarly, ζ_1 yields for $i = 1, 2$:

$$\lambda_{1i} = -\frac{1}{2}\left(\frac{1}{\tau} + \alpha\right) \pm \sqrt{\frac{1}{4}\left(\frac{1}{\tau} + \alpha\right)^2 - \frac{2\alpha}{\tau}}. \tag{7.53}$$

These results are obtained using the characteristic Eqs. (7.42-7.43), which rely on the conditions given in Eq. (7.13). Hence, these solutions are only valid if they fulfil these conditions.

Finally we compare the response to small perturbations between discrete and distributed delays with sinusoidal coupling function. The response to these perturbations is given by the solution with the largest real part, corresponding to the slowest relaxing perturbation mode for $\text{Re}(\lambda) < 0$, and the fastest diverging mode for $\text{Re}(\lambda) > 0$. The parameters ω and K are chosen according to the Delayed Coupling Theory of vertebrate segmentation [56]. The results are plotted in Figs. 7.3 and 7.4, and discussed in the next paragraph.

Discussion

As shown in Section 6.2, discrete and distributed delays change stability at the same values of $\Omega\tau$, where the lines in Fig. 7.3 cross $\text{Re}(\lambda) = 0$. However, these figures show that there are differences in resynchronization and desynchronization dynamics between the case with discrete and distributed delays in the coupling. In unstable intervals of $\Omega\tau$ [$\text{Re}(\lambda) > 0$], the real part of λ for distributed delays in the coupling is larger than in the case of discrete delays. Hence, in systems with distributed delays in the coupling, the synchronized steady state is left with larger perturbation growth rate as compared to discrete delays in these regions. Intervals of $\Omega\tau$ with stable solutions [$\text{Re}(\lambda) < 0$] show different behavior. In these
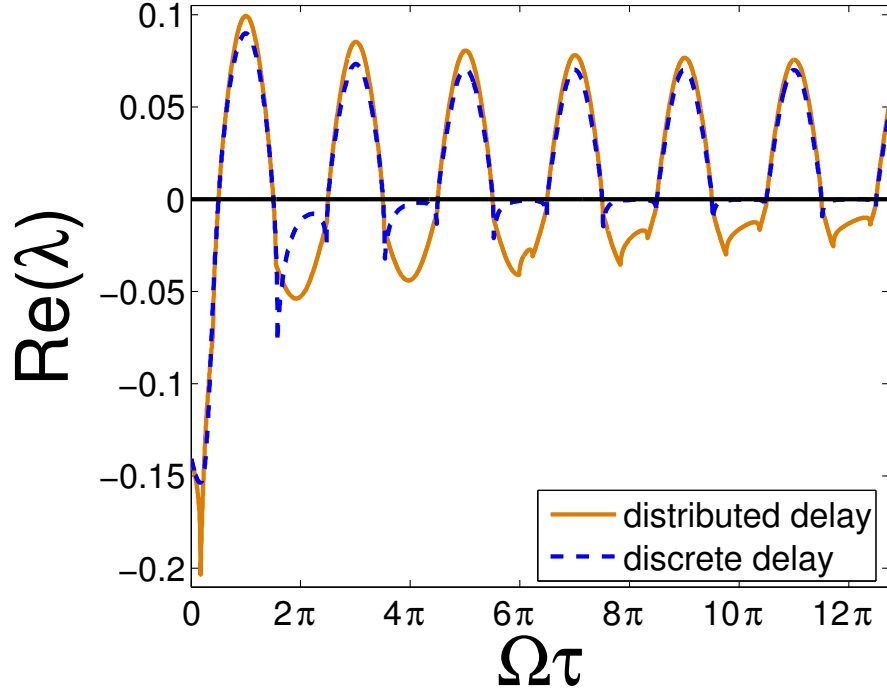
Figure 7.3.: Re(λ) plotted versus $\Omega\tau$ for the λ with the largest real part. Plots show results for $N = 2$ coupled oscillators with intrinsic frequencies $\omega = 0.223\,\mathrm{min}^{-1}$, coupling strength $K = 0.07\,\mathrm{min}^{-1}$, nearest neighbour interaction, and sinusoidal coupling function.

regions there are intervals, where distributed delays resynchronize faster than discrete delays, but also intervals where we find exactly the opposite behaviour. This will be investigated more closely in the next subsections.

The imaginary part associated with the λ with the largest real part, denotes the frequency of oscillation of the perturbation decay [19]. Hence, in intervals of $\Omega\tau$ where the solutions λ have a non-zero imaginary part, the perturbation decays in an oscillatory manner, see Fig. 7.4.

These results for Re(λ) and Im(λ) can be compared with simulation results. We simulated systems of $N = 2$ oscillators coupled with discrete or distributed delays for $\Omega\tau = 5.6$ and obtained the time evolution of the order parameter $r(t)$. Initially the systems were set to steady state and a small random perturbation was added to each phase, such that the initial order parameter was in the interval [0.99, 0.999]. Then we let each oscillator in the system evolve uncoupled with
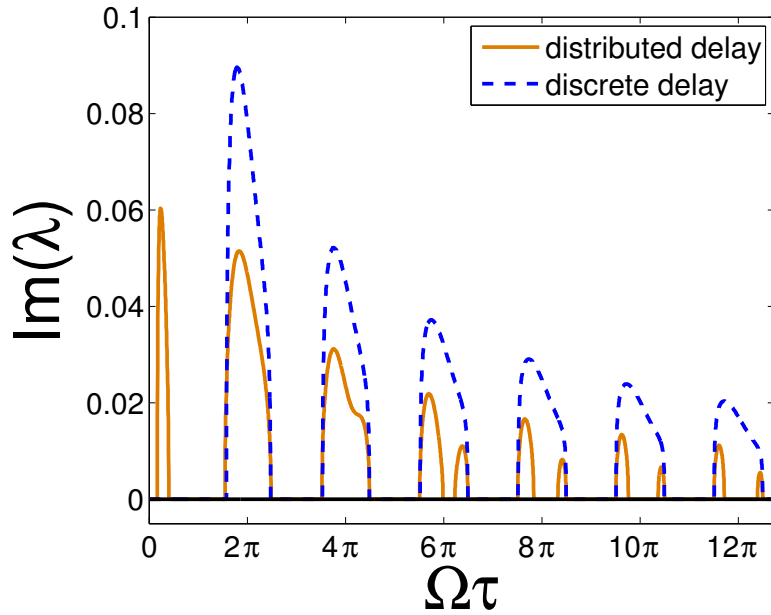
Figure 7.4.: Im(λ) plotted versus $\Omega\tau$ for the λ with the largest real part. Plots show results for $N = 2$ coupled oscillators with intrinsic frequencies $\omega = 0.223\,\mathrm{min}^{-1}$, coupling strength $K = 0.07\,\mathrm{min}^{-1}$, nearest neighbour interaction, and sinusoidal coupling function.
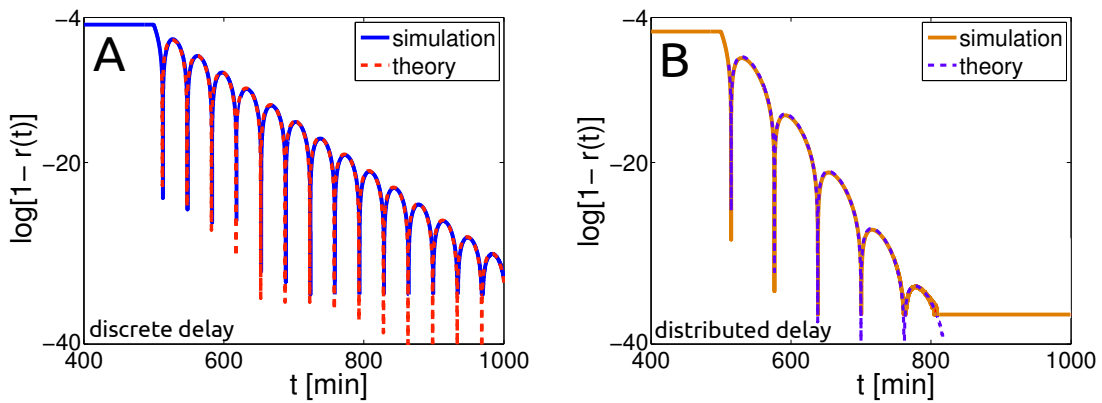

Figure 7.5.: $\log[1 - r(t)]$ vs. t from simulation plotted with predictions from theory for the largest $\mathrm{Re}(\lambda)$, see Figs. 7.3-7.4, for discrete (A) and distributed delays (B). Plots show results for $N = 2$ oscillators with $\omega = 0.223\,\mathrm{min}^{-1}$, $K = 0.07\,\mathrm{min}^{-1}$, $\Omega\tau = 5.6$, nearest neighbour interactions, and sinusoidal coupling.

the frequency Ω of the steady state to generate the necessary phase history for delay systems. A simple Euler forward iteration method was implemented, and an iteration step-size of $dt = 0.005\,\mathrm{min}$ was used. We iterated the system until the steady state was reached. The order parameter was measured and logarithmically plotted as $1 - r(t)$ versus t. These simulation results are plotted in Fig. 7.5 for discrete (A) and distributed (B) delays with solid lines. The dashed lines in Fig. 7.5 show the analytically predicted time evolution of the order parameter Eq. (7.10), with decay rates and frequencies from Figs. 7.3 and 7.4 at $\Omega\tau = 5.6$, which are in nice agreement with the simulation results.

We will now investigate the coupling function more closely to understand the differences in transient dynamics between discrete and distributed delays.

Separating the argument of the coupling function into the contribution of the mean delay and that of the perturbation

Here we take a closer look at the sinusoidal coupling function, for which the results on the dynamics close to the steady state, shown in Figs. 7.3 and 7.4, were obtained. The phase differences that are evaluated by the coupling function have two distinct sources; the incoherence of a system which is not in steady state and the communication delay. If the system of oscillators is close to the steady state, the phases and frequencies of the different oscillators in the system are close to each other, and the instantaneous phase differences are expected to be small. We write for the coupling term h:

$$h = \sin\left(-\theta_k(t) + \int_0^\infty ds\, g(s)\theta_l(t-s)\right), \tag{7.54}$$

and for the perturbed phase-locked solution given in Eq. (6.6):

$$\theta_k(t) = \Omega t + \epsilon q_k(t), \tag{7.55}$$

where $\epsilon \ll 1$. This is substituted into the coupling term:

$$h = \sin\left(-\Omega t - \epsilon q_k(t) + \int_0^\infty ds\, g(s)\left[\Omega t - \Omega s + \epsilon q_l(t-s)\right]\right), \tag{7.56}$$

and yields after evaluation of the perturbation related and delay related terms:

$$h = \sin\left(-\Omega\tau + \epsilon\left[-q_k(t) + \int_0^\infty ds\, g(s)q_l(t-s)\right]\right). \tag{7.57}$$

68

We define:

$$\hat{\epsilon} = \epsilon \left[-q_k(t) + \int_0^\infty ds \, g(s) \, q_l(t-s) \right], \qquad (7.58)$$

and use the trigonometric relation $\sin(f+g) = \sin(f)\cos(g) + \sin(g)\cos(f)$:

$$h = \sin(\hat{\epsilon})\cos(\Omega\tau) - \sin(\Omega\tau)\cos(\hat{\epsilon}). \qquad (7.59)$$

The term $\hat{\epsilon}$ denotes the difference of perturbations entering the coupling function, composed of the present perturbation on oscillator k, and a weighted sum over the past perturbations on oscillator l.

Approximation of the coupling function inside stable regimes

We concentrate on values of $\Omega\tau$, in small intervals around multiple integers of 2π, i.e. around the centers of stable regions:

$$\Omega\tau \approx 2\pi j \quad \text{with} \quad j \in \mathbb{N}. \qquad (7.60)$$

These correspond to values of $\Omega\tau$ for which the mean delay τ is approximately equal to multiples of the period of oscillation, and therefore the sine and cosine term in Eq. (7.59) yield:

$$\sin(\Omega\tau) \approx 0 \quad \text{and} \quad \cos(\Omega\tau) \approx 1. \qquad (7.61)$$
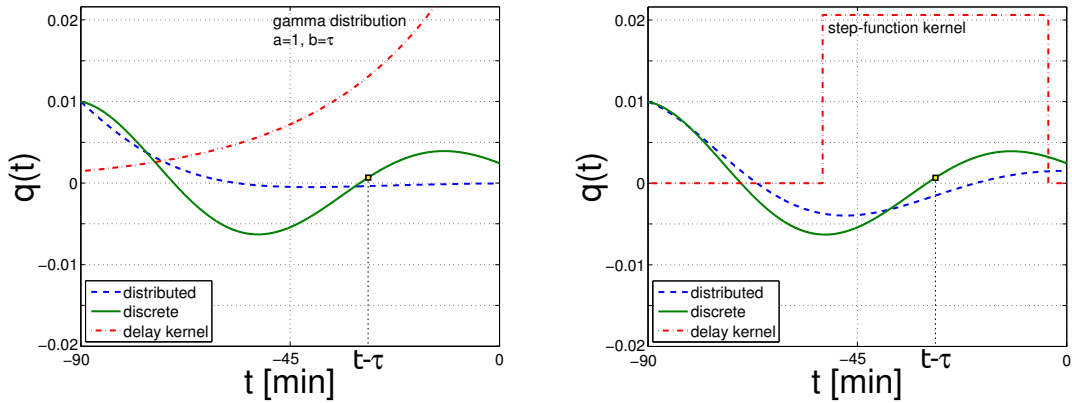

Figure 7.6.: Plots show decay of perturbations on oscillator l for discrete and distributed delays with decay rates and frequencies for a system of $N = 2$ oscillators, and parameters $K = 0.07\,\mathrm{min}^{-1}$, $\Omega\tau = 2\pi$ and $\omega = 0.223\,\mathrm{min}^{-1}$. The yellow square denotes $q(t-\tau)$ for discrete delay.
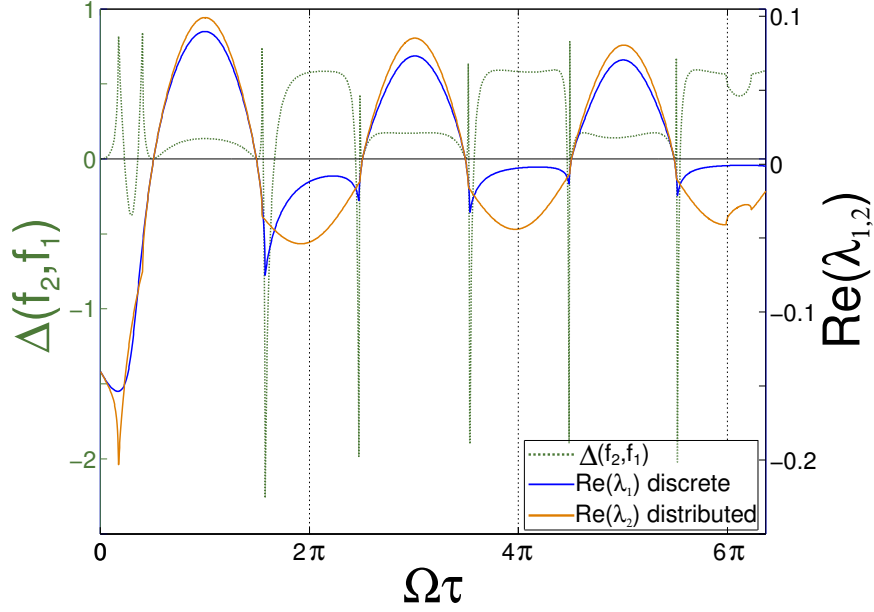
Figure 7.7.: Plot of $\Delta(f_2, f_1)$ for a system of $N = 2$ oscillators, and parameters $K = 0.07\,\mathrm{min}^{-1}$, and $\omega = 0.223\,\mathrm{min}^{-1}$. This corresponds to Figs. 7.3-7.4. $\mathrm{Re}(\lambda)$ for discrete and distributed delays is plotted for comparison.

This implies that only an odd function remains of Eq. (7.59), after substituting Eqs. (7.61), such that the coupling is attractive:

$$h \approx \sin\left(\epsilon\left[-q_k(t) + \int_0^\infty ds\, g(s)\, q_l(t-s)\right]\right). \tag{7.62}$$

Note that the effect of the mean delay is accounted for in this approximation via Eqs. (7.61).

We now compare the argument $\hat{\epsilon}$ of the sine term in Eq. (7.62), which is different for different delay distributions. For a discrete delay, with $g_\delta(s) = \delta(s - \tau)$, the perturbation at one past time is taken into account, while in the case of distributed delays with a non-zero variance the perturbations of the entire past interval governed by the delay integral are summed up and weighted according to the delay distribution, see sketches in Fig. 7.6. We investigate the perturbations $-q_k(t) + \int_0^\infty ds\, g(s)\, q_l(t-s)$, substitute $q_k(t) = c_k \exp(\lambda t)$ with $c_k \equiv 1$, and define:

$$\text{discrete delays:} \quad f_1 \;=\; e^{\lambda_1 t}\left(e^{\lambda_1 \tau} - 1\right), \tag{7.63}$$

$$\text{distributed delays:} \quad f_2 \;=\; e^{\lambda_2 t}(\hat{g}(\lambda_2) - 1), \tag{7.64}$$

70

where $\hat{g}(\lambda_2) = (1 + \lambda_2 \tau)^{-1}$ is the Laplace transform of the gamma distribution, and the $\lambda_{1,2} \in \mathbb{C}$ are given in Figs. 7.3-7.4 for the different τ. We calculate $\Delta(f_2, f_1) = f_2 - f_1$ in order to see whether the hypothesis holds true, that distributed delays also account for the perturbations around the mean delay, and hence result in larger $\hat{\epsilon}$ compared to discrete delays. The result is plotted in Fig. 7.7. We confirm that $\Delta(f_2, f_1) > 0$ in stable regions where the distributed delay, here given by a gamma distribution with $a = 1$ and $b = \tau$, resynchronizes faster than the discrete delay case with the same mean delay.

Hence, in the case of discrete delays, the sine function evaluates a smaller $\hat{\epsilon}$, which results in weaker coupling and smaller $|\text{Re}(\lambda)|$, as compared to distributed delays, see Fig. 7.3. The coupling with distributed delays takes into account perturbations on the phase of oscillator l at different past times around the mean delay τ, resulting in larger $\hat{\epsilon}$. Hence, coupling is stronger and resynchronization is faster, i.e. larger $|\text{Re}(\lambda)|$, compared to discrete delays, see Fig. 7.3.

Approximation of the coupling function close to changes in stability

In addition to integer multiples of 2π, we investigate values of $\Omega\tau$ in small intervals around odd multiples of $\pi/2$:

$$\Omega\tau \approx (2j+1)\frac{\pi}{2} \quad \text{with} \quad j \in \mathbb{N}, \tag{7.65}$$

for which the cosine and sine terms in Eq. (7.59) are:

$$\cos(\Omega\tau) \approx 0 \quad \text{and} \quad \sin(\Omega\tau) \approx 1. \tag{7.66}$$

Such states correspond to situations where the system is close to where stability of the solution changes between stable and unstable. In Eq. (7.59) only an even function of the expansion remains after substituting Eqs. (7.66):

$$h \approx -\cos\left(\epsilon\left[-q_k(t) + \int_0^\infty ds\, g(s)\, q_l(t-s)\right]\right). \tag{7.67}$$

The effect of the mean delay is accounted for via Eqs. (7.66). Depending on which side of $\Omega\tau = (2j+1)\frac{\pi}{2}$ with $j \in \mathbb{N}$ this expression is evaluated, corresponding to unstable or stable, the coupling function will drive the phases apart or force them towards resynchronization. We concentrate on the stable regimes.

We find that $\Delta(f_2, f_1) < 0$ close to the $\Omega\tau$ as given in Eq. (7.65), see Fig. 7.7. Therefore we conclude that the normalized sum over the perturbations picked

up by distributed delays is smaller than the perturbation at discrete delay τ, and hence the coupling with discrete delays resynchronizes faster than that with distributed delays.

Note that in the entire unstable regimes of $\Omega\tau$ where $\mathrm{Re}(\lambda) < 0$ we find that $\Delta(f_2, f_1) > 0$, and coupling with distributed delays leads to faster desynchronization compared to discrete delays.

Discrete delay is a limit case of gamma distributed delay

A closer look at the limit of $a \to \infty$ for the Laplace transform of the gamma distribution shows that:

$$\lim_{a \to \infty} \left(1 + \frac{\tau\lambda}{a}\right)^{-a} = e^{-\lambda\tau}, \tag{7.68}$$

which represents the approach to the discrete case by changing the shape parameter a of the gamma distribution. Since $\tau = ab$ in the above limit, b has to vanish in order to keep the mean τ constant, which implies for the variance σ_Γ^2
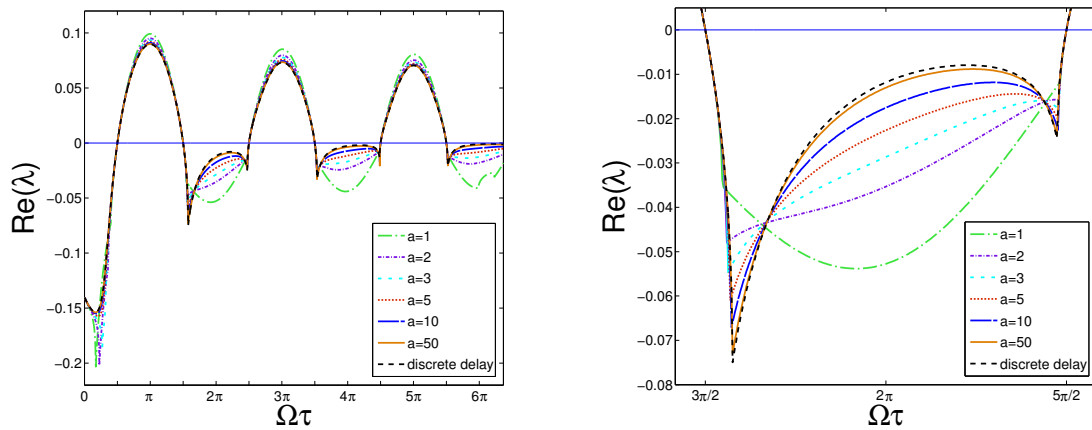
Figure 7.8.: $\mathrm{Re}(\lambda)$ plotted versus $\Omega\tau$ for different values of $a = \{1, 2, 3, 5, 10, 50\}$ of the gamma distribution. This is for a system of $N = 2$ oscillators with nearest neighbour interaction, periodic boundary conditions, intrinsic frequencies $\omega = 0.223\,\mathrm{min}^{-1}$, coupling strength $K = 0.07\,\mathrm{min}^{-1}$, and sinusoidal coupling. The right plot is a zoom of the second stable branch of the left plot.

and skewness γ_Γ of the gamma distribution:

$$
\begin{aligned}
a &\to \infty, \quad b \to 0, \\
\tau &= ab = \text{const.}, \\
\sigma_\Gamma^2 &= \tau b \to 0, \\
\gamma_\Gamma &= \frac{2}{\sqrt{a}} \to 0.
\end{aligned}
\tag{7.69}
$$

From this we see that in the limit $a \to \infty$, $b \to 0$, where the case of distributed delays approaches the discrete delay case with identical mean delay, the variance and the skewness of the delay distribution tend to zero. In Fig. 7.8 we show $\mathrm{Re}(\lambda)$ plotted versus $\Omega\tau$ for different values of a of the gamma distribution.

Our hypothesis, following the subsections on the approximation of the coupling function, is that increasing the variance and the skewness of the delay distribution will speed up resynchronization for systems of coupled phase oscillators, if the values of $\Omega\tau$ are close to integer multiples of 2π as given in Eq. (7.60). For values of $\Omega\tau$ close to odd multiples of $\pi/2$, we expect that an increasing variance and skewness will slow down resynchronization in such systems.

7.4.1. How variance and skewness influence synchrony dynamics

In order to investigate the influence of the variance and skewness on resynchronization and desynchronization properties close to the phase-locked solution independently, we use the two step delay distribution that is introduced in Appendix A.1, and given by Eqs. (A.1–A.2):

$$
g(s) = a\Pi\left(\frac{s - (\bar{m} - 0.5b)}{b}\right) + d\Pi\left(\frac{s - (\bar{m} + 0.5c)}{c}\right).
\tag{7.70}
$$

Here $\Pi(x) = \Theta(x + 0.5) - \Theta(x - 0.5)$ denotes the boxcar function, and Θ is the Heaviside function. The parameters a, b, c, d are the heights and widths of the two step functions. The Laplace transform associated to this distribution is:

$$
\hat{g}(\lambda) = \frac{e^{-m\lambda}}{2\lambda}\left\{\frac{1}{b}\left[e^{b\lambda} - 1\right] + \frac{1}{c}\left[1 - e^{-c\lambda}\right]\right\}.
\tag{7.71}
$$

The equation that has to be solved to determine these resynchronization properties is obtained by substituting the Laplace transform of the delay distribution
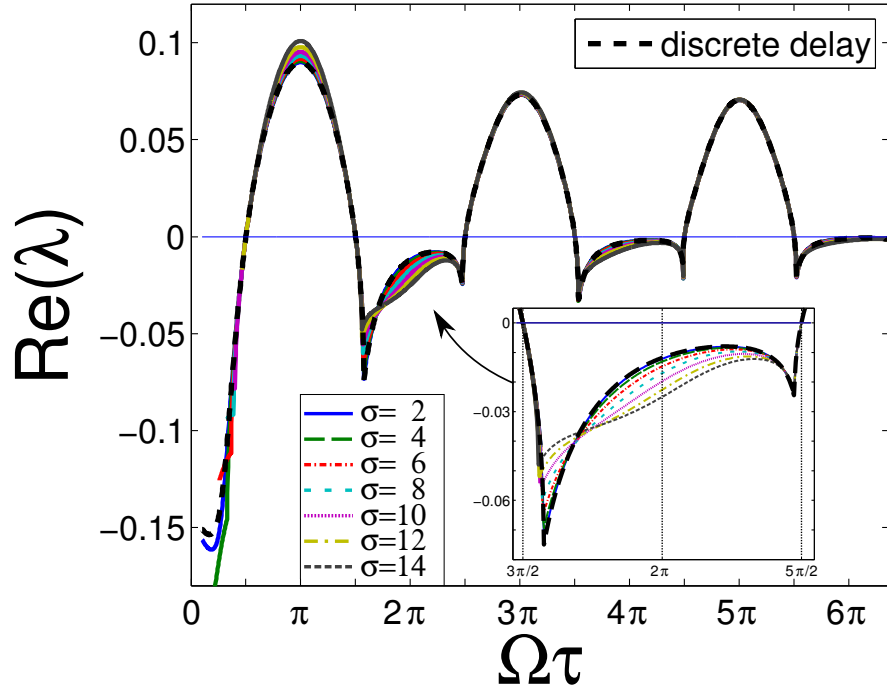
Figure 7.9.: Real part of the perturbation decay $[Re(\lambda) < 0]$ or growth $[Re(\lambda) > 0]$ plotted against $\Omega\tau$ for different values of the standard deviation and a fixed value of the skewness $\gamma = 0.92$ of the two step delay distribution. The dashed black line shows the discrete delay case, whereas the coloured lines denote the different standard deviations σ. $N = 2$ coupled oscillators with nearest neighbour interaction, periodic boundary conditions, $\omega = 0.223\,\text{min}^{-1}$, $K = 0.07\,\text{min}^{-1}$ and sinusoidal coupling. With increasing standard deviation the curves move further away from the discrete delay case – also see Fig. 7.10.

Eq. (7.71) into the characteristic Eq. (6.22), which yields the characteristic equation:

$$\frac{4\lambda_j}{e^{-\bar{m}\lambda_j}}\left(\frac{\lambda_j}{\alpha} + 1\right)\left\{\frac{1}{b}\left[e^{b\lambda_j} - 1\right] + \frac{1}{c}\left[1 - e^{-c\lambda_j}\right]\right\}^{-1} = \zeta_j, \qquad (7.72)$$

where $j = 1, 2$. We solve this equation numerically for the λ_j, using the trust-region dogleg algorithm, implemented in the fsolve function in Matlab, see [165, 166]. First we provide an overview and produce a plot analogous to Fig. 7.3 for the gamma distribution, but for the two step delay distribution. In order to accomplish this, we have to calculate the values of b, c and $\bar{m}$ of the two step
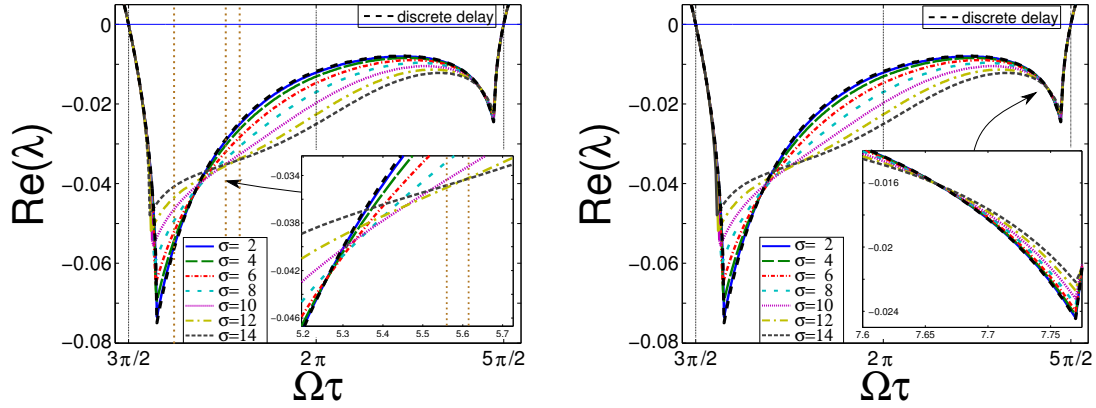
74

Figure 7.10.: Zooms of the second stable branch in Fig. 7.9. The insets show the resynchronization behaviour in dependence of the mean delay; from discrete delays synchronizing fastest, to distributed delays synchronizing fastest, and back.

delay distribution for each triple of τ, σ, γ in order to solve the characteristic Eq. (7.72). This is described in Appendix A.1 where the two step delay distribution is introduced. We choose a fixed pair of (σ, γ) and calculate the corresponding pair (b, c). Then, for each value of τ, we determine the corresponding value of $\bar{m}$, and solve Eq. (7.72) for the given triple of $\bar{m}, b, c$ for all ζ_j, which yields the λ_j.

Since negative delay times are undefined, we demand that the delay distribution does not expand to negative arguments. Therefore $(\bar{m} - b) \geq 0$, see Fig. A.1, has to be fulfilled. For larger variance this leads to minimal mean delays τ that can be realized for the chosen pair of (σ, γ), and the corresponding pair (b, c). Hence, the curves in Fig. 7.9 for distributed delays with different standard deviations σ start off at different values $\Omega \tau$.

Recall, that the dynamics of the slowest relaxing perturbation mode in stable systems is dominated by the eigenvalue λ_j with the largest real part that is smaller than zero. This real part is determined according to Eq. (7.72), and plotted in Fig. 7.9 for a fixed value of $\gamma = 0.92$ and different variances. The imaginary part denotes the frequency of oscillation of the perturbation decay dynamics and is plotted in Fig. 7.11.
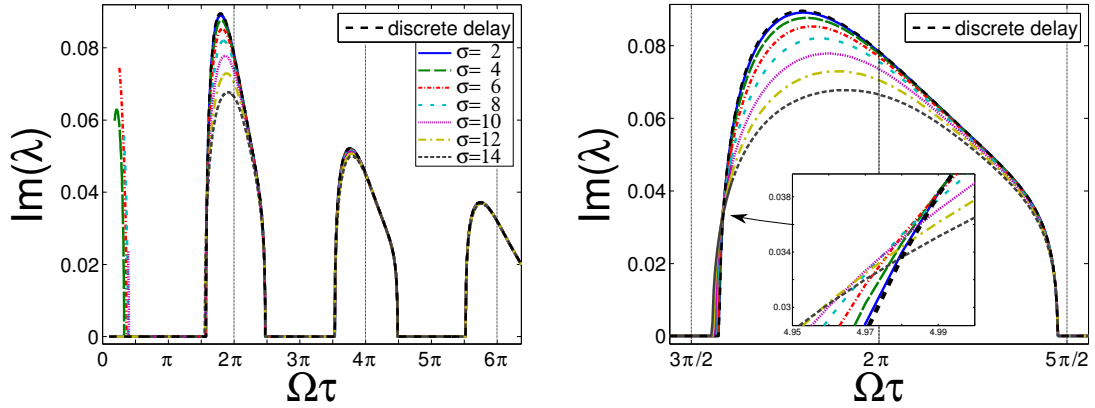
Figure 7.11.: Im(λ) corresponding to the real parts shown in Fig. 7.9, plotted versus $\Omega\tau$ for different values of the σ, and fixed skewness $\gamma = 0.92$ of the two step delay distribution. The right plot shows a zoom of the second stable branch. The imaginary part denotes for the frequency of oscillation with which the perturbation decays.

Discussion

The differences between the delay formulations are most prominent for small values of $\Omega\tau$. In Fig. 7.9 one can observe that with increasing values of $\Omega\tau$ the differences between discrete and distributed delays become smaller. We also observe that the difference between discrete delays, denoted by the dashed black line, compared to distributed delays increases with increasing variance. The value of the skewness $\gamma = 0.92$ is fixed. There are intervals of $\Omega\tau$, where discrete delays resynchronize faster, and regions where distributed delays resynchronize faster, compared to its counterpart. We found a qualitatively similar result before in the case of distributed delays governed by the gamma distribution, shown in Fig. 7.3. In unstable regions the phase-locked steady state desynchronizes fastest, for any corresponding value of $\Omega\tau$, when coupling involves distributed delays. The result on the steady state stability in Chapter 6, showing the independence of the stability of the phase-locked solutions on higher moments of the delay distribution but the first, is again confirmed. Independently of the variance and skewness, Re(λ) crosses zero at the same values of $\Omega\tau$.

The imaginary parts associated to the real parts shown in Fig. 7.9 are plotted in Fig. 7.11. We find that oscillatory behaviour can only be observed in stable

regions of the phase-locked solution, whereas in unstable regions the imaginary parts are zero for both delay cases. This can be explained by overshooting of the phases of the oscillators while trying to synchronize to those of their neighbours. The idea is that two oscillators that couple and have adjusted their phases almost entirely still see a phase difference due to the communication delay. This causes an overshooting as they try to synchronize to a common phase, since the communication delay does not change as the phases adjust. The overshooting does not occur in unstable regions of the phase-locked solution, where the oscillators repel each other due to the repulsive character of the coupling function.

We observe that in the first stable branch in Fig. 7.11 only distributed delays exhibit oscillatory behaviour, but discrete delays do not. This suggests that there is a critical delay value τ_c for the discrete delay case, below which no oscillatory behaviour is triggered. The case of distributed delays however expands due to the non-zero variance to delay values larger than τ_c, even if the mean of the distribution is smaller than τ_c.

In general it can be seen, that with increasing standard deviation the curves for distributed delays move further away from the case of discrete delays. As we have already observed for the real parts in Fig. 7.10, there are intervals within the stable regimes, where discrete delays have associated the smallest frequency during resynchronization, and other intervals where we find the opposite behaviour. This change takes place for values larger than $\Omega\tau \approx 5$, where the order is reversed. However, this is not a dominant effect, and for most values $\Omega\tau$ in stable regimes $\mathrm{Im}(\lambda)$ for discrete delays is the smallest. Hence, with increasing variance of distributed delays the perturbation decay frequency $\mathrm{Im}(\lambda)$ becomes smaller compared to the discrete delay case.

We now investigate the individual influences of the variance and the skewness of the delay distribution on resynchronization dynamics.

Influence of the variance on synchrony dynamics for fixed skewness

Here we choose fixed values of $\Omega\tau$ and plot $\mathrm{Re}(\lambda)$ as a function of the standard deviation σ of the two step delay distribution. This corresponds to a vertical cut through the curves in Fig. 7.10 at these fixed $\Omega\tau$, which is illustrated for three cases by the orange dotted verticals in both panels.

Those intersections are plotted at $\Omega\tau = \{5.61, 5.12, 5.57\}$ for three different fixed values of the skewness $\gamma = \{0.3, 0.6, 0.92\}$, which acts as an parameter.
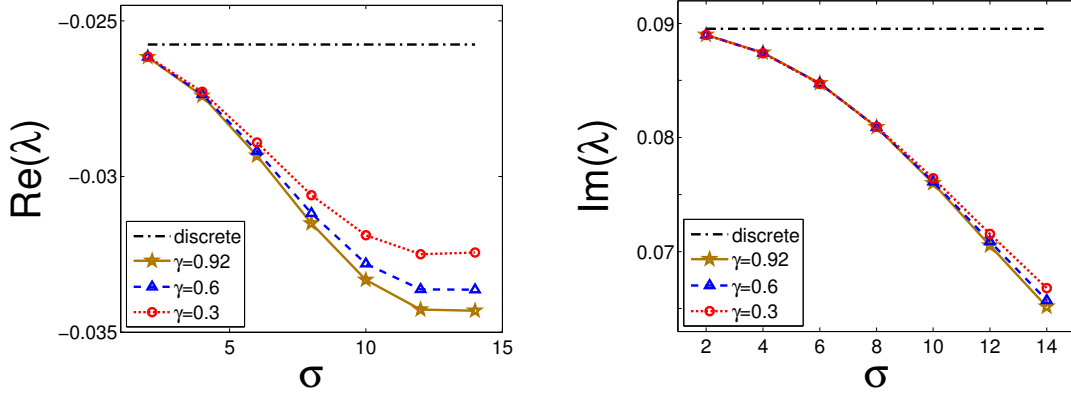
Figure 7.12.: Re(λ) and Im(λ) as a function of the standard deviation of the two step delay distribution. There are three curves for different fixed values of $\gamma = \{0.3, 0.6, 0.92\}$. This is at $\Omega\tau = 5.61$, which means $\Omega = 0.2669\,\text{min}^{-1}$ and $\tau = 21\,\text{min}$. The black dash dotted line is plotted for comparison to the value of the discrete delay, which has standard deviation zero.

These values are chosen because they represent three different dependencies of the resynchronization properties in dependence of the variance. These plots are shown in Figs. 7.12, 7.13 and 7.14, correspondingly.

In Fig. 7.12 where $\Omega\tau = 5.61$ ($\Omega = 0.2669\,\text{min}^{-1}$, $\tau = 21\,\text{min}$), we observe that the resynchronization rate $|\text{Re}(\lambda)|$ for small values of the standard deviation σ is comparable between discrete and distributed delays, independently of the skewness γ. With increasing σ however, distributed delays allow faster resynchronization compared to the case of discrete delays. The absolute value of Re(λ) increases, as σ increases. For values of the standard deviation above $\sigma = 12$ the increase in synchronization rate saturates and a minimum in Re(λ) is reached. We look at this minimum in more detail in Fig. 7.14. The growth of synchronization rate with increasing standard deviation σ is further enhanced by increasing the skewness γ, shown by the three different curves with red circle, blue triangle and yellow star markers. This effect is observed for sufficiently large σ. The imaginary part exhibits similar behaviour, and we can see that the frequency of perturbation decay becomes smaller, as the standard deviation σ increases. Here the effect of the skewness seems to be negligible.

The case $\Omega\tau = 5.12$ ($\Omega = 0.2873\,\text{min}^{-1}$, $\tau = 17.82\,\text{min}$) is shown in Fig. 7.13. We plotted the behaviour of the real and imaginary parts of λ for the same three
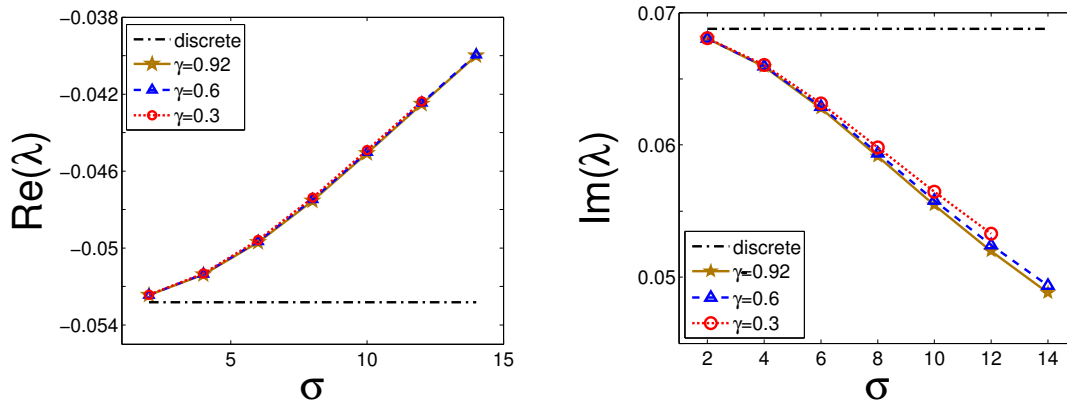
Figure 7.13.: Re(λ) and Im(λ) as a function of the standard deviation of the two step delay distribution. There are three curves for different fixed values of $\gamma = \{0.3, 0.6, 0.92\}$. This is at $\Omega\tau = 5.12$ for a system with $\Omega = 0.2873\,\mathrm{min}^{-1}$ and $\tau = 17.8\,\mathrm{min}$. The black dash dotted line is plotted for comparison to the value of the discrete delay, which has standard deviation zero.

different fixed values of γ as before in Fig. 7.12. In the left plot we see that in this case the real part Re(λ) of distributed delays has smaller absolute values compared to discrete delays given by the black dashed line. For small values of σ, Re(λ) is similar for discrete and distributed delays. As the variance is increased for this value of $\Omega\tau$, the moduli of Re(λ) for distributed delays become smaller. For all values of σ, discrete delays resynchronize fastest for this $\Omega\tau$, and the difference between discrete and distributed delays grows as the standard deviation σ increases. Comparison of the plots for the different values of the skewness show that the skewness has no noticeable effect. On the right hand side in Fig. 7.13 we plotted the imaginary part of λ. We find that the frequency of oscillation decreases with increasing variance, and depends only very weakly on the value of the skewness.

The findings related to Figs. 7.12 and 7.13 agree with the hypothesis we put forward, that increasing the variance and the skewness of the delay distribution will speed up resynchronization for systems of coupled phase oscillators, if the values of $\Omega\tau$ are close to integer multiples of 2π. Indeed there is a region around values of $\Omega\tau$ being multiples of 2π, where increasing the standard deviation of the delay distribution results in increased resynchronization rate $|\mathrm{Re}(\lambda)|$, when comparing distributed and discrete delays as was shown in Fig. 7.12. For
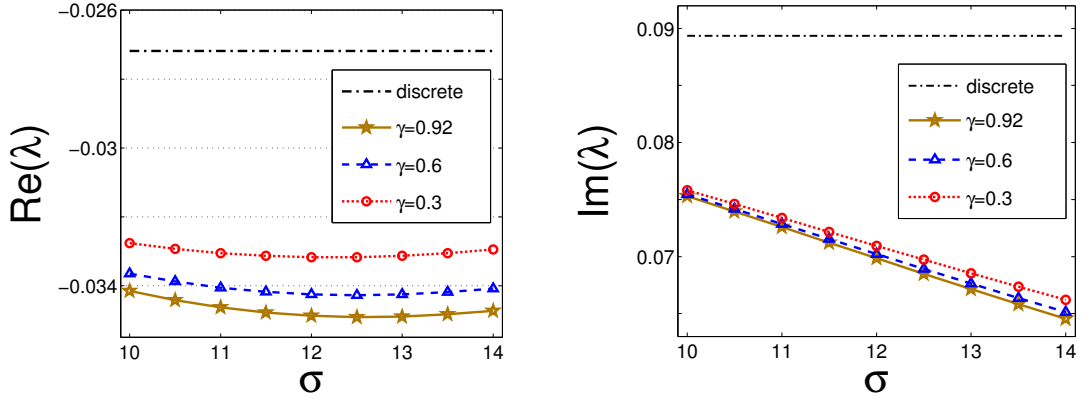
Figure 7.14.: Re(λ) and Im(λ) as a function of the standard deviation of the two step delay distribution. There are three curves for different fixed values of $\gamma = \{0.3, 0.6, 0.92\}$. This is at $\Omega\tau = 5.57$ for a system with $\Omega = 0.2688\,\mathrm{min}^{-1}$ and $\tau = 20.7\,\mathrm{min}$. The black dash dotted line is plotted for comparison to the value of the discrete delay, which has standard deviation zero.

sufficiently large values of the standard deviation, the skewness γ also affects resynchronization dynamics. It increases $|\mathrm{Re}(\lambda)|$ which implies faster resynchronization for larger values of the skewness. However the effect of the standard deviation is much larger. If one goes further away from these values of $\Omega\tau$ and approaches the ones close to odd multiples of $\pi/2$, given by Eq. (7.65), the above observed behaviour reverses and the discrete delay case resynchronizes fastest as shown in Fig. 7.13. In these intervals the skewness has almost no effect on resynchronization dynamics.

We now take a closer to look at the interval of $\Omega\tau$ where the transition between the different behaviours takes place. We look at Fig. 7.10, which contains a zoom of Fig. 7.9 with insets magnifying the regions where the influence of distributed delays reverses. One can see the region of $\Omega\tau$ close to $\Omega\tau = 5.25$ where the order of the curves changes the first time (left plot). In the region at approximately $\Omega\tau = 7.65$ it changes back to the initial ordering of the curves (right plot). Hence, systems coupled with distributed delays change their behaviour from synchronizing slower than the discrete delay case for values $\Omega\tau$ roughly smaller than $\Omega\tau = 5.25$, to synchronizing faster than the discrete delay, for larger values of $\Omega\tau$. This changes back to slower synchronization with distributed delays at about $\Omega\tau = 7.65$ on this stable branch. However, since not all

all curves cross at the same value of $\Omega\tau$ in this region where the resynchronization behaviour changes, one finds a minimum in the curve for the largest $\mathrm{Re}(\lambda)$. We show this in Fig. 7.14. This means that there is a pair of $(\sigma \approx 12, \gamma \approx 0.9)$ for which resynchronization rate $|\mathrm{Re}(\lambda)|$ has a maximum in the region of $\Omega\tau \approx 5.35$.

Influence of the skewness on synchrony dynamics for fixed values of the variance

Now we look at the influence that the skewness has on resynchronization dynamics for fixed values of the variance. We will first show plots similar to Fig. 7.9 for a system of two oscillators on a ring with identical intrinsic frequencies and distributed delays in the coupling. Here these plots show curves for fixed standard deviation $\sigma = 10$, and different values of the skewness. The black dashed line denotes the discrete delay case and the coloured lines the different values of the skewness γ. An overview for $\mathrm{Re}(\lambda)$ and $\mathrm{Im}(\lambda)$ as a function of $\Omega\tau$, for different skewness, is plotted in Fig. 7.15. Comparing these plots to the previous ones in Fig. 7.9, one can see that changing the skewness has a much smaller effect than changing the variance. The curves for the different values of γ almost cover each
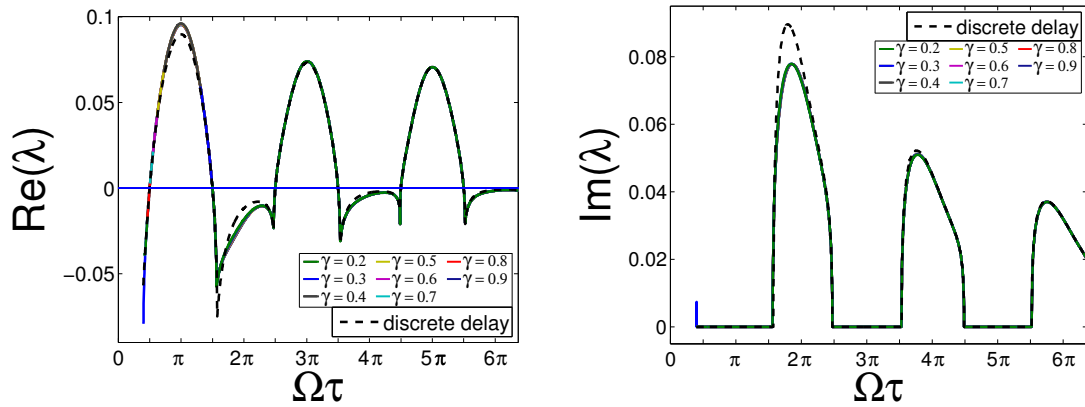
Figure 7.15.: $\mathrm{Re}(\lambda)$ and $\mathrm{Im}(\lambda)$ plotted versus $\Omega\tau$. The dashed black line represents the discrete delay case, the coloured lines denote for distributed delays. The standard deviation is fixed to $\sigma = 10$, and different values of the skewness $\gamma = \{0.2, 0.3, 0.4, 0.5, 0.6, 0.7, 0.8, 0.9\}$ are plotted. This is for a system of $N = 2$ oscillators with nearest neighbour interaction, periodic boundary conditions, $\omega = 0.223\,\mathrm{min}^{-1}$, $K = 0.07\,\mathrm{min}^{-1}$ and sinusoidal coupling.
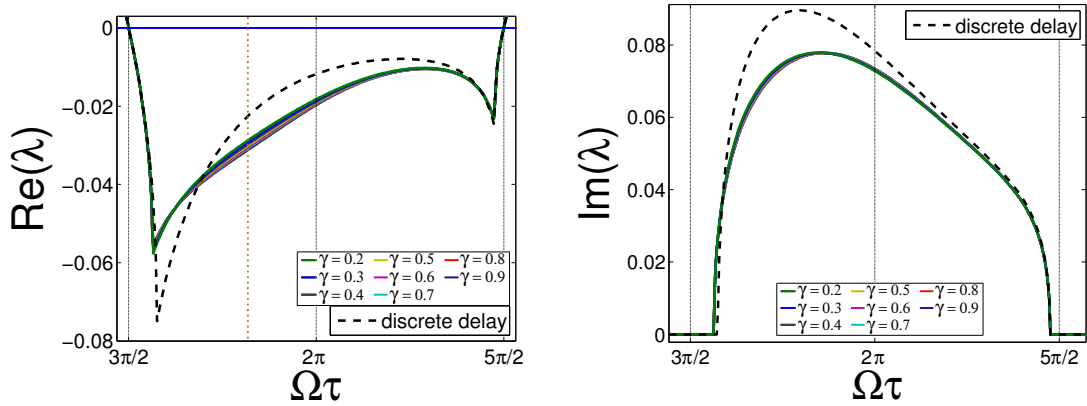
Figure 7.16.: Zooms of Fig. 7.15 highlighting a region where $\text{Re}(\lambda) < 0$, here the second stable branch.

other. The skewness ranges from values of $\gamma = 0.2$ up to 0.9 which is roughly the maximum skewness that can be realized with this two step delay distribution, see Appendix A.1. We also added a zoom of the second stable branch for each plot in Fig. 7.15. These are shown in Fig. 7.16.

At fixed $\Omega\tau = 5.61$ we make a cut as sketched by the orange dotted vertical in the left plot of Fig. 7.16. Then we plot the resynchronization rate given by $|\text{Re}(\lambda)|$ as a function of the skewness γ of the two step delay distribution for three different values of the standard deviation $\sigma = [3, 10, 14]$. These plots are shown in Fig. 7.17 for the real and imaginary parts of λ. We see that for small standard deviation σ as given by the red dotted line with circles, the skewness has almost no influence on resynchronization dynamics, and the resynchronization rate remains roughly constant as the skewness grows. For larger values of σ as given by the blue dashed curve with triangle markers, and the dark yellow curve with star markers, we observe that the skewness influences resynchronization properties. In these cases $|\text{Re}(\lambda)|$ grows with increasing skewness γ. The frequency of oscillation, given by $\text{Im}(\lambda)$, as the system approaches the steady state is shown in the right plot in Fig. 7.17. It depends very weakly on the skewness γ. For small values of the standard deviation σ it is independent of the skewness γ. At larger values of the standard deviation $\sigma = \{10, 14\}$ one can observe a small influence. We conclude that the skewness γ has an influence on the resynchronization dynamics at these values of $\Omega\tau$ close to multiples of 2π. In this region
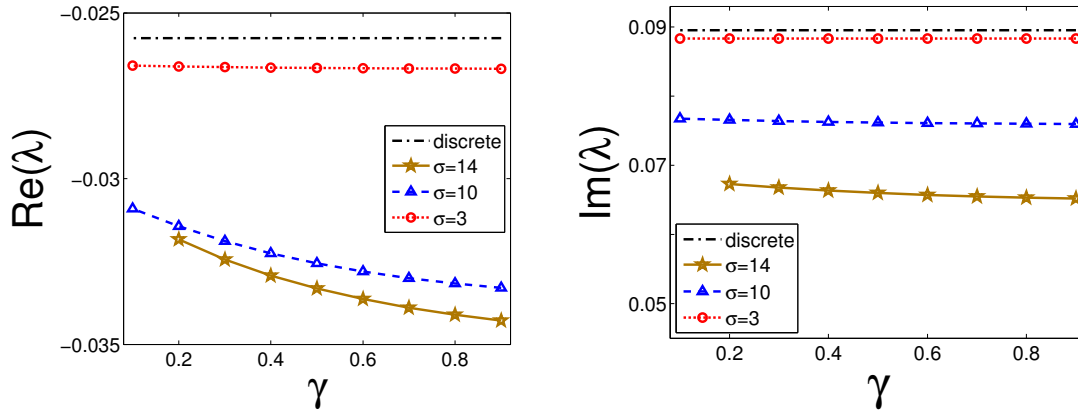
Figure 7.17.: Re(λ) and Im(λ) as a function of the skewness of the two step delay distribution. There are three curves for different fixed values of $\sigma = \{3, 10, 14\}$. This is at $\Omega\tau = 5.61$, sketched by the orange dotted line in Fig. 7.16, for a system with $\Omega = 0.2669\,\mathrm{min}^{-1}$ and $\tau = 21\,\mathrm{min}$. The black dash dotted line is plotted for comparison to the value of the discrete delay, which has standard deviation zero.

we find that increasing the skewness γ of the two step distribution for a fixed value of the standard deviation σ increases the resynchronization rate $|\mathrm{Re}(\lambda)|$. This is most pronounced for large values of the standard deviation. Compared to the influence that the standard deviation σ has, the influence of the skewness γ is much smaller.

7.4.2. The dependence of synchrony dynamics on the number of oscillators

The results on the differences in the linear response to small perturbations for discrete versus distributed delays in the coupling were obtained in systems of two phase oscillators with nearest neighbour coupling. We restricted our analysis to this most simple case to better understand the mechanism and effects that can be observed when replacing discrete with distributed delays in the coupling. Here we discuss and compare the largest real part of λ for system with different numbers of oscillators N. The characteristic equations for systems with discrete

delays and distributed delays with a gamma distribution are:

$$\text{discrete:} \qquad 2e^{\lambda_j \tau}\left(\frac{\lambda_j}{\alpha}+1\right)=\zeta_j, \qquad (7.73)$$

$$\text{gamma:} \qquad 2\left(1+\lambda_{ji}b\right)^a\left(\frac{\lambda_{ji}}{\alpha}+1\right)=\zeta_j, \qquad (7.74)$$

where $j = 1, 2, \ldots, N$ and $i = 1, 2, \ldots, a$, subject to the conditions:

$$\hat{g}(\lambda) \;\neq\; 0 \;\forall\; \lambda,$$
$$\alpha \;\neq\; 0. \qquad (7.75)$$

The ζ_j, $j = 1, 2, \ldots, N$ in Eqs. (7.73-7.74) are the eigenvalues of the coupling
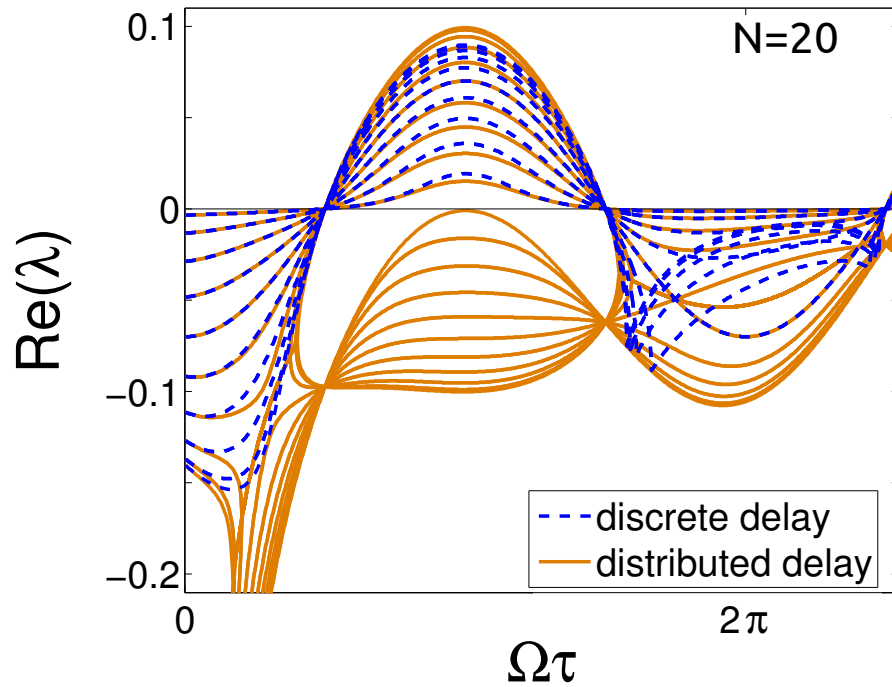
Figure 7.18.: All Re(λ), associated to the different perturbation modes, plotted vs. $\Omega\tau$ for $N = 20$ oscillators. This is for a system with coupling strength $K = 0.07\,\text{min}^{-1}$, intrinsic frequency $\omega = 0.223\,\text{min}^{-1}$, nearest neighbour interaction and sinusoidal coupling. The delay distribution is a gamma distribution with $a = 1$ and $b = \tau$.

matrix, obtained during the derivation, see Eqs. (6.17-6.18), of these characteristic equations, obtained by solving the eigenvalue problem $\zeta\vec{c} = \mathbb{D}\vec{c}$. These

eigenvalues are given by $\zeta_j = 2\cos(2\pi j/N)$ for nearest neighbour coupling on a $1D$ ring. With each new oscillator that is added to the system a new eigenvalue ζ_j emerges. This implies that new perturbation modes become possible. In the original 2-oscillator system there was only one perturbation mode that affects the synchrony in the system. This perturbation mode is given when the two oscillators in the system are perturbed by a small phase with different sign, shifting their phases towards or away from each other. Hence, this perturbation mode is related to nearest neighbours and constitutes the perturbation mode with the shortest wavelength in the system. When new oscillators are added, new perturbation modes with correspondingly longer wavelengths can exist in the system.

We plotted all solutions λ for a system of $N = 20$ phase oscillators coupled with discrete and distributed delays in Fig. 7.18. For each new oscillator that was added to the system, new solutions λ emerged for discrete and distributed delays. Their corresponding real parts move closer to zero in both, unstable and stable branches, and the difference between coupling with discrete opposed to coupling with distributed delays becomes smaller, see Fig. 7.18. Hence, for a growing number N of oscillators in the system, the solution with the largest real part dominating the dynamics close to steady state, changes in stable intervals of $\Omega\tau$, but does not in unstable intervals of $\Omega\tau$. The difference in response to small perturbations in stable regimes of $\Omega\tau$ is most pronounced for perturbation modes with short wavelengths, compared between discrete and distributed delays in the coupling. This is shown again in Fig. 7.19 where we plot the largest $\text{Re}(\lambda)$ versus $\Omega\tau$ for $N = 2, 3, 4, 10, 100, 1000$ oscillators. All plots show the same range of $\Omega\tau$. As the number of oscillators grows, all additional $\text{Re}(\lambda) < 0$ move towards zero, because long wavelength perturbation modes are added to the system, and nearest neighbour interaction counteracts these long wavelength modes less effectively. These are long-lived, and remain in the system when all other perturbation modes have already decayed. In the stable regimes with $\text{Re}(\lambda) > 0$, however, the perturbation modes with the shortest wavelengths grow first, and hence the linear dynamics are governed by these modes.

In summary, a qualitative explanation for these observations can be given in terms of the wavelengths associated to the perturbation modes in the system. The strictly local interactions in systems with nearest neighbour coupling respond most effectively to perturbation modes with short wavelength. In Fig. 7.18 this becomes obvious when looking at the resynchronization rates for the
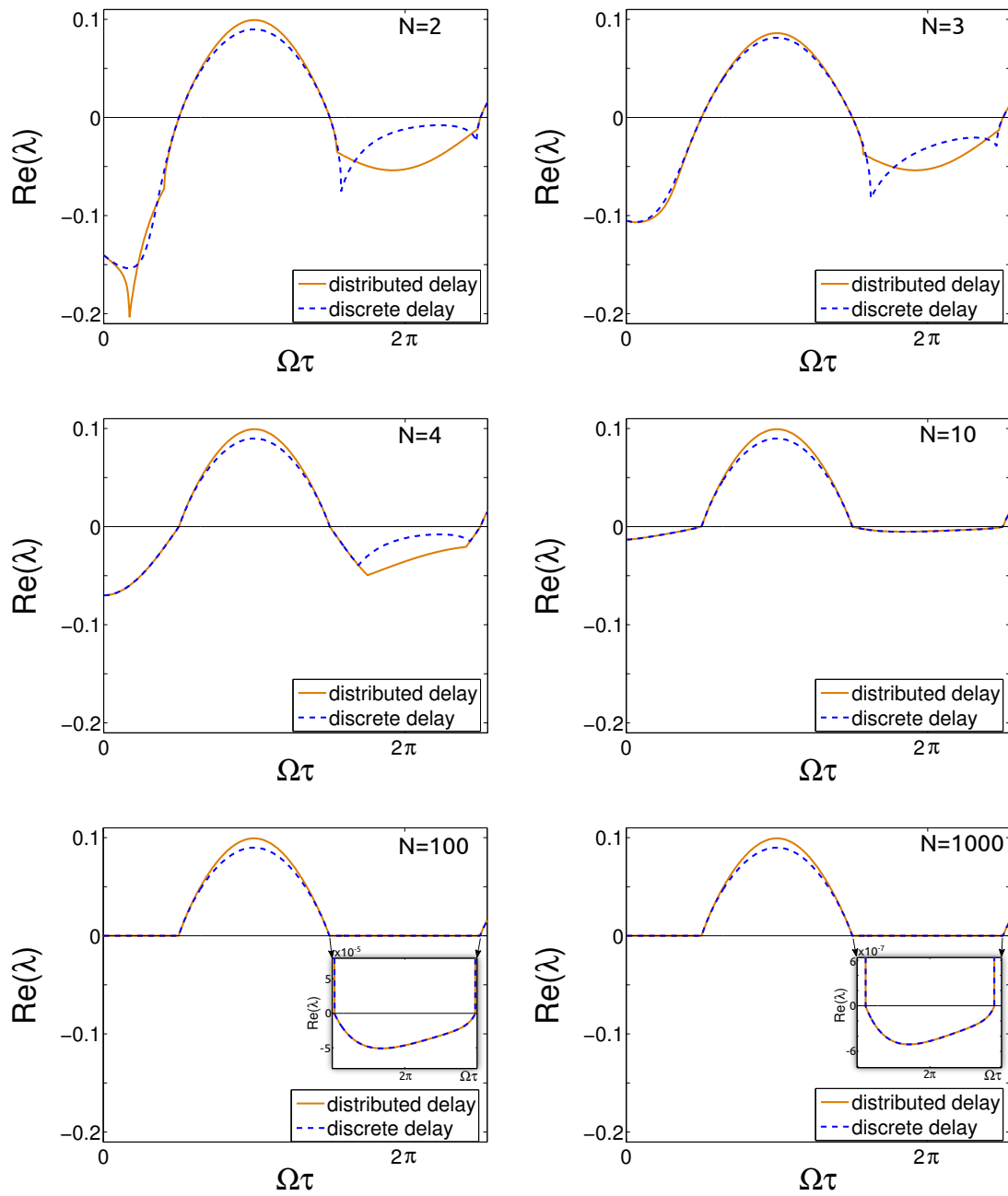
Figure 7.19.: Largest Re(λ) plotted vs. $\Omega\tau$ for different N. This is for a system with coupling strength $K = 0.07\,\mathrm{min}^{-1}$, intrinsic frequency $\omega = 0.223\,\mathrm{min}^{-1}$, nearest neighbour interaction and sinusoidal coupling. The delay distribution is a gamma distribution with $a = 1$ and $b = \tau$.

response to the different perturbation modes in the system. With each new oscillator added to the $1D$ chain, the wavelengths of the associated perturbation modes become longer and decay more slowly. The short ranged interactions are least effective in counteracting these long wavelength perturbation modes.

7.5. Synchrony dynamics in systems with arbitrary coupling topologies

Thus far we have focused on the stability of the phase-locked steady state and on the resynchronization dynamics close to the steady state. The characteristic equation associated to the system, as given by Eq. (6.21), was used to determine linear stability and resynchronization or desynchronization rates. The results were plotted as $\mathrm{Re}(\lambda)$ versus $\Omega\tau$ to show the stability given by the sign of $\mathrm{Re}(\lambda)$ and the resynchronization or desynchronization rate given by the value of $\mathrm{Re}(\lambda)$, see e.g. Fig. 7.3. Plots that show $\mathrm{Im}(\lambda)$ plotted versus $\Omega\tau$ depict the frequency of the dynamics close to steady state, see Fig. 7.4. These results hold for coupling topologies that are characterized by an equal number of connections for each oscillator in the system.

What can we learn for phase-locked systems with an arbitrary number of connections for each oscillator? We return to the characteristic Eq. (6.19):

$$\frac{1}{\hat{g}(\lambda)}\left(\frac{\lambda}{\alpha}+1\right)c_k = \frac{1}{n_k}\sum_{l=1}^{N} d_{kl}\,c_l, \tag{7.76}$$

where n_k denotes the number of connections of each oscillator independently. We define $d_{kl}^* \equiv d_{kl}/n_k$, which gives

$$\frac{1}{\hat{g}(\lambda)}\left(\frac{\lambda}{\alpha}+1\right)c_k = \sum_{l=1}^{N} d_{kl}^*\,c_l, \tag{7.77}$$

i.e.

$$\zeta^*\vec{c} = \mathbb{D}^*\vec{c}, \tag{7.78}$$

where:

$$\zeta^* \equiv \frac{1}{\hat{g}(\lambda)}\left(\frac{\lambda}{\alpha}+1\right). \tag{7.79}$$

This description governs all coupling topologies, where each oscillator can have a different number of connections n_k, but the total coupling strength is conserved for each oscillator. Hence, the right hand side of Eq. (7.79) only contains the influence of the delay distribution $g(s)$, given by its Laplace transform $\hat{g}(\lambda)$, and the left hand side contains all variables related to the coupling topology. These are the eigenvalues ζ_j^*, $j = 1, 2, \ldots, N$, of the coupling matrix $\mathbb{D}^*$.

Coupling matrices with real eigenvalues

For coupling topologies with bidirectional coupling between pairs of oscillators and $d_{kl}^* \in \mathbb{R}$, the resulting coupling matrices are Hermitian. For Hermitian matrices the spectrum of eigenvalues is purely real [144]. We now look at plots similar to Fig. 7.3, but add a new dimension that accounts for different values of $\mathrm{Re}(\zeta_j^*)$ in a given interval. This yields Figs. 7.20-7.21, where the stability given
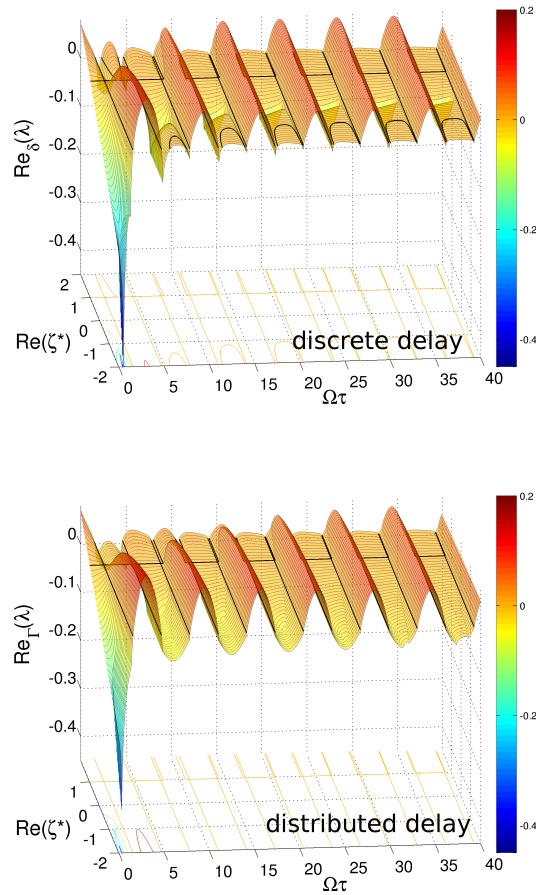
Figure 7.20.: $\mathrm{Re}_\delta(\lambda)$ and $\mathrm{Re}_\Gamma(\lambda)$ plotted versus $\mathrm{Re}(\zeta_j^*)$ and $\Omega\tau$. This is for a system of $N = 10$ oscillators with identical intrinsic frequencies $\omega = 0.224\,\mathrm{min}^{-1}$ and coupling strength $K = 0.07\,\mathrm{min}^{-1}$. The delay kernel $g(s)$ for the lower plot is a gamma distribution with scale parameter $b = \tau$ and shape parameter $a = 1$. The upper plot shows the discrete delay with a Dirac delta delay kernel. Black lines mark the intersections of the surface with the zero plane.
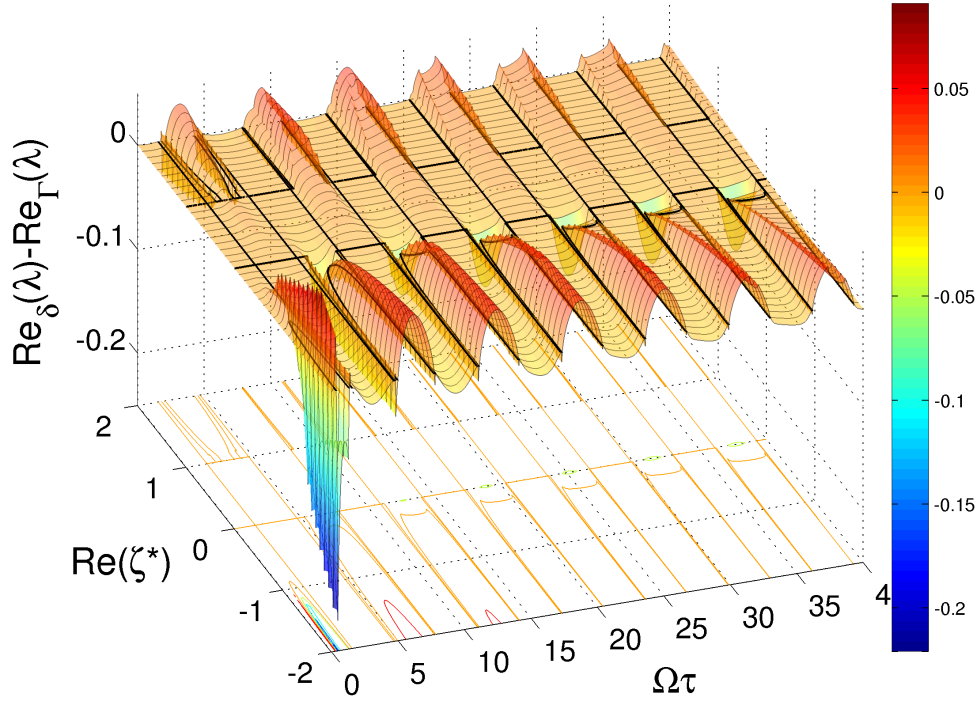
Figure 7.21.: Difference of $\text{Re}_\delta(\lambda)$ (discrete) and $\text{Re}_\Gamma(\lambda)$ (distributed) plotted versus $\text{Re}(\zeta_j^*)$ and $\Omega\tau$. This is plotted for a system of $N = 10$ oscillators with identical intrinsic frequencies $\omega = 0.223\,\text{min}^{-1}$ and coupling strength $K = 0.07\,\text{min}^{-1}$. Compare with single plots in Fig. 7.20.

by $\text{Re}(\lambda)$ is plotted versus $\Omega\tau$ and $\text{Re}(\zeta_j^*)$. The surface above the $\Omega\tau - \text{Re}(\zeta_j^*)$ plane shows the re- and desynchronization rates for all coupling topologies governed by the eigenvalues $\text{Re}(\zeta_j^*)$.

We remember from Chapter 6, that for coupling topologies where each oscillator has the same number of neighbours, stability does not change when comparing discrete and distributed delays. The stability depends only on the mean of the delay distribution. Using plots as described above for discrete and distributed delays, can give an idea whether the result on the steady state stability in Chapter 6 also holds for other coupling topologies. That is especially interesting for coupling topologies, that do not fall into the category as the ones for which this result holds. Note that it may not be possible to realize every $\text{Re}(\zeta_j^*)$, because an associated coupling topology might not exist.

This is shown in Fig. 7.20. We dropped the index j from the notation, since only the λ_j with the largest $\mathrm{Re}(\lambda_j)$ is plotted. It can be observed that there are differences in resynchronization and desynchronization rates for discrete and distributed delays. One can also see this, when moving from negative values of $\mathrm{Re}(\zeta^*)$ towards positive values, the stability can change from stable to unstable for fixed values of $\Omega\tau$. For different (unspecified) coupling topologies the differences in $\mathrm{Re}(\lambda)$ between discrete and distributed delays have different magnitudes. Plotting $\mathrm{Re}_\delta(\lambda) - Re_\Gamma(\lambda)$ versus $\Omega\tau$ and $\mathrm{Re}(\zeta^*)$ in Fig. 7.21, that can be seen more easily. There are large differences close to $\mathrm{Re}(\zeta^*) = 0$ and as one moves to larger values of $|Re(\zeta^*)|$. Note, that the information on stability itself is lost in this plot and not represented by the sign of $\mathrm{Re}_\delta(\lambda) - \mathrm{Re}_\Gamma(\lambda)$.

Coupling matrices with complex eigenvalues

Coupling topologies that also include unidirectional connections are not described by Hermitian matrices, because they are not symmetric [144]. In Fig. 7.22 we choose a fixed value of $\Omega\tau = 5.61$ and plot $\mathrm{Re}(\lambda)$ versus $\zeta^* \in \mathbb{C}$ for discrete on the left, and for distributed delays on the right hand side. Given the result in
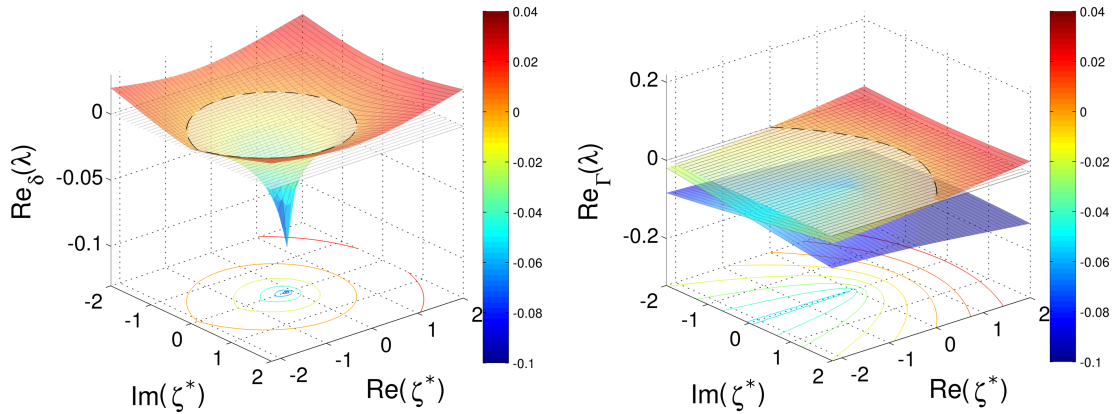
Figure 7.22.: $\mathrm{Re}_{\delta/\Gamma}(\lambda)$ plotted versus $\mathrm{Re}(\zeta^*)$ and $\mathrm{Im}(\zeta^*)$ for discrete (δ) and distributed (Γ) delays. The largest $\mathrm{Re}(\lambda)$ is plotted and the intersection curve with the zero plane where $\mathrm{Re}(\lambda) = 0$ is marked by a black dashed line. The system has identical oscillators with intrinsic frequency $\omega = 0.224\,\mathrm{min}^{-1}$ for fixed $\Omega\tau = 5.61$ ($\Omega = 0.2669\,\mathrm{min}^{-1}$, $\tau = 21\,\mathrm{min}$). The delay kernel $g(s)$ for the right plot is a gamma distribution with scale parameter $b = \tau$ and shape parameter $a = 1$. The left plot which shows the discrete delay has a Dirac delta delay kernel.
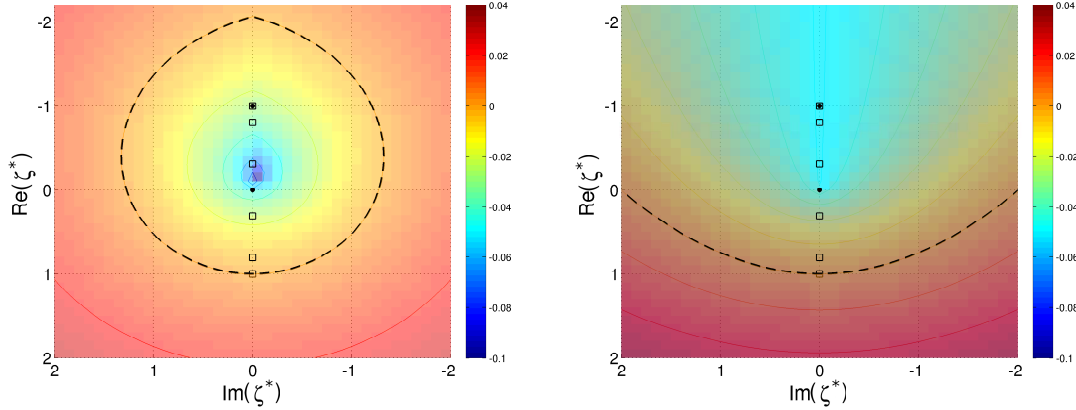
Figure 7.23.: Contour plot of $\text{Re}(\lambda)$ in the $\text{Re}(\zeta^*)$ - $\text{Im}(\zeta^*)$ plane. The values of $\text{Re}(\lambda)$ are given by the colourbar. Those plots correspond to Fig. 7.22. The black, dashed curve shows where $\text{Re}(\lambda) = 0$, and hence stability changes. The dots denote the ζ^* associated to mean-field coupling, and the squares the ζ^* for nearest neighbour coupling.

Chapter 6, we know that for this choice of $\Omega\tau$, the steady state is stable for all coupling topologies where each oscillator has the same number of connections. This means, all eigenvalues ζ^*, associated to these topologies, have to lie in regions of the $\text{Re}(\zeta^*) - Im(\zeta^*)$ plane, where the largest $\text{Re}(\lambda)$ is smaller than zero.

With mean field coupling we find for a system of N oscillators, that the eigenvalues ζ^* of the topology matrix are given by 1 and 0, independent of the number of oscillators. For nearest neighbour coupling the N eigenvalues of the topology, divided by $n_k = 2 \, \forall \, k$, all lie on a line between -1 and 1. They are given by:

$$\zeta_j^* = \frac{\zeta_j}{2} = \cos\left(\frac{2\pi j}{N}\right), \quad j = 1, 2, \ldots, N. \tag{7.80}$$

We have plotted the associated ζ^* for nearest neighbour coupling ($n_k = 2$), shown by the black squares, and the mean field case ($n_k = N$), denoted by black dots for a system of $N = 10$ oscillators into Fig. 7.23. As expected, all ζ^* lie at positions in the $\text{Re}(\zeta^*) - \text{Im}(\zeta^*)$-plane where $\text{Re}(\lambda) < 0$. If the round-shaped region in the left plot of Fig. 7.23 for discrete delay is the only region with solely negative values $\text{Re}_\delta(\lambda)$, then all values of ζ/n_k for coupling topologies included by the result in Chapter 6 have to lie in this region. Since $\text{Re}_\Gamma(\lambda)$ takes on different values, and cuts the zero plane at different lines (except for $\text{Im}(\zeta^*) \approx 0$ and $\text{Re}(\zeta^*) = -1$), we

know that coupling topologies whose associated ζ^* lie outside the region where $\mathrm{Re}_\delta(\lambda) < 0$ but $\mathrm{Re}_\Gamma(\lambda) > 0$, have different stability. We conclude that there could exist coupling topologies for which the stability of the steady state is different for discrete and distributed delays. We will encounter such a case in the next chapter for phase-locked solutions with non-zero phase lags on a ring topology.

7.6. Summary

The dynamics of systems close to steady state were investigated in Chapter 7. We considered different coupling topologies, such as mean field (global) and nearest neighbour (local) interactions. In the previous chapter we had shown that the stability and global frequency of the steady state only depends on the mean delay. This is true for all connection topologies characterized by an equal number of connections for each oscillator. Here we have shown, that the synchrony dynamics in systems with nearest neighbour interactions and gamma distributed delays are different from those with discrete delays, as shown in Figs. 7.3-7.4. Close to steady state the linearized dynamics, driven by the coupling function, are controlled by the phase differences introduced by the mean delay and by the perturbation. If the mean delay is equal to integer multiples of the period of oscillation, the according contribution to the phase difference is not seen by 2π-periodic coupling functions. Hence in such cases, the evaluation of the instantaneous phase differences due to the perturbation, which are small close to steady state, yields weak resynchronization in the case of coupling with discrete delays. Distributed delays however, also consider phase differences associated to the perturbation at times around the mean delay time. Therefore the effective phase differences evaluated are larger, and resynchronization is stronger, as shown in Fig. 7.7.

Values of the mean delay with $\Omega\tau$ close to odd multiples of $\pi/2$ induce large phase differences in the coupling function. These are averaged out by distributed delays that also take into account the delay times around the mean delay which are associated to smaller, delay related, phase differences.

These findings do not hold for all coupling topologies. We found that the linear dynamics in mean-field coupled systems of phase oscillators are independent of the shape of the delay distribution. Hence in this case, distributed delays with a mean equal to the discrete delay yields the same resynchronization properties,

see Fig. 7.1.

In Subsection 7.4.1 we quantified the influences of the shape of the delay distribution on synchrony dynamics. In a system of $N = 2$ identical oscillators with $\omega = 0.223 \, \text{min}^{-1}$, $K = 0.07 \, \text{min}^{-1}$, coupled via nearest neighbour interaction, we showed how synchrony dynamics depends on the variance and skewness of the delay distribution. We observed increasingly different dynamic responses to small perturbations as the variance and skewness were increased.

The role of number of oscillators in the system was addressed in Subsection 7.4.2. With an increasing number of oscillators on a $1D$ chain more perturbation modes with increasing wavelengths become possible. Short ranged interactions are least effective counteracting these long wavelength perturbation modes. We found that the differences in resynchronization rates between coupling with discrete and distributed delays decreased as the wavelength of the perturbation modes increased.

In Section 7.5 we looked at systems of coupled phase oscillators with arbitrary coupling topologies and different delay formulations. For phase-locked solutions, in systems whose characteristic equation is of the type of Eq. (7.79), we treated the eigenvalues of the connectivity matrix as a parameter. This allowed us to get a broad overview on stability properties, especially for more complex coupling topologies, where the eigenvalues of the connectivity matrix are hard to determine, or change in time. Time-dependent coupling topologies, e.g. [13, 38], correspond to series of points $\zeta^*(t)$ which are the eigenvalues associated to the topology. Hence the resynchronization properties are then given by the $\text{Re}(\lambda)$ associated to that series of points $\zeta^*(t)$. For fixed values of $\Omega\tau$ we also found the regions in parameter space $\text{Re}(\zeta^*) - \text{Im}(\zeta^*)$ where stable phase-locked solutions are possible: the regions in the $\text{Re}(\zeta^*) - Im(\zeta^*)$-plane where $\text{Re}(\lambda) < 0$. These regions were compared for the two delay formulations, see Figs. 7.22 and 7.23.

8. The *m*-twist Steady State Solution on a Ring

In this chapter we focus on solutions on rings of oscillators where all oscillators synchronize to a global frequency Ω but keep a constant phase lag to their nearest neighbours, denoted by $\pm\Delta$. We refer to such solutions as *m*-twist solutions [37, 38] or splay states [93, 167]. In biological systems these solutions have been studied in many different situations, reaching from developmental processes to systems of *Physarum* plasmodial slime mold [38, 168, 169].

We study a ring topology, equivalent to a $1D$ chain of oscillators with periodic boundary conditions. For this topology we obtain results for the global frequency and linear stability [35, 37] of these solutions. The oscillators couple only to their nearest neighbours:

$$\dot{\theta}_k(t) = \omega + \frac{K}{2} \sum_{l=k\pm 1} h\left(-\theta_k(t) + \int_0^\infty ds\, g(s)\theta_{k-l}(t-s)\right),\qquad(8.1)$$

$\theta_k(t)$ denotes the phase of oscillator k at time t, $k = 1, 2, \ldots, N$ numbers the oscillators in the system, $g(s)$ is the normalized delay distribution, h is an arbitrary 2π periodic coupling function, K denotes the coupling strength and ω is the intrinsic frequency of each oscillator. We restrict our attention to a simplified situation where all oscillators have a common intrinsic frequency ω.

8.1. Global frequency of *m*-twist steady states

We obtain the global frequency Ω, for the *m*-twist steady states of Eq. (8.1), from Eq. (2.9) and Eq. (8.1):

$$\Omega = \omega + \frac{K}{2} \sum_{l=k\pm 1} h(-\Omega\tau + \Delta l),\qquad(8.2)$$

where:

$$\Delta = \frac{2\pi m}{N}.\qquad(8.3)$$

For a sinusoidal coupling function h we obtain:

$$\Omega = \omega + \frac{K}{2}\left[\sin(-\Omega\tau + \Delta) + \sin(-\Omega\tau - \Delta)\right], \tag{8.4}$$

which can be simplified with the trigonometric relation $\sin(g \pm f) = \cos(f)\sin(g) \pm \cos(g)\sin(f)$, see [144]. The global frequency of the m-twist steady state with sinusoidal coupling is thus given by:

$$\Omega = \omega - K\sin(\Omega\tau)\cos(\Delta). \tag{8.5}$$

Hence for sinusoidal coupling, the frequency of the m-twist solution with $\Delta = 0$ is recovered in the limit $\frac{m}{N} \to 0$, and of course for $m = 0$. This result matches the finding in [35].

With respect to the system discussed in Chapters 6 and 7, with $m = 0$, there are now regimes of $\frac{m}{N}$ in Eq. (8.3) for $m \geq 1$, for which the coupling becomes repulsive. This is the case for $\frac{1}{4} < \frac{m}{N} < \frac{3}{4}$, since such values of $\frac{m}{N}$ result in $\cos(\Delta) < 0$. For example, $\Delta = \pi$ realized by $m = N/2$, makes the coupling repulsive [35]. Note, that this can only be realized for even numbers N of oscillators in the system, since $m \in \mathbb{N}_0$.

Discussion

Plots of Ω versus $\Omega\tau$ obtained from Eq. (8.5) with $m = 0, 1, 2$ for discrete and distributed delays are given in Fig. 8.1. The dashed lines denote the unstable regimes of the solution and the solid lines the stable branches. We discuss the stability analysis in the next section.

We find that the global frequency depends on the value of m. For a system of $N = 5$ oscillators, the cases with $m = \{3, 4\}$ are not explicitly shown in Fig. 8.1, since they are identical to the cases with $m = \{2, 1\}$, respectively. The case $m = 4$ yields the same result as $m = 1$. Only the signs of Δ change with respect to their two nearest neighbours. This is absorbed by the coupling function and the reflection symmetry $\omega \to -\omega$, $\theta_k \to -\theta_k$ of the system. For $m = 3$ and $m = 2$ we find, that in both cases $\cos(\Delta) \approx -0.809$. Hence, they have the same global frequencies. We do not plot $m = 5$ since it is clear by looking at Eq. (8.3), that all oscillators are separated by $\Delta = 2\pi$ from their nearest neighbours. This however is not seen by the 2π periodic coupling function and yields the same result as $m = 0$.

We plotted both, discrete and distributed delays, in independent plots because steady state stability is altered between the delay formulations for $m = 1, 2$. The differences in stability can be seen, when comparing the points where solid lines change to dashed lines and vice versa. For $m = 0$ there is no difference in stability between discrete and distributed delays as predicted. The result on the steady state stability in section 6.3 shows that the phase-locked solution with no phase lags obeys the same stability condition for discrete and distributed delays. In the next section we show how stability can be determined for m-twist solutions on a ring. Then we compare the impact of the different delay types.

8.2. Linear stability of m-twist steady states

The stability of the m-twist solution is determined by means of linear stability analysis. We ask how the system at its steady state responds to a small perturbation. This is studied for linearized dynamics, which are valid close to the steady state [19]. For unstable steady states the perturbation will grow; in the case that steady states are stable, the perturbation will converge to zero with a perturbation decay rate given by $\mathrm{Re}(\lambda)$. Following this idea, we add a perturbation $q_k(t)$ to the phases of the m-twist solution:

$$\theta_k(t) = \Omega t + \Delta k + \epsilon q_k(t), \tag{8.6}$$

with $\epsilon \ll 1$ and substitute that back into Eq. (8.1):

$$\Omega + \epsilon \dot{q}_k(t) = \omega + \frac{K}{2} \sum_{l=k\pm 1} h\left(-\Omega\tau + \Delta l + \epsilon\left[-q_k(t) + \int_0^\infty ds\, g(s) q_l(t-s)\right]\right), \tag{8.7}$$

where τ is the mean of the delay distribution, given by its first moment. Here $\Delta(k+l) - \Delta k = \Delta l$. Taylor expansion for $\epsilon \ll 1$ leads to:

$$\Omega + \epsilon \dot{q}_k(t) = \omega + \frac{K}{2} \sum_{l=k\pm 1} h(-\Omega\tau + \Delta l) +$$
$$\frac{K}{2} \sum_{l=k\pm 1} \left(\epsilon h'(-\Omega\tau + \Delta l)\left[-q_k(t) + \int_0^\infty ds\, g(s) q_l(t-s)\right]\right) + O\left(\epsilon^2\right), \tag{8.8}$$

with h' being the first derivative of h with respect to its argument. Equation (8.8) can be separated in powers of ϵ to yield the equation for the global frequency in steady state:

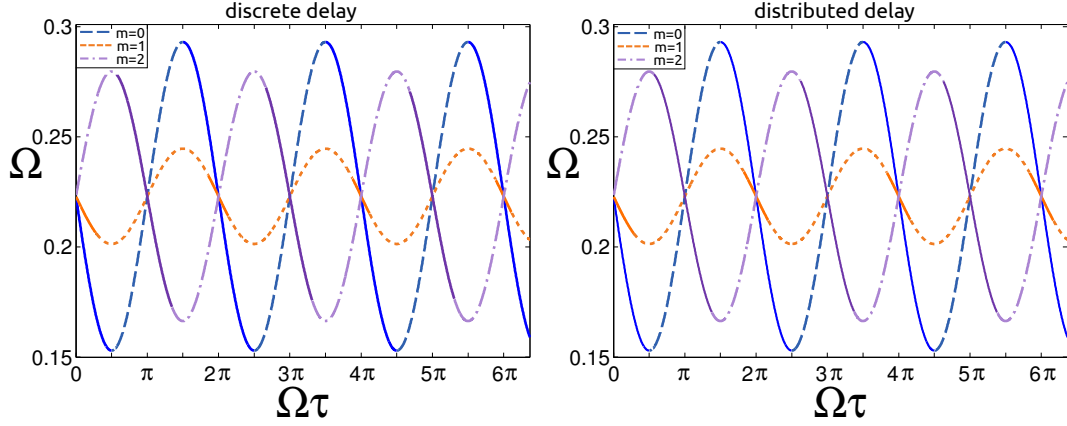$$\epsilon^0: \quad \Omega = \omega + \frac{K}{2} \sum_{l=k\pm 1} h(-\Omega\tau + \Delta l), \tag{8.9}$$

97

Figure 8.1.: Ω plotted versus $\Omega\tau$ for sinusoidal coupling. Each plot shows three curves for different m-twist states $m = \{0, 1, 2\}$. The system parameters are $\omega = 0.223\,\text{min}^{-1}$, $K = 0.07\,\text{min}^{-1}$, $N = 5$ oscillators and nearest neighbour coupling with periodic boundary conditions. The distributed delay kernel is the gamma distribution with parameters $a = 1$ and $b = \tau$. Solid lines denote stable, discontinuous lines unstable m-twist solutions.

and the dynamic equations for the time evolution of the perturbation:

$$\epsilon^1: \quad \dot{q}_k(t) = \frac{K}{2} \sum_{l=k\pm 1} \left(\epsilon h'(-\Omega\tau + \Delta l) \left[-q_k(t) + \int_0^\infty ds\, g(s) q_l(t-s) \right] \right). \quad (8.10)$$

We proceed our analysis with a sinusoidal coupling function h, use the following trigonometric relations [144]:

$$\sin(g \pm f) = \cos(f)\sin(g) \pm \cos(g)\sin(f), \quad (8.11)$$

$$\cos(g \pm f) = \cos(g)\cos(f) \mp \sin(g)\sin(f), \quad (8.12)$$

and confirm the global frequency Ω as previously determined in Eq. (8.5):

$$\Omega = \omega - K\sin(\Omega\tau)\cos(\Delta), \quad (8.13)$$

consistent with Eq. (8.5). Next we introduce a perturbation of the form $q_k(t) = c_k e^{\lambda t}$ in Eq. (8.10), that then reads:

$$\begin{aligned}
c_k \lambda &= \frac{K}{2} \sum_{l=k\pm 1} \cos(-\Omega\tau + \Delta l) \left[-c_k + \int_0^\infty ds\, g(s) c_l e^{-\lambda s} \right] \quad (8.14) \\
&= \frac{K}{2} \{ \cos(\Omega\tau - \Delta)[c_{k+1}\hat{g}(\lambda) - c_k] + \cos(\Omega\tau + \Delta)[c_{k-1}\hat{g}(\lambda) - c_k] \},
\end{aligned}$$

98

where $\hat{g}(\lambda)$ denotes the Laplace transform of $g(s)$:

$$\hat{g}(\lambda) = \int_0^\infty ds\, g(s)\, e^{-\lambda s}.$$

Defining:

$$\begin{aligned} A &= \cos(\Omega\tau - \Delta), \\ B &= \cos(\Omega\tau + \Delta), \end{aligned} \tag{8.15}$$

and comparing Eq. (8.11) and Eq. (8.12) yields:

$$\begin{aligned} A + B &= 2\cos(\Omega\tau)\cos(\Delta), \\ A - B &= 2\sin(\Omega\tau)\sin(\Delta). \end{aligned} \tag{8.16}$$

The characteristic equation

After rearranging and applying the latter definitions, Eq. (8.14) implies:

$$c_k \lambda = \frac{K}{2}\{\hat{g}(\lambda)[A c_{k+1} + B c_{k-1}] - c_k(A+B)\}, \tag{8.17}$$

which can be further rewritten using $\vec{c} = (c_1, c_2, \ldots, c_N)^T$. It contains the components associated to the different perturbation modes. Note that further rearrangement of the equation:

$$(2\lambda + K(A+B)) c_k = K\hat{g}(\lambda)[A c_{k+1} + B c_{k-1}], \tag{8.18}$$

allows only λ for which $\hat{g}(\lambda)$ is well defined and:

$$\hat{g}(\lambda) \neq 0. \tag{8.19}$$

In matrix notation the characteristic equation then reads:

$$\left(\frac{2\lambda + K(A+B)}{K\hat{g}(\lambda)}\right)\vec{c} = \mathbb{D}\vec{c}, \tag{8.20}$$

where $\mathbb{D}$ is the connectivity matrix for a system of N oscillators:

$$\mathbb{D} = \begin{pmatrix} 0 & A & 0 & \ldots & \ldots & \ldots & 0 & B \\ B & 0 & A & 0 & \ldots & \ldots & 0 & 0 \\ 0 & B & 0 & A & 0 & \ldots & 0 & 0 \\ \vdots & & \ddots & \ddots & \ddots & & & \vdots \\ \vdots & & & \ddots & \ddots & \ddots & & \vdots \\ 0 & 0 & 0 & \ldots & B & 0 & A & 0 \\ 0 & 0 & 0 & \ldots & \ldots & B & 0 & A \\ A & 0 & 0 & \ldots & \ldots & \ldots & B & 0 \end{pmatrix}. \tag{8.21}$$

The eigenvalues of this matrix can be found using the solutions to the N-th cyclotomic polynomial, see Appendix A.6 and [163, 164], which are the N roots of unity as given by:

$$w_j^k = \exp\left(i\frac{2\pi j k}{N}\right) \quad \text{where} \quad j = 1, 2, \dots, N. \tag{8.22}$$

We use them to construct the eigenvectors $\vec{c}$:

$$\vec{c}_j = (w_j^1, w_j^2, \dots, w_j^N)^T, \tag{8.23}$$

with $w^N = w^0 = 1$ and $w^{-1} = w^{N-1}$. see Eq. (8.22). We find from the evaluation of the right hand side of Eq. (8.20):

$$\mathbb{D}\vec{c} = \begin{pmatrix} Aw^2 + Bw^N \\ Aw^3 + Bw \\ \vdots \\ Aw + Bw^{N-1} \end{pmatrix} = \underbrace{\left(Aw + Bw^{N-1}\right)}_{=\zeta_j} \begin{pmatrix} w^1 \\ w^2 \\ \vdots \\ w^N \end{pmatrix}, \tag{8.24}$$

that a term $Aw + Bw^{N-1}$ can be separated of each component of the vector $\mathbb{D}\vec{c}$, which must be the eigenvalues ζ_j of the matrix $\mathbb{D}$ for N oscillators on a ring. Simplifying the term for the eigenvalues using $w^{N-1} = w^N, w^{-1} = w^{N-1}$, yields an expression for the complex eigenvalues ζ_j:

$$\zeta_j = (A + B)\cos\left(\frac{2\pi j}{N}\right) + i(A - B)\sin\left(\frac{2\pi j}{N}\right), \quad j = 1, 2, \dots, N. \tag{8.25}$$

With the definitions in Eq. (8.16), one finds that these eigenvalues are purely real for $\Omega\tau = \pi n$, $n \in \mathbb{N}$ and purely imaginary for $\Omega\tau = \frac{\pi}{2}(2n + 1)$, $n \in \mathbb{N}$. One can also see that for $m = \frac{N}{4}(2n + 1)$, with $n \in \mathbb{N}$ the real part $\text{Re}(\zeta_j) = 0$ and for $m = \frac{N}{2}n$, $n \in \mathbb{N}$ the imaginary part $\text{Im}(\zeta_j) = 0$.

Given the solution for the ζ_j given by Eq. (8.25), the characteristic equations for discrete delays and distributed delays with a gamma distribution, can be written as:

$$\text{discrete:} \quad e^{\lambda_j \tau}\left(\frac{2\lambda_j + K(A + B)}{K}\right) = \zeta_j, \tag{8.26}$$

$$\text{gamma:} \quad \left(1 + \lambda_{ji} b\right)^a \left(\frac{2\lambda_{ji} + K(A + B)}{K}\right) = \zeta_j, \tag{8.27}$$

where $j = 1, 2, \dots, N$, and $i = 0, 1, \dots, a$. We substituted the delay dependent Laplace transforms given by Eq. (7.27) and Eq. (7.25). The gamma distribution has the parameters $a = 1$ and $b = \tau$ for all examples that are treated in this
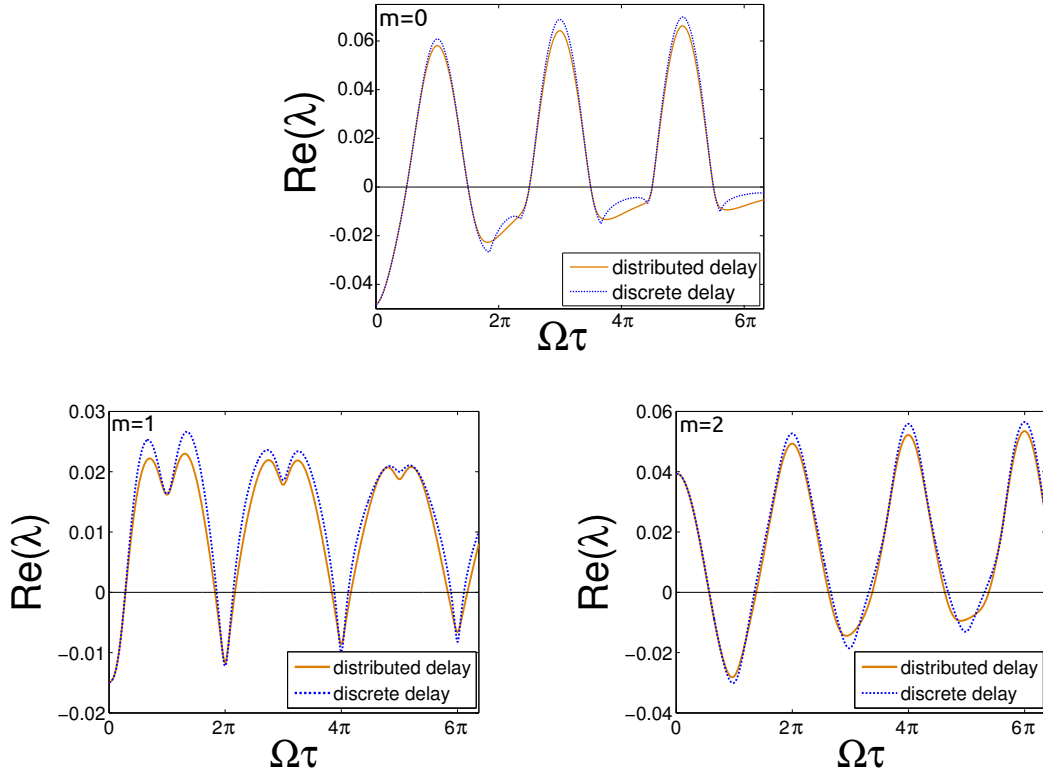
Figure 8.2.: Largest Re(λ) plotted versus $\Omega\tau$ for sinusoidal coupling. Three plots for different m-twist states $m = \{0, 1, 2\}$, intrinsic frequency $\omega = 0.223\,\text{min}^{-1}$, coupling strength $K = 0.07\,\text{min}^{-1}$, $N = 5$ oscillators and nearest neighbour coupling with periodic boundary conditions. The curves are obtained, solving Eq. (8.26-8.27). The distributed delay kernel is the gamma distribution with parameters $a = 1$ and $b = \tau$. Note the different stability boundaries of the two delay cases, see zoom in Fig. 8.3

chapter. This constitutes the case of an exponential distribution. These expressions can be analyzed to determine the solutions λ. Parameter choices satisfying $\text{Re}\left(\lambda_j\right) < 0 \ \forall \ j$, are stable with the global frequency given by Eq. (8.13). If there is a $\text{Re}\left(\lambda_j\right) > 0$ the solution is unstable, since at least one perturbation mode grows exponentially close to steady state.

We solve Eqs. (8.26) and (8.27), using the trust-region dogleg algorithm, implemented in the fsolve function in Matlab, see [165, 166]. Then we plotted the results for $N = 5$ oscillators and $m = \{0, 1, 2\}$ in Fig. 8.2, and a zoom of the second stable branch, with $\text{Re}(\lambda) < 0$, for $m = 1$ in Fig. 8.3.
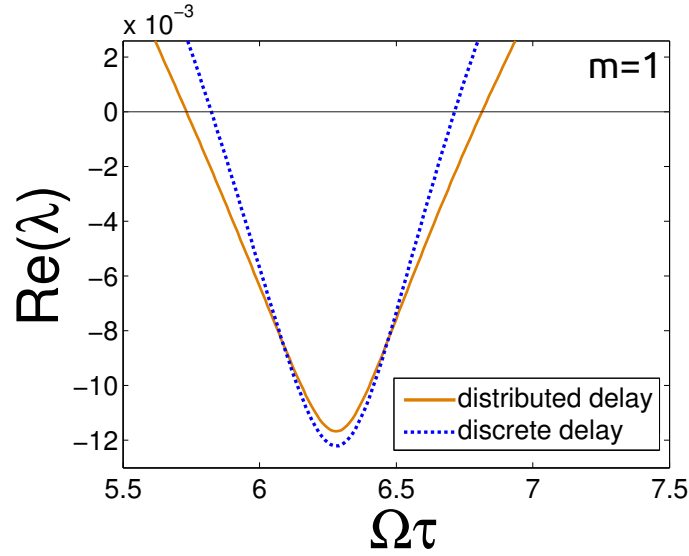
Figure 8.3.: Zoom of Fig. 8.2, for $m = 1$, second stable branch. The curves for distributed delays show an extended stable interval of $\Omega\tau$ compared to discrete delay.

Discussion

The plots in Fig. 8.2 compare the stable and unstable regions with discrete and distributed delays, for m-twist steady states with different values m. Positive values of $\text{Re}(\lambda)$ denote unstable regimes. Perturbations grow in these regions as the system evolves. The unstable mode grows exponentially in time with a growth rate given by the value of $\text{Re}(\lambda)$. Negative values depict stable parameter regimes of $\Omega\tau$. The last perturbation mode that is present in the system decays exponentially with a decay constant given by $\text{Re}(\lambda)$. That information was used in Fig. 8.1, which shows the global frequencies Ω in dependence of $\Omega\tau$ to mark stable and unstable solutions. One can see that the stability of m-twist steady states on a $1D$-ring depends on the winding number m [35], and also changes for different formulations of the delay, if $m > 0$. The stable regions are larger for distributed delays with a gamma distribution, compared to the case of discrete delays. These results show that the findings on the stability of phase-locked solutions with no phase lags in Chapter 6, Section 6.3, do not extend to m-twist steady states with $m \neq 0$.

8.3. Summary

In this chapter we investigated the stability of m-twist steady states and the linearized dynamics close to these steady states in systems of delay coupled phase oscillators. We found that by introducing distributed delays with non-zero variance the intervals of $\Omega\tau$ that govern stable m-twist steady states are enlarged compared to discrete delays for all $m \neq 0$. This is shown in Figs. 8.2-9.1. A previous result [35] on m-twist steady states reported that finite discrete time delays allow stable m-twist steady states in certain ranges of $\Omega\tau$ that do not allow stable solutions in systems without delay. Hence, they have found that discrete delays can expand the range and stability of possible phase-locked patterns. These stable regions seem to be increased even further by distributed delays with non-zero variance for m-twist solutions with $m \neq 0$. In order to determine the dependence of the stable regimes on the variance of the delay distribution, simulations with the two-step delay distribution such as in Chapter 6 presented could be performed.

9. Dynamics Approaching the *m*-twist Steady States

In the previous chapter we have discussed the expression for the global frequency of the general m-twist solution [35] and the characteristic equation that determines the linear stability of steady state solutions. We found that for $m > 0$ linear stability of the m-twist steady states is affected by distributed delays.

In this chapter we derive the relation between the order parameter and the perturbation decay and growth rates. We are interested in the dynamics, as the system approaches the m-twist steady states. Finally, we compare the analytically obtained results with simulations.

9.1. Relation between order parameter and perturbation modes

The measure of the system's synchrony is given by the order parameter $r(t)$, but the perturbation decay rates are given by $x = \text{Re}(\lambda)$ and $y = \text{Im}(\lambda)$. A relation between $r(t)$ and λ is derived in order to compare analytically obtained solutions λ, and measured order parameters from simulation. We proceed similarly as in Section 7.2, but with Eq. (8.6):

$$\theta_k(t) = \Omega t + \Delta k + \epsilon q_k(t),$$

for the perturbed m-twist solution that describes the time evolution of the phases of the oscillators. Combined with Eq. (1.3), this gives:

$$r(t)e^{i\Xi(t)} \equiv \frac{1}{N} \sum_{k=1}^{N} e^{i\theta_k(t)},$$

for the synchronization order parameter $r(t)$. That means:

$$r(t)e^{i\Xi(t)} = \frac{1}{N} \sum_{k=1}^{N} e^{i(\Omega t + \Delta k + \epsilon q_k(t))}. \tag{9.1}$$

Rearranging equation Eq. (9.1) yields:

$$r(t)e^{i(\Xi(t)-\Omega t)} = \frac{1}{N}\sum_{k=1}^{N}[\cos(\Delta k + \epsilon q_k(t)) + i\sin(\Delta k + \epsilon q_k(t))]. \qquad (9.2)$$

We are interested in the modulus of the order parameter $r(t)$. Squaring the last equation eliminates the phases:

$$r(t)^2 = \frac{1}{N^2}\left\{\left(\sum_{k=1}^{N}\cos(\Delta k + \epsilon q_k(t))\right)^2 + \left(\sum_{k=1}^{N}\sin(\Delta k + \epsilon q_k(t))\right)^2\right\}, \qquad (9.3)$$

and since $\epsilon \ll 1$, we expand the sine and cosine terms to second order in ϵ:

$$\cos(\Delta k + \epsilon q_k(t)) = \cos(\Delta k) - \epsilon q_k(t)\sin(\Delta k) - \frac{\epsilon^2}{2}q_k(t)\cos(\Delta k) + O\left(\epsilon^3\right),$$

$$\sin(\Delta k + \epsilon q_k(t)) = \sin(\Delta k) + \epsilon q_k(t)\cos(\Delta k) - \frac{\epsilon^2}{2}q_k(t)\cos(\Delta k) + O\left(\epsilon^3\right). \; (9.4)$$

These expressions are substituted into Eq. (9.3). The sum over the zero order term in each expansion is zero inside both squared brackets, meaning $\sum_{k=1}^{N}\sin(\Delta k) = 0$ and $\sum_{k=1}^{N}\cos(\Delta k) = 0$, see [163, 164], and Appendix A.6. Hence, there are two terms left in the squared brackets, one with order ϵ and the other with ϵ^2. Dropping terms of order ϵ^2 and higher yields:

$$r(t)^2 = \frac{1}{N^2}\left\{\left(\sum_{k=1}^{N}\epsilon q_k(t)\sin(\Delta k)\right)^2 + \left(\sum_{k=1}^{N}\epsilon q_k(t)\cos(\Delta k)\right)^2\right\}. \qquad (9.5)$$

The time-dependent perturbation is then given by:

$$\epsilon q_k(t) = \frac{1}{2}\left(c_k e^{\lambda t} + c_k^* e^{\lambda^* t}\right) = e^{xt}\left[c_k^{Re}\cos(yt) - c_k^{Im}\sin(yt)\right], \qquad (9.6)$$

where $\lambda = x + iy$ and $c_k = c_k^{Re} + ic_k^{Im}$. Here x denotes the perturbation decay rate and y the frequency of oscillation of the decay process. We use Eq. (8.22) to substitute the terms c_k^{Re} and c_k^{Im} in Eq. (9.6), which is then substituted into Eq. (9.5):

$$r(t)^2 = \frac{e^{2xt}}{N^2}\left\{\left(\sum_{k=1}^{N}\left[\cos\left(\frac{2\pi k}{N}\right)\cos(yt) - \sin\left(\frac{2\pi k}{N}\right)\sin(yt)\right]\sin(\Delta k)\right)^2\right\} +$$

$$\frac{e^{2xt}}{N^2}\left\{\left(\sum_{k=1}^{N}\left[\cos\left(\frac{2\pi k}{N}\right)\cos(yt) - \sin\left(\frac{2\pi k}{N}\right)\sin(yt)\right]\cos(\Delta k)\right)^2\right\}. \qquad (9.7)$$

For $m = 1$, such that $\Delta k = \frac{2\pi k}{N}$, we evaluate the product inside the squared braces:

$$r(t)^2 = \frac{e^{2xt}}{N^2} \left\{ \left(\sum_{k=1}^{N} \left[\sin\left(\frac{2\pi k}{N}\right) \cos\left(\frac{2\pi k}{N}\right) \cos(yt) - \sin^2\left(\frac{2\pi k}{N}\right) \sin(yt) \right] \right)^2 \right\} + $$

$$\frac{e^{2xt}}{N^2} \left\{ \left(\sum_{k=1}^{N} \left[\cos^2\left(\frac{2\pi k}{N}\right) \cos(yt) - \cos\left(\frac{2\pi k}{N}\right) \sin\left(\frac{2\pi k}{N}\right) \sin(yt) \right] \right)^2 \right\}. \quad (9.8)$$

We use the trigonometric relations taken from [144]:

$$\cos(f)\sin(f) = \frac{1}{2}\sin(2f), \quad (9.9)$$

$$\sin^2(f) = \frac{1}{2}(1 - \cos(2f)), \quad (9.10)$$

$$\cos^2(f) = \frac{1}{2}(1 + \cos(2f)), \quad (9.11)$$

to rewrite the terms in Eq. (9.8). Noting that:

$$\sum_{k=1}^{N} \cos\left(\frac{4\pi k}{N}\right) = 0, \quad (9.12)$$

$$\sum_{k=1}^{N} \sin\left(\frac{4\pi k}{N}\right) = 0. \quad (9.13)$$

Eq. (9.8) can be drastically simplified to obtain:

$$\log[r(t)] = xt + \log(2). \quad (9.14)$$

This is the desired relation between order parameter $r(t)$ and the λ for the slowest decaying perturbation mode. We use Eq. (9.14) to compare analytically obtained results for λ, e.g. Fig. 8.2, with simulations of the system that yield the time series $r(t)$.

Comparison to simulation results

In the last chapter we found that the stability of the m-twist steady state and the dynamics close to steady state for $m > 0$ are altered by distributed delays represented using a gamma distribution, as compared to discrete delays. Here we compare to simulation results with a sinusoidal coupling function. The initial phase history necessary for the simulation of delay systems was given by evolving the uncoupled oscillators with an intrinsic frequency equal to the global frequency of the 1-twist steady state.
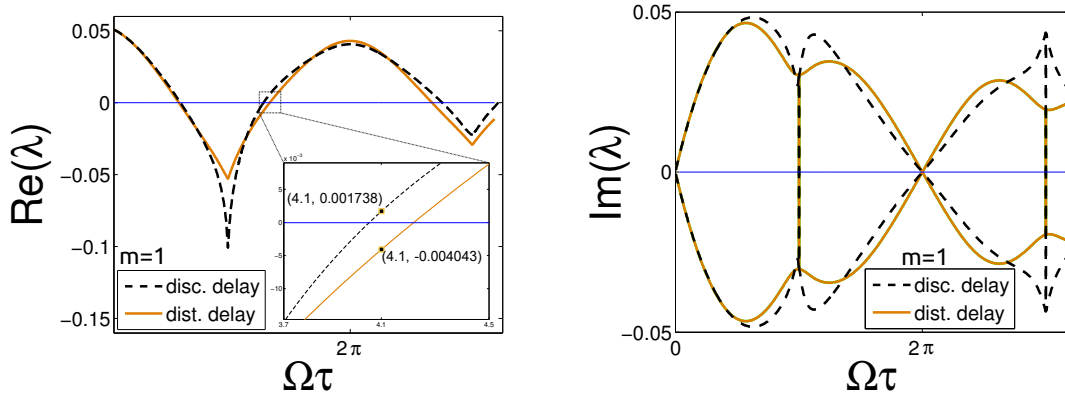
Figure 9.1.: Re(λ) and Im(λ) versus $\Omega\tau$ for discrete and distributed delays. The distributed delay kernel is the gamma distribution with parameters $a = 1$ and $b = \tau$. The inset shows the analytically obtained values of Re(λ) at $\Omega\tau = 4.1$ ($\tau = 21.09\,\text{min}$, $\Omega = 0.1944$). This is for sinusoidal coupling, $\omega = 0.223\,\text{min}^{-1}$, $K = 0.07\,\text{min}^{-1}$, $N = 3$ oscillators and nearest neighbour coupling with periodic boundary conditions.

We simulate a system of $N = 3$ oscillators with a mean communication delay of $\tau = 21.09\,\text{min}$, at $\Omega\tau = 4.1$. These parameters are chosen, because at this value
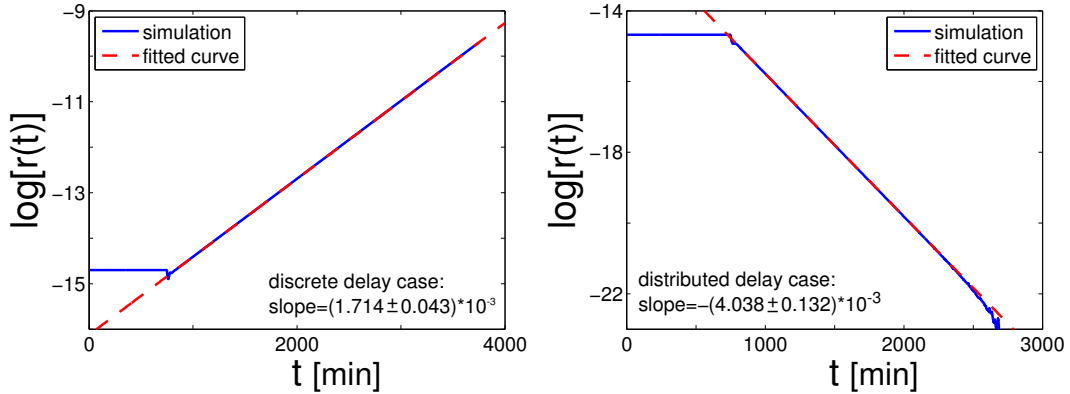
Figure 9.2.: $\log[r(t)]$ plotted versus t for $N = 3$ identical oscillators. The fitted dashed curves in red have slope $(1.714 \pm 0.043) \times 10^{-3}$ (left) and $-(4.038 \pm 0.132) \times 10^{-3}$ (right). Here $K = 0.07\,\text{min}^{-1}$, $\omega = 0.223\,\text{min}^{-1}$, $\tau = 21.09\,\text{min}$, with sinusoidal coupling function and $m = 1$ twist. The distributed delay kernel is the gamma distribution with parameters $a = 1$ and $b = \tau$.

of the mean delay the analytically obtained solution for the case with discrete delays is unstable, while the case with distributed delays is stable. The corresponding interval of $\Omega\tau$ is shown in the left plot of Fig. 9.1, which shows the analytically obtained curves for $\mathrm{Re}(\lambda)$ in dependence of $\Omega\tau$. These were obtained using the trust-region dogleg algorithm, implemented in the fsolve function in Matlab, see [165, 166].

The order parameter was measured in simulation, and plotted logarithmically versus time in Fig. 9.2 for both delay cases. It can be seen that for discrete delays the order parameter grows exponentially, as expected for an unstable solution. In the case of distributed delays the perturbation decays exponentially, hence the solution is stable. This confirms the analytically obtained results on linear stability at this value of $\Omega\tau$. We also measured the slopes of the curves and compared to value of $\mathrm{Re}(\lambda)$, obtained analytically from the characteristic Eqs. (8.26) and (8.27). The slopes of the fitted curves confirm the results at $\Omega\tau = 4.1$ shown in Fig. 9.2.

9.2. Summary

This last chapter addressed resynchronization dynamics in response to a small perturbation about m-twist steady states. Looking at Fig. 8.2, we observe that the resynchronization rate $|\mathrm{Re}(\lambda)|$ depends on the value of $\Omega\tau$, and is different comparing discrete and distributed delays. There are intervals of $\Omega\tau$ where coupling with distributed delays leads to faster resynchronization or desynchronization and also intervals where exactly the opposite can be observed. This could be explained with similar reasoning as in Chapter 7, where we separated the phase differences seen by the coupling function into real existing phase differences and those introduced by the mean delay. In this case however, there is an additional influence of the fixed phase difference Δ between the oscillators that has to be taken into account. The intervals of $\Omega\tau$ in which coupling with distributed delays resynchronizes faster than with discrete delays are not conserved, since the stable and unstable regimes shift to other values of $\Omega\tau$ for m-twist solutions with $m \geq 1$.

10. Conclusions and Outlook

In this thesis we studied the effects of distributed delays in systems of coupled phase oscillators. We focused on the linear stability of the steady states. In addition, the transient dynamics close to the steady states of phase-locked solutions with and without phase lags were investigated. For our analysis we used tools from dynamical systems theory [19, 154], including characteristic equations obtained linearising around the steady states of the system. These dynamic equations were then employed to ask how such systems react to small perturbations when close to the steady state.

In Chapters 1 and 2 we presented a short introduction on synchronization phenomena in systems of coupled phase oscillators. Some historical examples of synchronization and the first explanation attempts [4, 16] were summarised to make the reader familiar with the topic. Phase-locked solutions were introduced, where all oscillators synchronize to a global frequency and share the same phase. Another type of solution also sharing a common global frequency in steady state was introduced, having specific non-zero phase relations between neighbouring oscillators. We discussed two major coupling topologies, the mean-field approximation for global interactions between the oscillators, and local interactions mediated by nearest neighbour coupling. Such interactions, which include the exchange of signals between different parts in the system, require time to be completed. This is what we call a time delay in communication processes. If time delays in the system are of the order of the timescales that govern the dynamics, they can lead to qualitatively new behavior and cannot be neglected [68]. We compared different types of time delays in the coupling, distinguishing between the influence of one discrete past time and entire intervals of the past.

In Chapter 3 we introduced the vertebrate segmentation clock, that provides the rhythm for the formation of somites, which set the template for segmented structures in growing vertebrates [98]. The clock and wavefront mechanism of vertebrate segmentation [96] proposes temporal oscillations that are arrested

111

and thereby translated into spatial patterns by a travelling wavefront. We discussed experimental evidence for different parts of this clock [99, 116, 117, 140, 142] and its biochemical functionality.

There are experiments [123, 126] that suggest the existence of an auto-inhibitory feedback loop with time delays in the expression of certain genes, leading to cyclic gene expression [63]. On the tissue level, patterns of locally synchronized gene expression levels have been observed [116]. The locally acting Delta-Notch signalling pathway [130] has been shown to be involved in coupling individual oscillations [32, 99, 101], and therefore leading to locally synchronized regions.

Finally we introduced the Delayed Coupling Theory of vertebrate segmentation [56]. It is based on the concept of the clock and wavefront mechanism. This model of delay coupled phase oscillators with discrete delays in the coupling successfully predicted the dependence of the length of somites on the time delays of intercellular communication [113]. Motivated by this model, we asked whether the approximation of discrete delays in the coupling captures all effects of the delayed signalling in the tissue. In order to investigate this, we formulated a model of coupled phase oscillators with distributed delays in the coupling. We ask what effects are introduced when considering the entire past of the neighbours, as compared to discrete delays homogeneous and constant in time.

In Chapter 4 we present an outline on how the remainder of the thesis is organised.

In Chapter 5 we introduced a model of coupled phase oscillators with distributed delays in the coupling. Details were given on how distributed delays are formulated, as compared to other types of interaction delays.

In Chapter 6 we show that the global frequency of the phase-locked steady state only depends on the mean of the delay distribution. It is given by Eq. (6.5) which is the same as for discrete delay, if the mean of the delay distribution equals the discrete delay. We also obtain an important result on the linear stability of the phase-locked steady state with no phase lags. The result is valid for a large class of coupling topologies; we only demand the number of connections to neighbours to be equal for all oscillators in the system. For such systems we can extend the linear stability condition for systems with discrete delays, obtained by Earl and Strogatz [155], to systems with distributed delays. We show that the stability condition only depends on the mean of the delay distribution, but not on

higher moments associated to the shape or symmetry of the distribution. Hence, if the mean of the delay distribution equals the value of the discrete delay, the steady state stability condition given in Eq. (6.39) is not altered by coupling with distributed delays.

With regard to the Delayed Coupling Theory of vertebrate segmentation [56], we conclude that the approximation with discrete delays in the coupling yields the same results for steady state properties of the system, as compared to distributed delays in the coupling. Hence in systems of coupled phase oscillators with an equal number of connections for each oscillator, steady state results do not depend on the shape of the delay distribution, and a formulation with discrete delay is sufficient.

In Chapter 7 we investigated the linear dynamics close to steady state in response to a small perturbation. We asked whether the synchronization dynamics are affected by using distributed delays instead of discrete delays in the coupling. We found that the linear dynamics in response to small perturbations can depend on the shape of the delay distribution, but not necessarily for all coupling topologies. In mean-field coupled systems, for example, there are no differences between the two models of the delay, see Fig. 7.1. For systems of oscillators with nearest neighbour sinusoidal coupling we find that the resynchronization dynamics depend on the shape of the delay distribution, see e.g. Figs. 7.3 and 7.19. Hence we conclude that, depending on the coupling topology, there can be different dynamic response to small perturbations when using coupling with distributed delays, as compared to discrete delays.

The phase differences evaluated by the coupling function consist of the instantaneous phase difference present in the system, and an additional phase difference introduced by the coupling delay. In a system close to a stable steady state, the instantaneous phase differences are small, and the coupling strength depends strongly on the phase difference imposed by the delay. For discrete delays, the delay induced phase difference has no effects when close to multiples of 2π, because the coupling function is 2π-periodic. Hence the coupling is weak due to the small instantaneous phase difference present in the system. Distributed delays however also consider values around that 2π-multiple mean delay value, and therefore couple more strongly. This results in faster resynchronization. Close to odd multiples of $\pi/2$ this behavior is reversed, since the delay induced phase difference has its maximum and results in strong coupling with discrete

delay. Distributed delays in turn also consider times around these odd multiples of $\pi/2$ and hence couple less strongly.

In the remainder of this chapter we quantified the influence of the variance and skewness of a two-step delay distribution on resynchronization dynamics for different values of the mean. The two-step delay distribution was introduced in Appendix A.1. We found that for fixed values of the skewness, an increasing variance favours the differences in resynchronization rates between discrete and distributed delays, as shown in Figs. 7.12-7.14. The impact on synchrony dynamics changing the skewness for fixed values of the variance is much smaller, see Fig. 7.17.

In Chapter 8 we investigated the linear stability of the steady states of phase-locked solutions with non-zero phase lags, so-called m-twists or splay states [37, 93]. We considered a one-dimensional system of phase oscillators with nearest neighbour interaction and periodic boundary conditions. Previous results for these m-twist solutions showed that discrete delay expands the range and stability of possible phase-locked solutions with $m \neq 0$ [35]. Our results show that coupling with distributed delays can lead to an additional increase of stable regions.

In Chapter 9 we addressed the resynchronization dynamics of m-twists. We derived a relation between the Kuramoto order parameter and the perturbation decay and growth rates in Eq. (9.14). This relation was then used to test the results in Fig. 9.2. Systems of $N = 3$ oscillators with discrete and distributed delays in the coupling were simulated, sharing the same mean delay value τ, and the order parameter time evolution was recorded. We plotted the time series data from simulation and fitted these curves using Eq. (9.14). The slope of perturbation decay for distributed delays matched the analytically obtained value, within the error of the linear least square fit. Also the predicted perturbation growth in the case of coupling with discrete delays was confirmed. See Fig. 9.2 for these results.

Outlook

In the last paragraphs we recapitulated the results on steady state stability and the differences in linear dynamic response to small perturbations in systems of coupled phase oscillators with discrete and distributed delays in the coupling.

The steady state stability does not depend on the shape of the delay distribution for synchronized phase-locked solutions, nor on the dimension. This holds in systems with arbitrary coupling topologies with the constraint that each oscillator couples to the same number of other oscillators in the system. Hence, all steady state results in systems of delay coupled phase oscillators with an equal number of connections for each oscillator, are sufficiently described by the discrete delay approximation.

For m-twist or splay state solutions in these systems we found that for all $m \neq 0$ the stability of the steady state is dependent on the shape of the delay distribution. This could be relevant for systems of delay coupled oscillators where such solutions are observed; for example in apical area oscillations during dorsal closure in the fruit fly *Drosophila melanogaster* [170, 171] or in the circadian clock for the left and right suprachiasmatic nuclei [172]. Antiphase oscillations of endothelium and smooth muscle $[Ca^{2+}]_i$ in vasomotion of rat mesenteric small arteries have been reported in [173]. Such oscillations are abundant and have been observed in neuronal [174, 175], mechanical [176], chemical [177], and superconducting systems [178]. Anti-phase oscillations constitute a special case of the splay state or m-twist solutions, namely the case of $m = N/2$ where N denotes the number of oscillators in the system. The analysis on the linear dynamics in response to small perturbation for the m-twist or splay state solutions has not been completed. An analysis more in depth of the qualitative and quantitative dependence of the m-twist steady state stability and response to small perturbations on the shape of the delay distribution should be conducted.

The results on the linear dynamic response to small perturbations in Chapter 7 for phase-locked solutions without phase lags suggest that distributed delays in nearest neighbour coupling can enhance the ability to react to small perturbations when the mean delay is close to a multiple of the uncoupled oscillator's period.

Current experimental work suggests that cells taken from zebrafish embryos might soon allow to conduct in vitro experiments where individual cells can be brought into contact, and anti-phase or in-phase synchronized states of cyclic gene expression might be observable. If the mean delay time for Delta-Notch coupling could be changed in these cells, such that the mean delay value is altered and the respective state becomes unstable, data on desynchronization rates could be obtained and compared to the two modelling approaches with

discrete and distributed delays. In combination with a molecular model of the Delta-Notch signalling pathway that connects to experimental accessible data, the model with distributed delays in the coupling could describe the dynamic response more realistically, if data on statistics of the time delays involved in the signalling process is accessible.

We have not assessed, whether the observed results in Chapter 7 are present in $2D$ or $3D$. All calculations and simulations were carried out in $1D$ systems. Simulation of the dynamics of many phase oscillators with distributed delays in the coupling, for systems with $D > 1$ is computationally expensive. The convolution of the delay distribution and the phase history of the coupled neighbour has to be conducted for all oscillators in the system individually. The question whether the effects on the linear dynamical response to small perturbations are present in higher dimensional systems is nevertheless interesting, since not all systems of coupled phase oscillators can be described by one-dimensional chains.

Part III.

APPENDICES

A.

A.1. Distribution composed of two adjacent boxcar functions

Here a delay distribution is introduced for which the second and third central moments can be changed independently for a constant first moment. I.e., the variance and the skewness can be changed independently for a fixed value of the mean of the delay distribution. With $a, b, c, d, \bar{m} \in \mathbb{R}^+$, we define the delay
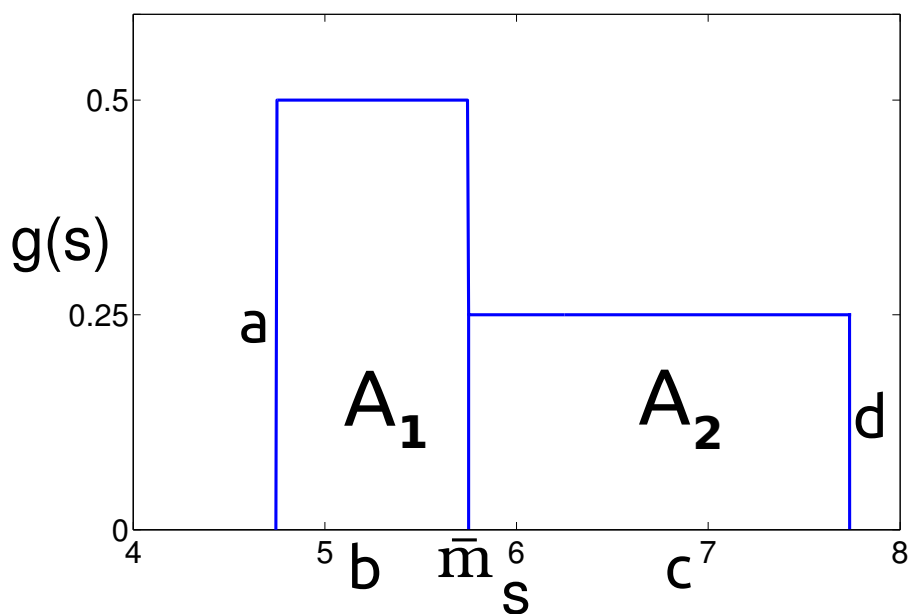

Figure A.1.: Sketch of the two step delay distribution. A_1 and A_2 are the areas of the two steps, b and c denote for the widths, a and d for the heights of the steps and $\bar{m}$ is the median of the two step delay distribution. Each step is normalized to $A_1 = A_2 = 0.5$.

distribution which is shown in Fig. A.1 by:

$$g(s) = \begin{cases} a & \forall \ (\bar{m} - b) \le s \le \bar{m} \\ d & \forall \ \bar{m} < s \le (\bar{m} + c) \\ 0 & \text{elsewhere,} \end{cases} \tag{A.1}$$

which can be expressed in terms of boxcar functions Π [179, 180]:

$$g(s) = a\Pi\left(\frac{s - (\bar{m} - 0.5b)}{b}\right) + d\Pi\left(\frac{s - (\bar{m} + 0.5c)}{c}\right), \tag{A.2}$$

where $\Pi(x) = H(x + 0.5) - H(x - 0.5)$, and H denotes the Heaviside function. We refer to $g(s)$ as the two step delay distribution. For the areas A_1 and A_2 of the two boxcar functions we demand that:

$$\begin{aligned} A_1 &= A_2 = 0.5, \\ A_1 &= ab, \\ A_2 &= cd, \end{aligned} \tag{A.3}$$

such that

$$\begin{aligned} a &= \frac{0.5}{b} \\ d &= \frac{0.5}{c}. \end{aligned} \tag{A.4}$$

We will now derive the mean τ, variance σ^2 and skewness γ for this delay distribution. The first moment or mean of the delay distribution is given by:

$$\tau = \int_{\bar{m}-b}^{\bar{m}} ds \, s \, a + \int_{\bar{m}}^{\bar{m}+c} ds \, s \, d, \tag{A.5}$$

i.e.

$$\tau = \bar{m} - \frac{1}{4}(b - c). \tag{A.6}$$

By definition the variance is given by:

$$\sigma^2 = \int_{\bar{m}-b}^{\bar{m}} ds \, a \, (s - \tau)^2 + \int_{\bar{m}}^{\bar{m}+c} ds \, d \, (s - \tau)^2, \tag{A.7}$$

and with the relations given in Eq. (A.4) yields:

$$\sigma^2 = (\bar{m} - \tau)^2 - \frac{1}{2}(\bar{m} - \tau)[b - c] + \frac{1}{6}\left[b^2 + c^2\right]. \tag{A.8}$$

Eq. (A.6) and Eq. (A.8) imply:

$$\sigma^2 = \frac{1}{48}\left(5b^2 + 6bc + 5c^2\right). \tag{A.9}$$

The third moment of the delay distribution, the skewness, is a measure of the symmetry of the shape of the distribution; this is defined as:

$$\gamma = \frac{1}{\sigma^3}\left(\int_{\bar{m}-b}^{\bar{m}} ds\, a\, (s-\tau)^3 + \int_{\bar{m}}^{\bar{m}+c} ds\, d\, (s-\tau)^3\right), \tag{A.10}$$

which evaluated and given in terms of $b, c, \bar{m}$ and τ reads:

$$\gamma = \frac{1}{8\sigma^3}\left([b^3 - c^3] + 4(\bar{m}-\tau)[b^2 + c^2] + 6(\bar{m}-\tau)^2[b-c] + 8(\bar{m}-\tau)^3\right). \tag{A.11}$$

Plugging Eq. (A.6) in for the terms $(\bar{m}-\tau)$ yields in this case the skewness in dependence of c, b and σ:

$$\gamma = \frac{1}{32\sigma^3}\left(c^3 - bc^2 + b^2c - b^3\right). \tag{A.12}$$

Our goal is to calculate the parameters $b, c, \bar{m}$ for any given set of γ, σ, τ where $\bar{m}$ is given by τ, b, c:

$$\bar{m} = \tau + \frac{1}{4}(b-c), \tag{A.13}$$

and we can use Eqs. (A.9) and (A.12) to calculate c, b. First we introduce the substitution:

$$\alpha = b + c \quad \text{and} \quad \beta = b - c, \tag{A.14}$$

and calculate the relation:

$$\left(\alpha^2\beta + \beta^3\right) = 2b^3 - 2b^2c + 2bc^2 - 2c^3. \tag{A.15}$$

With this relation we can rewrite Eq. (A.12) in terms of α, β:

$$32\gamma\sigma^3 = -\frac{1}{2}\left(\alpha^2\beta + \beta^3\right). \tag{A.16}$$

Expressing Eq. (A.12) also in terms of α, β yields:

$$48\sigma^2 = 4\alpha^2 + \beta^2. \tag{A.17}$$

Now Eq. (A.17) can be rearranged for α and substituted into Eq. (A.16) which results in a third order polynomial in β:

$$\frac{3}{4}\beta^3 + 12\sigma^2\beta + 64\gamma\sigma^3 = 0, \tag{A.18}$$

that is used to determine the β. With Eq. (A.17) α can be calculated using the β and σ. Parameters b, c are obtained by re-substitution:

$$b = \frac{\alpha + \beta}{2} \quad \text{and} \quad c = \frac{\alpha - \beta}{2}. \tag{A.19}$$

This means that we can calculate b and c by solving the third order polynomial in β given by Eq. (A.18), the second order polynomial in α given by Eq. (A.17) and resubstituting according to Eq. (A.19) for any given pair of (σ, γ). Note that the skewness of this delay distribution has an upper bound γ_{max}, see Fig. A.2. Furthermore, note that not every possible triplet (τ, σ, γ) can be realized, even if $\gamma < \gamma_{max}$, if the distribution is only defined for non-negative values. Only triplets of (τ, σ, γ) for which $\bar{m} - b \geq 0$ is fulfilled exist in this case. This is important to us, because negative delay times do not exist.

The Laplace transform $\hat{g}(\lambda)$ [181] of $g(s)$, used in Chapter 6, is defined as:

$$\hat{g}(\lambda) = \int_0^\infty ds\, g(s) e^{-\lambda s}. \tag{A.20}$$
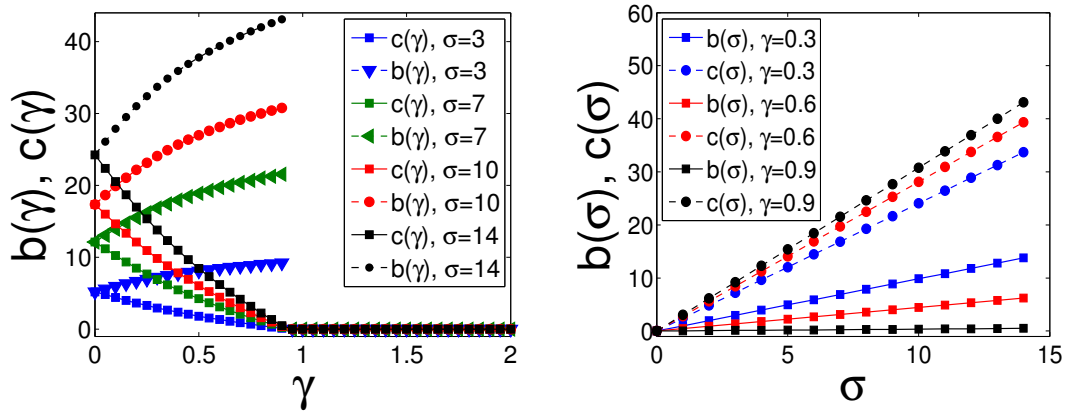
Figure A.2.: The left plot shows the dependence of the width b and c on the skewness γ of the two step delay distribution for three different fixed standard deviations σ. The maximum skewness γ, for which b and c are both positive and have imaginary part equal to zero, that can be realized is $\gamma_{max} \approx 0.92$. On the right side the figure shows the dependence of the width b and c on the standard deviation σ for three different fixed values of the skewness γ. With increasing skewness the difference in the width of the two steps increases and so does the hight since the two are connected via the constant area of each of the steps.

This is obtained by rewriting Eq. (A.2) in terms of Heaviside functions H, using the relation [182]:

$$\Pi\left(\frac{t-X}{Y}\right) = H(t-X+0.5Y) - H(t-X-0.5Y), \tag{A.21}$$

which applied to Eq. (A.2) yields:

$$g(s) = a\left[H(s-\bar{m}-b) - H(s-\bar{m})\right] + d\left[H(s-\bar{m}) - H(s-\bar{m}-c)\right]. \tag{A.22}$$

The Laplace transform of a shifted Heaviside function [183, 184] is given by:

$$\mathcal{L}[H(t-r)] = \frac{1}{\lambda}e^{-r\lambda}. \tag{A.23}$$

Using the linearity property of the Laplace operator [152] we find:

$$\mathcal{L}[af(s) + dk(s)] = a\mathcal{L}[f(s)] + d\mathcal{L}[k(s)] = a\hat{f}(\lambda) + d\hat{k}(\lambda). \tag{A.24}$$

We use this property given in the above equation and the expression of Laplace transform for shifted Heaviside functions as given by Eq. (A.23) to obtain the Laplace transform of Eq. (A.22):

$$\hat{g}(\lambda) = \frac{e^{-\bar{m}\lambda}}{2\lambda}\left\{\frac{1}{b}\left[e^{b\lambda}-1\right] + \frac{1}{c}\left[1-e^{-c\lambda}\right]\right\}. \tag{A.25}$$

Approximation to determine the maximum skewness

We expect a maximum skewness for $b \rightarrow 0$ and finite c or vice versa due to the symmetry of the distribution. In this limit Eqs. (A.9) and (A.12) for the variance and skewness of the two step delay distribution read:

$$\tilde{\sigma} \approx \pm c\sqrt{\frac{5}{48}},$$

$$\gamma_{max} \approx \frac{c^3}{32\tilde{\sigma}^3}.$$

Now if we plug the first into the second equation we get:

$$\gamma_{max} \approx \pm\frac{1}{32}\left(\frac{48}{5}\right)^{\frac{3}{2}} = \pm 0.929516, \tag{A.26}$$

which is the maximum value for the skewness that we had found plotting b and c versus the skewness – see Fig. A.2. In the case of $c \rightarrow 0$ and finite b one obtains the same result. We choose the solution with the plus sign for the approximation of the maximum value of the skewness.

A.2. The gamma distribution

The gamma distribution is a continuous probability distribution supported on $[0, \infty)$ with two parameters: $a > 0$, the so-called shape parameter, and $b > 0$, the scale parameter [144]. For integer a the gamma distribution represents the waiting time distribution [185] for a chain of a Poisson processes, each with rate $1/b$, to complete. The distribution is given by the following equation:

$$g_\Gamma(s; a, b) = s^{a-1} \frac{e^{-\frac{s}{b}}}{b^a \Gamma(a)}, \tag{A.27}$$

where $\Gamma(a)$ denotes the Gamma function evaluated at a. The mean τ_Γ of the distribution [186] is given by its two parameters:

$$\tau_\Gamma = ab, \tag{A.28}$$

which also determine the variance:

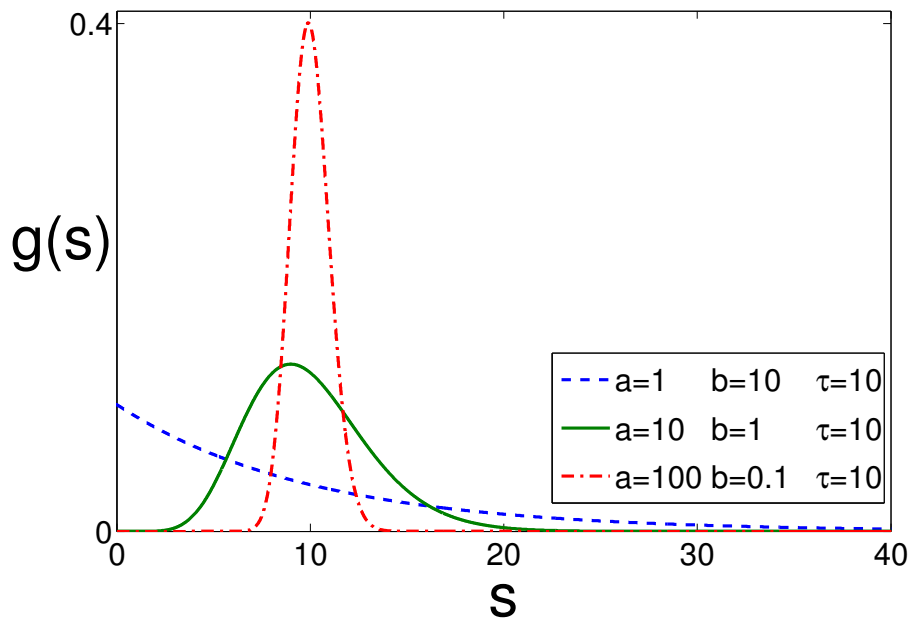$$\sigma_\Gamma^2 = ab^2. \tag{A.29}$$

Figure A.3.: Gamma distribution $g(s)$ plotted versus s for 3 different pairs of parameters a and b, such that the mean τ is constant.

The skewness γ_Γ, a measure of the symmetry of the distribution about its mean, is given by:

$$\gamma_\Gamma = \frac{2}{\sqrt{a}}, \qquad (A.30)$$

and only depends on the shape parameter a. With $a = 1$ the distribution is exponential with exponent $-1/b$. As can be seen by looking at the last equation, the skewness is maximal for the exponential case $a = 1$, which implies $\gamma_\Gamma = 2$, and becomes small for large values of a. This means that the gamma distribution becomes more symmetric as a increases – see Fig. A.3.

The Laplace transform $\hat{g}_\Gamma(\lambda)$ of the gamma distribution depends on the two distribution parameters and reads [152, 153]:

$$\hat{g}_\Gamma(\lambda) = (1 + b\lambda)^{-a}. \qquad (A.31)$$

A.3. Distribution composed of two Dirac delta peaks

Here we present another delay distribution for which the second and third central moments can be changed independently while the first moment is kept constant. It means that the variance and the skewness can be changed independently for a fixed value of the mean of the delay distribution. We define the delay distribution shown in Fig. A.4 by:

$$g(s) = \frac{1}{1+a} [a\delta(s - \bar{m}) + \delta(s - (\bar{m} + b))], \qquad (A.32)$$

where $a > 0$ is a real parameter that changes the hight of the first peak and $b > 0 \in \mathbb{R}$ changes the distance of the second peak with respect to the first one. The real parameter $\bar{m}$ denotes the position of the first delta peak with hight a, whereas $\bar{m} + b$ marks the position of the second delta peak with hight 1. For this delay distribution the mean τ, variance σ^2 and skewness γ are calculated in this section. The mean of the delay distribution is defined by:

$$\tau = \int_0^\infty ds\, g(s)s, \qquad (A.33)$$

and substituting Eq. (A.32) for $g(s)$ yields:

$$\tau = \bar{m} + \frac{b}{a+1}. \qquad (A.34)$$
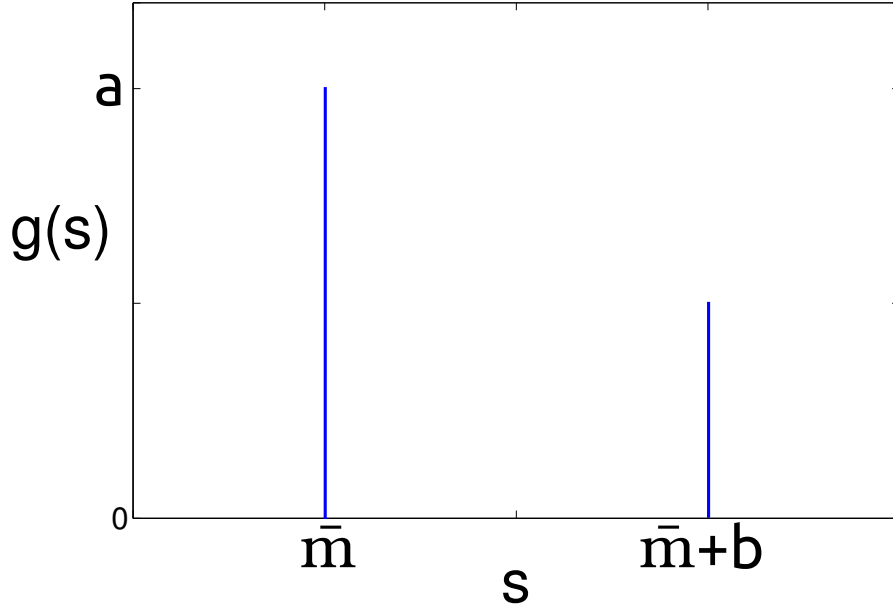
Figure A.4.

The variance is given by the second central moment about the mean of the delay distribution:

$$\sigma^2 = \int_0^\infty ds\, g(s)(s-\tau)^2, \tag{A.35}$$

which yields after substituting Eqs. (A.32) and (A.34):

$$\sigma^2 = \frac{ab^2}{(a+1)^2}. \tag{A.36}$$

The third central moment, the so-called skewness of the distribution is given by:

$$\gamma = \frac{1}{\sigma^3} \int_0^\infty ds\, g(s)(s-\tau)^3 = \frac{a(\bar{m}-\tau)^3 + (\bar{m}+b-\tau)^3}{\sigma^3(a+1)}. \tag{A.37}$$

For all $b > 0$ this can be further simplified:

$$\gamma = \frac{a-1}{\sqrt{a}}, \tag{A.38}$$

i.e. the skewness is independent of b and only depends on the hight of the first peak.

The Laplace transform of this delay distribution is given by:

$$\hat{g}(\lambda) = \frac{e^{-\lambda\bar{m}}}{a+1}\left(a + e^{-\lambda b}\right), \tag{A.39}$$

and depends on all parameters of the distribution.

126

A.4. Gerschgorin's circle theorem

Gerschgorin's circle theorem may be used to bound the spectrum of eigenvalues of complex $N \times N$ matrices.

Let $\mathbb{D} = \{d_{kl}\}$ be a complex $N \times N$ matrix and define $\sum_{l \neq k} |d_{kl}| \equiv r_k$. So called Gerschgorin discs are then defined by d_{kk}, the diagonal entry of $\mathbb{D}$, which denotes the center and r_k the radius. We introduce $\vec{c} = \{c_l\}$ for $l = 1, 2, \dots, N$ the eigenvector corresponding to the eigenvalue ζ. We omit the zero vector, such that $|c_k| > 0$. The theorem [156] states that:

All eigenvalues ζ of $\mathbb{D}$ lie within the at least one of the Gerschgorin discs.

Proof: $\zeta \vec{c} = \mathbb{D} \vec{c}$ written in terms of the components:

$$(\zeta - d_{kk})c_k = \sum_{l \neq k} d_{kl} c_l \text{ hence, } |\zeta - d_{kk}| \leq \sum_{l \neq k} |d_{kl}| \frac{|c_l|}{|c_k|}. \tag{A.40}$$

If the largest component of $\vec{c}$ is c_k, then these last ratios are ≤ 1, and ζ lies in the kth circle: $|\zeta - d_{kk}| \leq r_k$.

For matrices with solely zeros in the main diagonal $d_{kk} = 0$ holds, and all circles are centered at zero. In that case all solutions ζ satisfy $|\zeta| \leq r_k$, following Gerschgorin's theorem.

A.5. The Lambert W function

The Lambert W function [187], also referred to as the omega function, is a set of functions which are the inverse relation of:

$$f(w) = we^w \tag{A.41}$$

where $w = W(z)$ with $w, z \in \mathbb{C}$ and the defining equation for $W(z)$ is:

$$W(z)e^{W(z)} = z. \tag{A.42}$$

A.6. Roots of unity

In Section (9.1) we used for the approximation of the relation between the order parameter and λ that:

$$\sum_{k=1}^{N} e^{i\Delta k} = 0, \tag{A.43}$$

where $e^{i\Delta N} = 1$ and $e^{i\Delta} \neq 1$. Here by definition $\Delta = \frac{2\pi m}{N}$. The first condition holds because $m \in \mathbb{N}^+$. The second condition holds for $m \neq 0$ and if $\frac{m}{N} \notin \mathbb{N} \ \forall \ m, N$, which is always fulfilled since $m < N$ in our case. The case of $m = 0$ has to be excluded and yields a different result, namely:

$$\sum_{k=1}^{N} (1)^k = N, \tag{A.44}$$

which recovers the expression that was obtained for the relation of the order parameter and the λ's for the phase-locked state in Section 7.2.

For $m = 0, 1, \ldots, N - 1$ all $e^{i\Delta}$ are the nth roots of unity– see [163] and [164]. These are the solution to the polynomial:

$$x^n - 1 = 0, \tag{A.45}$$

where $n \in \mathbb{N}$ and we defined $x \equiv e^{i\Delta}$. With $x \neq 1$ and $x^N = 1$, Eq. (A.45) factorizes and we get:

$$(x - 1)(x^{n-1} + x^{n-2} + \cdots + x^1 + 1) = 0, \tag{A.46}$$

for which the first bracket cannot be zero since $x \neq 1$ by definition, and therefore:

$$(x^{n-1} + x^{n-2} + \cdots + x^1 + 1) \equiv \sum_{k=0}^{n-1} x^k = 0. \tag{A.47}$$

Since $e^{i\Delta N} = 1$, we find for Eq. (A.43):

$$\sum_{k=1}^{N} e^{i\Delta k} \equiv e^{i\Delta N} - 1 + \sum_{k=0}^{N-1} e^{i\Delta k} = 0. \tag{A.48}$$

B. Simulation methods

The programs for simulating systems of coupled phase oscillators with discrete and distributed delays are written in the C++ programming language. The GNU-Scientific Library (GSL) [188] was used to implement spline-interpolation and integration functions to perform the delay integrals. All simulations of Eqs. (5.1) have been carried out using Heun's method [189] or an Euler method [190, 191] with a step-length of $dt = 0.005$. For simulations with distributed delays and gamma function kernel, a cut-off for the tail of the distribution at finite delay was defined. This was chosen such that the resulting error was negligible. Random numbers for setting random initial conditions were generated using the Mersenne-Twister random number generator [192, 193].

Bibliography

[1] Y. Kuramoto. Self-entrainment of a population of coupled nonlinear oscillators. In H. Araki, editor, *International Symposium on Mathematical Problems in Theoretical Physics*, volume 39 of *Lecture Notes in Physics*, pages 420–422, NY, USA, 1975. Springer.

[2] S. H. Strogatz. *Sync: The Emerging Science of Spontaneous Order*. Hyperion, New York, NY, USA, 2003.

[3] A. Pikovsky, M. G. Rosenblum, and J. Kurths. *Synchronization – A universal concept in nonlinear sciences*. Cambridge University Press, Cambridge, 2001.

[4] C. Huygens. On the pendulum clock – Horologium oscillatorium. Ithaca, New York: Cornell University Library, 1913. Parisiis: Apud F. Muguet, 1673.

[5] C. Huygens, A. Heckscher, and A. Oettingen. *Die Pendeluhr, Horologium oscillatorium*. Ostwalds Klassiker der exakten Wissenschaften. W. Engelmann, 1913.

[6] R. Dilão. Antiphase and in-phase synchronization of nonlinear oscillators: the Huygens's clocks system. *Chaos*, 19:023118, 2009.

[7] E. Kämpfer. *History of Japan – together with a description of the Kingdom of Siam*. (posthumous translation) James MacLehose & Sons, 1906.

[8] J. Buck, E. Buck, F. E. Hanson, J. F. Cae, L. Mets, and G. J. Atta. Control of flashing in fireflies IV. Free run pacemaking in a synchronic Pteroptyx. *J. Comp. Physiol. A*, 144:277–286, 1981.

[9] P. Hadley, M. R. Beasley, and K. Wiesenfeld. Phase locking of Josephson-junction series arrays. *Phys. Rev. B*, 38:8712–8719, 1988.

[10] K. Wiesenfeld, P. Colet, and S. H. Strogatz. Synchronization transitions in a disordered Josephson series array. *Phys. Rev. Lett.*, 76:404–407, 1996.

[11] Y. Kuramoto. *Chemical oscillations, waves, and turbulence.* Chemistry Series. Dover Publications, 2003.

[12] M. Dolnik and I. R. Epstein. Coupled chaotic chemical oscillators. *Phys. Rev. E*, 54:3361–3368, 1996.

[13] N. Fujiwara, J. Kurths, and A. Díaz-Guilera. Synchronization in networks of mobile oscillators. *Phys. Rev. E*, 83:7, 2011.

[14] M. Kawato and R. Suzuki. Two coupled neural oscillators as a model of the circadian pacemaker. *J. Theor. Biol.*, 86:547–575, 1980.

[15] A. T. Winfree. *The Geometry of Biological Time – Interdisciplinary Applied Mathematics.* Springer, 2001.

[16] A. T. Winfree. Biological rhythms and the behavior of populations of coupled oscillators. *J. Theor. Biol.*, 16:15–42, 1967.

[17] S. H. Strogatz. From Kuramoto to Crawford: exploring the onset of synchronization in populations of coupled oscillators. *Physica D*, 143:1–20, 2000.

[18] S. H. Strogatz and R. E. Mirollo. Stability of incoherence in a population of coupled oscillators. *J. Stat. Phys.*, 63:613–635, 1991.

[19] S. H. Strogatz. *Nonlinear dynamics and chaos: with applications to physics, biology, chemistry, and engineering.* Westview Press, 1994.

[20] Y. Kuramoto and D. Battogtokh. Coexistence of coherence and incoherence in nonlocally coupled phase oscillators. *Nonlinear Phenomena in Complex Systems*, 5:380–385, 2002.

[21] G. C. Sethia, A. Sen, and F. M. Atay. Clustered Chimera States in Delay-Coupled Oscillator Systems. *Phys. Rev. Lett.*, 100:144102, 2008.

[22] E. Ott, J. H. Platig, T. M. Antonsen, and M. Girvan. Echo phenomena in large systems of coupled oscillators. *Chaos*, 18:23, 2008.

[23] W. S. Lee, E. Ott, and T. M. Antonsen. Large coupled oscillator systems with heterogeneous interaction delays. *Phys. Rev. Lett.*, 103:044101, 2009.

[24] E. Ott and T. M. Antonsen. Long time evolution of phase oscillator systems. *Chaos*, 19:023117, 2009.

[25] G. Barlev, T. M. Antonsen, and E. Ott. The dynamics of network coupled phase oscillators: An ensemble approach. *Chaos*, 21:025103, 2011.

[26] W. S. Lee, J. G. Restrepo, E. Ott, and T. M. Antonsen. Dynamics and pattern formation in large systems of spatially-coupled oscillators with finite response times. *Chaos*, 21:023122, 2011.

[27] L. Glass and M. C. Mackey. *From Clocks to Chaos*. Princeton University Press, 1988.

[28] J. D. Murray. *Mathematical Biology*. Springer, 1993.

[29] J. A. Acebrón, L. L. Bonilla, C. J. Pérez-Vicente, F. Ritort, and R. Spigler. The Kuramoto model: A simple paradigm for synchronization phenomena. *Rev. Mod. Phys.*, 77:137–185, 2005.

[30] A. Sen, R. Dodla, and G. L. Johnston. Collective dynamics of delay-coupled limit cycle oscillators. *Pramana*, 64:465–482, 2005.

[31] E. M. Izhikevich. Phase models with explicit time delays. *Phys. Rev. E*, 58:905–908, 1998.

[32] I. H. Riedel-Kruse, C. Müller, and A. C. Oates. Synchrony dynamics during initiation, failure, and rescue of the segmentation clock. *Science*, 317:1911–1915, 2007.

[33] M. Bonnin, F. Corinto, and M. Gilli. A phase model approach for synchronization analysis of coupled nonlinear oscillators. In *Circuits and Systems (ISCAS), Proceedings of 2010 IEEE International Symposium*, pages 3385–3388, 2010.

[34] F. M. Atay. Distributed delays facilitate amplitude death of coupled oscillators. *Phys. Rev. Lett.*, 91:094101, 2003.

[35] R. Dodla, A. Sen, and G. L. Johnston. Phase-locked patterns and amplitude death in a ring of delay-coupled limit cycle oscillators. *Phys. Rev. E*, 69:056217, 2004.

[36] Y. Kyrychko, K. Blyuss, and E. Schöll. Amplitude death in systems of coupled oscillators with distributed-delay coupling. *Eur. Phys. J. B*, 84:307–315, 2011.

[37] A. D. Wiley, S. H. Strogatz, and M. Girvan. The size of the sync basin. *Chaos*, 16:015103, 2006.

[38] F. Peruani, M. E. Nicola, and L. G. Morelli. Mobility induces global synchronization of oscillators in periodic extended systems. *New J. Phys.*, 12:093029, 2010.

[39] A. A. Selivanov, J. Lehnert, T. Dahms, P. Hövel, A. L. Fradkov, and E. Schöll. Adaptive synchronization in delay-coupled networks of Stuart-Landau oscillators. *Phys. Rev. E*, 85:016201, 2012.

[40] E. Montbrio, D. Pazo, and J. Schmidt. Time delay in the Kuramoto model with bimodal frequency distribution. *Phys. Rev. E*, 74:5, 2006.

[41] E. Ott and T. M. Antonsen. Low dimensional behavior of large systems of globally coupled oscillators. *Chaos*, 18:037113, 2008.

[42] H. Kori and A. S. Mikhailov. Entrainment of randomly coupled oscillator networks by a pacemaker. *Phys. Rev. Lett.*, 93:254101, 2004.

[43] T.-W. Ko, S.-O. Jeong, and H.-T. Moon. Wave formation by time delays in randomly coupled oscillators. *Phys. Rev. E*, 69:056106, 2004.

[44] T.-W. Ko and G. B. Ermentrout. Effects of axonal time delay on synchronization and wave formation in sparsely coupled neuronal oscillators. *Phys. Rev. E*, 76:056206, 2007.

[45] K. Uriu, Y. Morishita, and Y. Iwasa. Random cell movement promotes synchronization of the segmentation clock. *P. Natl. Acad. Sci. USA*, 107:4979–4984, 2010.

[46] G. B. Ermentrout. The behavior of rings of coupled oscillators. *J. Math. Biol.*, 23:55–74, 1985.

[47] E. Niebur, H. G. Schuster, D. M. Kammen, and C. Koch. Oscillator-phase coupling for different two-dimensional network connectivities. *Phys. Rev. A*, 44:6895, 1991.

[48] P.-J. Kim, T.-W. Ko, H. Jeong, and H.-T. Moon. Pattern formation in a two-dimensional array of oscillators with phase-shifted coupling. *Phys. Rev. E*, 70:065201, 2004.

[49] J. G. Restrepo, E. Ott, and B. R. Hunt. Synchronization in large directed networks of coupled phase oscillators. *Chaos*, 16:015107, 2006.

[50] J. G. Restrepo, E. Ott, and B. R. Hunt. Onset of synchronization in large networks of coupled oscillators. *Phys. Rev. E*, 71:036151, 2005.

[51] B. B. Zhou and R. Roy. Isochronal synchrony and bidirectional communication with delay-coupled nonlinear oscillators. *Phys. Rev. E*, 75:026205, 2007.

[52] P. Perlikowski, S. Yanchuk, O. V. Popovych, and P. A. Tass. Periodic patterns in a ring of delay-coupled oscillators. *Phys. Rev. E*, 82:036208, 2010.

[53] V. M. Eguíluz, T. Pérez, J. Borge-Holthoefer, and A. Arenas. Structural and functional networks in complex systems with delay. *Phys. Rev. E*, 83:056113, 2011.

[54] L. S. Tsimring, N. F. Rulkov, M. L. Larsen, and M. Gabbay. Repulsive synchronization in an array of phase oscillators. *Phys. Rev. Lett.*, 95:014101, 2005.

[55] L. Bertini, G. Giacomin, and K. Pakdaman. Dynamical aspects of mean field plane rotators and the Kuramoto model. *J. Stat. Phys.*, 138:18, 2009.

[56] L. G. Morelli, S. Ares, L. Herrgen, C. Schröter, F. Jülicher, and A. C. Oates. Delayed coupling theory of vertebrate segmentation. *HFSP J.*, 3:55–66, 2009.

[57] S. H. Park, S. Kim, H.-B. Pyo, S. Lee, and S.-K. Lee. Time Delay Effects on Dynamic Patterns in a Coupled Neural Model. In *Proceedings of the First IEEE International Workshop on Biologically Motivated Computer Vision*, BMVC 2000, pages 268–275, London, UK, 2000. Springer-Verlag.

[58] D. H. Zanette. Structures and propagation in globally coupled systems with time delays. *Phys. Rev. E*, 62:13, 2000.

[59] B. Ermentrout and T.-W. Ko. Delays and weakly coupled neuronal oscillators. *Philos. T. Roy. Soc. A*, 367:1097–1115, 2009.

[60] O. Vallès-Codina, R. Möbius, S. Rüdiger, and L. Schimansky-Geier. Traveling echo waves in an array of excitable elements with time-delayed coupling. *Phys. Rev. E*, 83:036209, 2011.

[61] S. Rüdiger and L. Schimansky-Geier. Dynamics of excitable elements with time-delayed coupling. *J. Theor. Biol.*, 259:96–100, 2009.

[62] N. Kouvaris, L. Schimansky-Geier, and E. Schöll. Control of coherence in excitable systems by the interplay of noise and time-delay. *Eur. Phys. J-Spec. Top.*, 191:29–51, 2010.

[63] N. A. M. Monk. Oscillatory Expression of Hes1, p53, and NF-κB Driven by Transcriptional Time Delays. *Curr. Biol.*, 13:1409–1413, 2003.

[64] J. Lewis. Autoinhibition with transcriptional delay: A simple mechanism for the zebrafish somitogenesis oscillator. *Curr. Biol.*, 13:1398–1408, 2003.

[65] P. Feng. Dynamics of a Segmentation Clock Model with Discrete and Distributed Delays. *Int. J. Biomath.*, 03:399, 2010.

[66] S.-I. Niculescu, E. Verriest, L. Dugard, and J.-M. Dion. Stability and robust stability of time-delay systems: A guided tour. In L. Dugard and E. Verriest, editors, *Stability and Control of Time-delay Systems*, volume 228 of *Lecture Notes in Control and Information Sciences*, pages 1–71. Springer Berlin/Heidelberg, 1998.

[67] N. MacDonald, C. Cannings, F. C. Hoppensteadt, and L. A. Segel. *Biological Delay Systems: Linear Stability Theory*. Cambridge Studies in Mathematical Biology. Cambridge University Press, 2008.

[68] H. G. Schuster and P. Wagner. Mutual Entrainment of Two Limit Cycle Oscillators with Time Delayed Coupling. *Prog. Theor. Phys.*, 81:939–945, 1989.

[69] M. K. S. Yeung and S. H. Strogatz. Time delay in the Kuramoto model of coupled oscillators. *Phys. Rev. Lett.*, 82:648–651, 1999.

[70] E. Niebur, H. G. Schuster, and D. M. Kammen. Collective frequencies and metastability in networks of limit-cycle oscillators with time delay. *Phys. Rev. Lett.*, 67:2753–2756, 1991.

[71] S. Kim, S. H. Park, and C. S. Ryu. Multistability in coupled oscillator systems with time delay. *Phys. Rev. Lett.*, 79:2911–2914, 1997.

[72] D. V. Ramana Reddy, A. Sen, and G. L. Johnston. Time delay effects on coupled limit cycle oscillators at hopf bifurcation. *Physica D*, 129:15–34, 1999.

[73] D. G. Aronson, G. B. Ermentrout, and N. Kopell. Amplitude response of coupled oscillators. *Physica D*, 41:403–449, 1990.

[74] G. B. Ermentrout. Oscillator death in populations of "all to all" coupled nonlinear oscillators. *Physica D*, 41:219–231, 1990.

[75] M. P. Mehta and A. Sen. Death island boundaries for delay-coupled oscillator chains. *Phys. Lett. A*, 355:202–206, 2006.

[76] R. E. Mirollo and S. H. Strogatz. Amplitude death in an array of limit-cycle oscillators. *J. Stat. Phys.*, 60:245–262, 1990.

[77] Y. Yamaguchi and H. Shimizu. Theory of self-synchronization in the presence of native frequency distribution and external noises. *Physica D*, 11:212–226, 1984.

[78] D. V. Ramana Reddy, A. Sen, and G. L. Johnston. Time delay induced death in coupled limit cycle oscillators. *Phys. Rev. Lett.*, 80:5109–5112, 1998.

[79] S.-O. Jeong, T.-W. Ko, and H.-T. Moon. Time-delayed spatial patterns in a two-dimensional array of coupled oscillators. *Phys. Rev. Lett.*, 89:154104, 2002.

[80] K. L. Cooke and Z. Grossman. Discrete Delay, Distributed Delay and Stability Switches. *J. Math. Anal. Appl.*, 86:592–627, 1982.

[81] K. I. Tsianos and M. G. Rabbat. Distributed consensus and optimization under communication delays. In *Communication, Control, and Computing, 2011 49th Annual Allerton Conference*, pages 974–982, 2011.

[82] J. Zhou and Z. Liu. Synchronized patterns induced by distributed time delays. *Phys. Rev. E*, 77:056213, 2008.

[83] X. Liang, M. Tang, M. Dhamala, and Z. Liu. Phase synchronization of inhibitory bursting neurons induced by distributed time delays in chemical coupling. *Phys. Rev. E*, 80:066202, 2009.

[84] K. Gu. An improved stability criterion for systems with distributed delays. *Int. J. Robust Nonlin.*, 13:819–831, 2003.

[85] L. Ji and Q. S. Li. Turing pattern formation in coupled reaction-diffusion system with distributed delays. *J. Chem. Phys.*, 123:94509, 2005.

[86] H. Özbay, C. Bonnet, and J. Clairambault. Stability analysis of systems with distributed delays and application to hematopoietic cell maturation dynamics. In *Decision and Control, 2008. CDC 2008. 47th IEEE Conference*, pages 2050–2055, 2008.

[87] X. Liao, K.-W. Wong, and Z. Wu. Bifurcation analysis on a two-neuron system with distributed delays. *Physica D*, 149:123–141, 2001.

[88] X. Liao, S. Li, and G. Chen. Bifurcation analysis on a two-neuron system with distributed delays in the frequency domain. *Neural Networks*, 17:545–561, 2004.

[89] H. Zhao. Global asymptotic stability of Hopfield neural network involving distributed delays. *Neural Networks*, 17:47–53, 2004.

[90] C. H. Li and S.-Y. Yang. Synchronization in Linearly Coupled Dynamical Networks with Distributed Time Delays. *Int. J. Bifurcat. Chaos*, 18:2039–2047, 2008.

[91] Karmeshu, V. Gupta, and K. Kadambari. Neuronal model with distributed delay: analysis and simulation study for gamma distribution memory kernel. *Biological Cybern.*, 104:369–383, 2011.

[92] G. Keqin and S.-I. Niculescu. Additional dynamics in transformed time-delay systems. *IEEE T. Automat. Contr.*, 45:572–575, 2000.

[93] S. H. Strogatz and R. E. Mirollo. Splay states in globally coupled Josephson arrays: Analytical prediction of Floquet multipliers. *Phys. Rev. E*, 47:220–227, 1993.

[94] C. B. Kimmel, W. W. Ballard, S. R. Kimmel, B. Ullmann, and T. F. Schilling. Stages of embryonic development of the zebrafish. *Dev. Dyn.*, 203:253–310, 1995.

[95] J. Cachat, A. Stewart, L. Grossman, S. Gaikwad, F. Kadri, K. M. Chung, N. Wu, K. Wong, S. Roy, C. Suciu, and et al. Measuring behavioral and endocrine responses to novelty stress in adult zebrafish. *Nat. Protoc.*, 5:1786–99, 2010.

[96] J. Cooke and E. C. Zeeman. A clock and wavefront model for control of the Number of repeated structures during animal morphogenesis. *J. Theor. Biol.*, 58:455–476, 1976.

[97] L. Wolpert, C. Tickle, T. Jessell, P. Lawrence, and E. Meyerowitz. *Principles of Development.* Oxford University Press, USA, 4th edition, 2010.

[98] A. C. Oates, L. G. Morelli, and S. Ares. Patterning embryos with oscillations: structure, function and dynamics of the vertebrate segmentation clock. *Development*, 139, 2012.

[99] Y. J. Jiang, B. L. Aerne, L. Smithers, C. Haddon, D. Ish-Horowicz, and J. Lewis. Notch signalling and the synchronization of the somite segmentation clock. *Nature*, 408:475–479, 2000.

[100] K. Horikawa, K. Ishimatsu, E. Yoshimoto, S. Kondo, and H. Takeda. Noise-resistant and synchronized oscillation of the segmentation clock. *Nature*, 441:719–723, 2006.

[101] E. M. Özbudak and J. Lewis. Notch Signalling Synchronizes the Zebrafish Segmentation Clock but Is Not Needed To Create Somite Boundaries. *PLoS Genet.*, 4:11, 2008.

[102] J. Cooke. The problem of periodic patterns in embryos. *Philos. T. Roy. Soc. B*, 295:509–524, 1981.

[103] O. Pourquie. The vertebrate segmentation clock. *J. Anat.*, 199:169–175, 2001.

[104] O. Pourquié. Vertebrate somitogenesis. *Annu. Rev. Cell Dev. Biol.*, 17:311–350, 2001.

[105] D. Roellig, L. G. Morelli, S. Ares, F. Jülicher, and A. C. Oates. SnapShot: The segmentation clock. *Cell*, 145:800–800.e1, 2011.

[106] A. Oates, N. Gorfinkiel, M. González-Gaitán, and C.-P. Heisenberg. Quantitative approaches in developmental biology. *Nat. Rev. Genet.*, 10:517–530, 2009.

[107] W. Driever and C. Nusslein-Volhard. The bicoid protein determines position in the Drosophila embryo in a concentration-dependent manner. *Cell*, 54:95–104, 1988.

[108] J. B. Gurdon, P. Harger, A. Mitchell, and P. Lemaire. Activin signalling and response to a morphogen gradient. *Nature*, 371:487–492, 1994.

[109] A. M. Turing. The chemical basis of morphogenesis. *B. Math. Biol.*, 52:37–72, 1952.

[110] H. Meinhardt. *Models of biological pattern formation*. Academic Press, 1982.

[111] O. Pourquié. The Segmentation Clock: Converting Embryonic Time into Spatial Pattern. *Science*, 301:328–330, 2003.

[112] C. Schröter and A. C. Oates. Segment Number and axial identity in a segmentation clock period mutant. *Curr. Biol.*, 20:1254–1258, 2012.

[113] L. Herrgen, S. Ares, L. G. Morelli, C. Schröter, F. Jülicher, and A. C. Oates. Intercellular coupling regulates the period of the segmentation clock. *Curr. Biol.*, 20:1244–1253, 2010.

[114] K. Uriu, Y. Morishita, and Y. Iwasa. Traveling wave formation in vertebrate segmentation. *J. Theor. Biol.*, 257:385–396, 2009.

[115] S. D. Hester, J. M. Belmonte, J. S. Gens, S. G. Clendenon, and J. A. Glazier. A multi-cell, multi-scale model of vertebrate segmentation and somite formation. *PLoS Comput. Biol.*, 7:e1002155, 2011.

[116] I. Palmeirim, D. Henrique, D. Ish-Horowicz, and O. Pourquié. Avian hairy gene expression identifies a molecular clock linked to vertebrate segmentation and somitogenesis. *Cell*, 91:639–648, 1997.

[117] M. Maroto, J. K. Dale, M.-L. Dequèant, A.-C. Petit, and O. Pourquié. Synchronised cycling gene oscillations in presomitic mesoderm cells require cell-cell contact. *Int. J. Dev. Biol.*, 49:309–315, 2005.

[118] A. C. Oates and R. K. Ho. Hairy/E(spl)-related (Her) genes are central components of the segmentation oscillator and display redundancy with the delta/notch signaling pathway in the formation of anterior segmental boundaries in the zebrafish. *Development*, 129:2929–2946, 2002.

[119] C. Gomez, E. M. Özbudak, J. Wunderlich, D. Baumann, J. Lewis, and O. Pourquié. Control of segment number in vertebrate embryos. *Nature*, 454:335–339, 2008.

[120] V. E. Prince, L. Joly, M. Ekker, and R. K. Ho. Zebrafish hox genes: genomic organization and modified colinear expression patterns in the trunk. *Development*, 125:407–420, 1998.

[121] A. C. Oates, A. E. E. Bruce, and R. K. Ho. Too Much Interference: Injection of Double-Stranded RNA Has Nonspecific Effects in the Zebrafish Embryo. *Dev. Biol.*, 224:20–28, 2000.

[122] A. C. Oates, C. Müller, and R. K. Ho. Cooperative function of deltaC and her7 in anterior segment formation. *Dev. Biol.*, 280:133–149, 2005.

[123] Y. Masamizu, T. Ohtsuka, Y. Takashima, H. Nagahara, Y. Takenaka, K. Yoshikawa, H. Okamura, and R. Kageyama. Real-time imaging of the somite segmentation clock: revelation of unstable oscillators in the individual presomitic mesoderm cells. *P. Natl. Acad. Sci. USA*, 103:1313–1318, 2006.

[124] A. Aulehla, W. Wiegraebe, V. Baubet, M. B. Wahl, C. Deng, M. Taketo, M. Lewandoski, and O. Pourquié. A beta-catenin gradient links the clock

and wavefront systems in mouse embryo segmentation. *Nat. Cell Biol.*, 10:186–193, 2008.

[125] Y. Takashima, T. Ohtsuka, A. González, H. Miyachi, and R. Kageyama. Intronic delay is essential for oscillatory expression in the segmentation clock. *P. Natl. Acad. Sci. USA*, 108:3300–3305, 2011.

[126] H. Hirata, S. Yoshiura, T. Ohtsuka, Y. Bessho, T. Harada, K. Yoshikawa, and R. Kageyama. Oscillatory expression of the bHLH factor Hes1 regulated by a negative feedback loop. *Science*, 298:840–843, 2002.

[127] C. Schröter, L. Herrgen, A. Cardona, G. J. Brouhard, B. Feldman, and A. C. Oates. Dynamics of zebrafish somitogenesis. *Dev. Dyn.*, 237:545–553, 2008.

[128] H. B. Tiedemann, E. Schneltzer, S. Zeiser, I. Rubio-Aliaga, W. Wurst, J. Beckers, G. K. H. Przemeck, and M. Hrabé De Angelis. Cell-based simulation of dynamic expression patterns in the presomitic mesoderm. *J. Theor. Biol.*, 248:120–129, 2007.

[129] B. Novák and J. J. Tyson. Design principles of biochemical oscillators. *Nat. Rev. Mol. Cell Biol.*, 9:981–991, 2008.

[130] S. Artavanis-Tsakonas, M. D. Rand, and R. J. Lake. Notch signaling: cell fate control and signal integration in development. *Science*, 284:770–776, 1999.

[131] A.-C. Tien, A. Rajan, and H. J. Bellen. A notch updated. *J. Cell Biol.*, 184:621–629, 2009.

[132] D. Sprinzak, A. Lakhanpal, L. Lebon, L. A. Santat, M. E. Fontes, G. A. Anderson, J. Garcia-Ojalvo, and M. B. Elowitz. Cis-interactions between Notch and Delta generate mutually exclusive signalling states. *Nature*, 465:86–90, 2010.

[133] D. Sprinzak, A. Lakhanpal, L. LeBon, J. Garcia-Ojalvo, and M. B. Elowitz. Mutual inactivation of notch receptors and ligands facilitates developmental patterning. *PLoS Comput. Biol.*, 7:e1002069, 2011.

[134] S. A. Holley, R. Geisler, and C. Nüsslein-Volhard. Control of her1 expression during zebrafish somitogenesis by a delta-dependent oscillator and an independent wave-front activity. *Gene. Dev.*, 14:1678–1690, 2000.

[135] M. Itoh, C.-H. Kim, G. Palardy, T. Oda, Y.-J. Jiang, D. Maust, S.-Y. Yeo, K. Lorick, G. J. Wright, L. Ariza-McNaughton, and et al. Mind Bomb Is a Ubiquitin Ligase that Is Essential for Efficient Activation of Notch Signaling by Delta. *Cell*, 4:67–82, 2003.

[136] D. Jülich, C. Hwee Lim, J. Round, C. Nicolaije, J. Schroeder, A. Davies, R. Geisler, J. Lewis, Y.-J. Jiang, and S. A. Holley. beamter/deltaC and the role of Notch ligands in the zebrafish somite segmentation, hindbrain neurogenesis and hypochord differentiation. *Dev. Biol.*, 286:391–404, 2005.

[137] R. E. Baker, S. Schnell, and P. K. Maini. A clock and wavefront mechanism for somite formation. *Dev. Biol.*, 293:116–26, 2006.

[138] K. Uriu, Y. Morishita, and Y. Iwasa. Synchronized oscillation of the segmentation clock gene in vertebrate development. *J. Math. Biol.*, 61:207–229, 2010.

[139] F. Giudicelli, E. M. Özbudak, G. J. Wright, and J. Lewis. Setting the Tempo in Development: An Investigation of the Zebrafish Somite Clock Mechanism. *PLoS Comput. Biol.*, 5:e150, 2007.

[140] A. Sawada, M. Shinya, Y. J. Jiang, A. Kawakami, A. Kuroiwa, and H. Takeda. Fgf/MAPK signalling is a crucial positional cue in somite boundary formation. *Development*, 128:4873–4880, 2001.

[141] J. Dubrulle, M. J. McGrew, and O. Pourquié. FGF signaling controls somite boundary position and regulates segmentation clock control of spatiotemporal Hox gene activation. *Cell*, 106:219–232, 2001.

[142] A. Aulehla, C. Wehrle, B. Brand-Saberi, R. Kemler, A. Gossler, B. Kanzler, and B. G. Herrmann. Wnt3a plays a major role in the segmentation clock controlling somitogenesis. *Dev. Cell*, 4(3):395–406, 2003.

[143] L. G. Morelli and F. Jülicher. Precision of genetic oscillators and clocks. *Phys. Rev. Lett.*, 98:228101, 2007.

[144] I. N. Bronstein, K. A. Semendjajew, G. Grosche, and E. Zeidler. *Teubner-Taschenbuch der Mathematik*. Teubner, 2003.

[145] B. Alberts, D. Bray, J. Lewis, M. Raff, K. Roberts, and J. D. Watson. *Molecular Biology of the Cell*. Garland Publications, 1994.

[146] R. Schlicht and G. Winkler. A delay stochastic process with applications in molecular biology. *J. Math. Biol.*, 57:613–648, 2008.

[147] K. Josić, J. M. López, W. Ott, L. Shiau, and M. R. Bennett. Stochastic Delay Accelerates Signaling in Gene Networks. *PLoS Comput. Biol.*, 7:e1002264, 2011.

[148] S. Ruan and R. S. Filfil. Dynamics of a two-neuron system with discrete and distributed delays. *Physica D*, 191:323–342, 2004.

[149] K. Gopalsamy and X. He. Stability in asymmetric hopfield nets with transmission delays. *Physica D*, 76:344–358, 1994.

[150] J. K. Hale and S. M. V. Lunel. *Introduction To Functional Differential Equations*. Applied Mathematical Sciences. Springer-Verlag, 1993.

[151] H. Heuser. *Lehrbuch der Analysis*. Lehrbuch: Mathematik. Teubner, 2006.

[152] D. V. Widder. *The Laplace transform*. Princeton Mathematical Series. Princeton University Press, 1946.

[153] F. W. Olver, D. W. Lozier, R. F. Boisvert, and C. W. Clark. *NIST Handbook of Mathematical Functions*. Cambridge University Press, New York, NY, USA, 1st edition, 2010.

[154] R.C. Hilborn. *Chaos and nonlinear dynamics: an introduction for scientists and engineers*. Oxford University Press, 2000.

[155] M. Earl and S. H. Strogatz. Synchronization in oscillator networks with delayed coupling: A stability criterion. *Phys. Rev. E*, 67:036204, 2003.

[156] S. Gerschgorin. Über die Abgrenzung der Eigenwerte einer Matrix. *Izv. Akad. Nauk. UdSSR Otd. Fiz.-Mat. Nauk*, 7:749–754, 1931.

[157] H. E. Bell. Gershgorin's Theorem and the Zeros of Polynomials. *Am. Math. Mon.*, 72:292–295, 1965.

[158] G. Strang. *Introduction to Applied Mathematics*. 1986.

144

[159] R. M. Corless, G. H. Gonnet, D. E. G. Hare, D. J. Jeffrey, and D. E. Knuth. On the Lambert W Function. In *Advances in Computational Mathematics*, pages 329–359. Springer-Verlag, 1996.

[160] H. Shinozaki and T. Mori. Robust stability analysis of linear time-delay systems by Lambert W function: Some extreme point results. *Automatica*, 42:1791–1799, 2006.

[161] F. Maghami Asl and A. Galip Ulsoy. Analytical solution of a system of homogeneous delay differential equations via the Lambert function. In *Proceedings of the American Control Conference, 2000.*, volume 4, pages 2496–2500, 2000.

[162] C. Hwang and Y.-C. Cheng. A note on the use of the Lambert W-function in the stability analysis of time-delay systems. *Automatica*, pages 1979–1985, 2005.

[163] D. Dummit. *Abstract Algebra.* John Wiley & Sons Canada, Limited, 1995.

[164] G. H. Hardy and E. M. Wright. *An introduction to the theory of numbers.* Clarendon Press, 5th edition, 1995.

[165] M. J. D. Powell. A hybrid method for nonlinear equations. In P. Rabinowitz, editor, *Numerical Methods for Nonlinear Algebraic Equations*, pages 87–114. Gordon and Breach, 1970. (Proc. Conf., Univ. Essex, Colchester, 1969).

[166] M. J. D. Powell. A fortran subroutine for solving systems of nonlinear algebraic equations. In P. Rabinowitz, editor, *Numerical Methods for Nonlinear Algebraic Equations*, pages 115–162. Gordon and Breach, 1970. (Proc. Conf., Univ. Essex, Colchester, 1969).

[167] W. Zou and M. Zhan. Splay states in a ring of coupled oscillators: From local to global coupling. *SIAM J. Appl. Dyn. Syst.*, 8:1324–1340, 2009.

[168] J. Collins and I. Stewart. A group-theoretic approach to rings of coupled biological oscillators. *Biol. Cybern.*, 71:95–103, 1994.

[169] A. Takamatsu, R. Tanaka, H. Yamada, T. Nakagaki, T. Fujii, and I. Endo. Spatiotemporal Symmetry in Rings of Coupled Biological Oscillators of *Physarum* Plasmodial Slime Mold. *Phys. Rev. Lett.*, 87:078102, 2001.

[170] J. Solon, A. Kaya-Copur, J. Colombelli, and D. Brunner. Pulsed forces timed by a ratchet-like mechanism drive directed tissue movement during dorsal closure. *Cell*, 137:1331–1342, 2009.

[171] A. Sokolow, Y. Toyama, D. Kiehart, and G. Edwards. Cell ingression and apical shape oscillations during dorsal closure in drosophila. *Cell Imaging*, 102:969–979, 2012.

[172] H. O. De La Iglesia, J. Meyer, A. Carpino, and W. J. Schwartz. Antiphase oscillation of the left and right suprachiasmatic nuclei. *Science*, 290:799–801, 2000.

[173] A. Rahman, A. Hughes, V. Matchkov, H. Nilsson, and C. Aalkjaer. Antiphase oscillations of endothelium and smooth muscle $[Ca2+]_i$ in vasomotion of rat mesenteric small arteries. *Cell Calcium*, 42:536–547, 2007.

[174] G. S. Cymbalyuk, E. V. Nikolaev, and R. M. Borisyuk. In-phase and antiphase self-oscillations in a model of two electrically coupled pacemakers. *Biol. Cybern.*, 71:153–160, 1994.

[175] M. Zeitler, A. Daffertshofer, and C. C. A. M. Gielen. Asymmetry in pulse-coupled oscillators with delay. *Phys. Rev. E*, 79:065203, 2009.

[176] B. Blazejczyk-Okolewska, J. Brindley, K. Czolczynski, and T. Kapitaniak. Antiphase synchronization of chaos by noncontinuous coupling: two impacting oscillators. *Chaos Soliton. Fract.*, 12:1823–1826, 2001.

[177] V. Vanag, L. Yang, M. Dolnik, A. Zhabotinsky, and I. Epstein. Oscillatory cluster patterns in a homogeneous chemical system with global feedback. *Nature*, 406:389–91, 2000.

[178] I. B. Schwartz and K. Y. Tsang. Antiphase switching in josephson-junction arrays. *Phys. Rev. Lett.*, 73:2797–2800, 1994.

[179] R. N. Bracewell. *The Fourier transform and its applications*. McGraw-Hill series in electrical and computer engineering. McGraw Hill, 2000. "Rectangle Function of Unit Hight and Base".

[180] E. W. Weisstein. Boxcar function. From MathWorld – A Wolfram Web Resource. http://mathworld.wolfram.com/BoxcarFunction.html Accessed Dec. 13, 2011. Keywords: Rectangle Function.

[181] W. D. Day. *Introduction to Laplace transforms for radio and electronic engineers*. Wireless World Book. Iliffe, 1960.

[182] E. W. Weisstein. Heaviside step function. From MathWorld – A Wolfram Web Resource. Accessed Dec. 28, 2011. Keywords: Heaviside step function.

[183] B. Davies. *Integral transforms and their applications*. Applied mathematical sciences. Springer-Verlag, 1978.

[184] D. Zwillinger. *Handbook of Integration*. AK Peters Series. Jones and Bartlett, 1992.

[185] A. Papoulis and S. U. Pillai. *Probability, random variables, and stochastic processes*. McGraw-Hill electrical and electronic engineering series. McGraw-Hill, 2002.

[186] E. W. Weisstein. Gamma distribution. From MathWorld – A Wolfram Web Resource. `http://mathworld.wolfram.com/GammaDistribution. html` Accessed Dec. 13, 2011. Keywords: Gamma Distribution.

[187] E. W. Weisstein. Lambert w-function. From MathWorld – A Wolfram Web Resource. `http://mathworld.wolfram.com/LambertW-Function. html` Accessed Dec. 10, 2011. Keywords: Lambert-W function.

[188] M. Galassi, J. Davies, J. Theiler, B. Gough, G. Jungman, M. Booth, and F. Rossi. *GNU Scientific Library Reference Manual*. Network Theory Ltd., 2003.

[189] U. M. Ascher and L. R. Petzold. *Computer Methods for Ordinary Differential Equations and Differential-Algebraic Equations*. Society for Industrial and Applied Mathematics, 1997.

[190] W. H. Press, S. A. Teukolsky, W. T. Vetterling, and B. P. Flannery. *Numerical Recipes: The Art of Scientific Computing*. Cambridge University Press, 1987.

[191] A. K. Kaw, E. E. Kalu, and G. Besterfield. *Numerical Methods with Applications*. Lulu, 2008.

[192] M. Matsumoto and T. Nishimura. Mersenne Twister: A 623-dimensionally equidistributed uniform pseudorandom number generator. *Discrete Math.*, 8:3–30, 1998.

[193] H. Haramoto, M. Matsumoto, T. Nishimura, F. Panneton, and P. L'Ecuyer. Efficient Jump Ahead for F2-Linear Random Number Generators. *IN-FORMS J. Comp.*, 20:385–390, 2008.

Versicherung

Hiermit versichere ich, dass ich die vorliegende Arbeit ohne unzulässige Hilfe Dritter und ohne Benutzung anderer als der angegebenen Hilfsmittel angefertigt habe; die aus fremden Quellen direkt oder indirekt übernommenen Gedanken sind als solche kenntlich gemacht. Die Arbeit wurde bisher weder im Inland noch im Ausland in gleicher oder ähnlicher Form einer anderen Prüfungsbehörde vorgelegt.

Die Arbeit wurde am Max-Planck-Institut für Physik komplexer Systeme angefertigt und von Prof. Dr. Frank Jülicher, Dr. Saúl Ares und Dr. Luis G. Morelli betreut.

Ich erkenne die Promotionsordnung der Fakultät Mathematik und Naturwissenschaften der Technischen Universität Dresden an.

_____

Lucas Wetzel